

Design of a microfluidic chip for three dimensional hydrodynamic  
focusing in cell cytometry applications

Anthony Tony

A Thesis

In The Department

of

Mechanical and Industrial Engineering

Presented in Partial Fulfillment of the Requirements

For the Degree of

Master of Applied Science (Mechanical and Industrial Engineering) at

Concordia University

Montreal, Quebec, Canada

December 2011

© Anthony Tony, 2011

**CONCORDIA UNIVERSITY**

**School of Graduate Studies**

This is to certify that the thesis prepared

By: **Anthony Tony**

Entitled: **Design of a microfluidic chip for three dimensional hydrodynamic focusing  
in cell cytometry applications**

and submitted in partial fulfillment of the requirements for the degree of

**Master of Applied Science (Mechanical Engineering)**

complies with the regulations of the University and meets the accepted standards with respect to originality and quality.

Signed by the final examining committee:

\_\_\_\_\_ Dr. M.D. Pugh , Chair

\_\_\_\_\_ Dr. A. Bagchi , External Examiner

\_\_\_\_\_ Dr. J. Dargahi, Examiner

\_\_\_\_\_ Dr. S. Narayanswamy, Supervisor

Approved by

\_\_\_\_\_  
Chair of Department or Graduate Program Director

\_\_\_\_\_  
Dean of Faculty

Date

\_\_\_\_\_

## ABSTRACT

### Design of a microfluidic chip for three dimensional hydrodynamic focusing in cell cytometry applications

Anthony Tony

The Focusing of cells is an important part of cytometry applications and can be achieved by different techniques. 3D hydrodynamic focusing has generated considerable interest over the last few years, owing to its simplicity and its independence from an electric potential for focusing. Current 3D hydrodynamic focusing devices require multilayer structures necessitating complex fabrication. Moreover, the existing designs show poor efficiencies in focusing. In the present work, three novel 3D hydrodynamic focusing designs consisting of a main channel for sample fluid flow and three pairs of side channels for focusing are proposed and modelled. A novel three dimensional hydrodynamic focusing design is proposed and simulated. In order to develop the numerical model for three dimensional focusing designs, a theoretical review of parameters affecting the fluid flow in microfluidic structure has been performed.

Simulation was performed using COMSOL Multiphysics with diluted glycerol as the sample fluid and DI water as sheath flow fluid. The effects of fluid velocities in the channels were studied. In Design III, the overall efficiency is less than that in the first two designs, but the advantage of this design lies in the possibility of a simpler fabrication. Subsequently, parameters such as velocity and viscosity were studied in the case of Design III, and the ideal velocity condition was identified as 150  $\mu\text{m}/\text{sec}$  for the sample

flow, 350 $\mu\text{m}/\text{sec}$  for the first sheath flow, and 550 $\mu\text{m}/\text{sec}$  for the second sheath. Simulations were carried out with sample and sheath flow fluids that have different viscosities. It was concluded that the effect of focusing is primarily dependent on the velocity rather than on the viscosity of the fluid.

*'And now these three remain: faith, hope and love. But the greatest of these is love'.*

**- 1 Corinthians 13:13**

Dedicated to my Love, Mother and God Almighty

-Anthony Tony

## Table of Contents

Table of Contents .....	vii
List of Figures .....	xi
List of Tables .....	xiv
List of Symbols .....	xv
1 INTRODUCTION: .....	1
1.1 Flow Cytometry.....	3
1.2 Fluid focusing in microfluidic chips .....	5
1.2.1 Narrowing channel section .....	6
1.2.2 Electrokinetic focusing .....	6
1.2.3 Dielectrophoresis focusing.....	7
1.2.4 Optical forces .....	8
1.2.5 Magnetic Focusing.....	10
1.3 Three Dimensional Focusing .....	12
1.3.1 Electrophoresis Focusing .....	12
1.3.2 Hydrodynamic focusing.....	13
1.4 Three Dimensional Hydrodynamic focusing .....	15
1.5 Material for Microfluidic Manufacture .....	23
1.6 Thesis Motivation.....	23

1.7	Thesis Objective and Scope .....	24
1.8	Organization of the Thesis in Manuscript-Based Format .....	25
2	THEORETICAL DESIGN .....	28
2.1	Hydrodynamics of Microfluidics .....	28
2.1.1	Shear stress.....	29
2.1.2	Reynolds Number .....	30
2.1.3	Laminar flow.....	31
2.1.4	Péclet number.....	31
2.1.5	Diffusion .....	31
2.1.6	Dean Number .....	32
2.1.7	Entrance Length .....	33
2.1.8	Velocity Ratio .....	34
2.1.9	Fluidic resistance .....	36
2.1.10	Surface tension.....	36
2.2	Single Phase Flow in Microfluidics .....	37
2.3	Numerical Simulation .....	39
2.3.1	Governing Equations .....	39
2.3.2	Modeling.....	41
2.3.3	Model Introduction .....	41
2.3.4	Constants.....	43



2.3.5	Mesh and Validation .....	43
2.3.6	Model Validation .....	45
2.4	Summary .....	50
3	A NOVEL THREE DIMENSIONAL HYDRODYNAMIC FOCUSING DESIGN IN MICRO FLUIDICS .....	51
3.1	Introduction: .....	51
3.2	Literature Review .....	52
3.3	Theoretical Design Considerations .....	56
3.4	Simulation .....	59
3.4.1	Design I .....	60
3.4.2	Design II .....	64
3.4.3	Design III .....	67
3.5	Results and Discussion .....	71
3.6	Summary .....	73
4	EFFECT OF VELOCITY AND VISCOSITY PARAMETERS ON HYDRODYNAMIC FOCUSING IN THE PROPOSED DESIGN .....	74
4.1	Introduction .....	74
4.2	Hydrodynamic Focusing .....	75
4.3	Design: .....	76
4.4	Simulation: .....	78

4.5	Viscous Effect in Focusing .....	83
4.6	Results and Discussion:.....	87
4.7	Summery .....	88
5	PRILIMINARY FABRICATION .....	89
5.1	Introduction .....	89
5.2	Photolithography .....	91
5.3	Silanisation.....	94
5.4	Soft lithography.....	95
5.5	Oxygen plasma bonding.....	97
5.6	Summary .....	98
6	CONCLUSION AND FUTURE WORK.....	99
6.1	Future work .....	101
	REFERENCES .....	102

## List of Figures

Figure 1.1: Fluorescence active Cell Sorter .....	5
Figure 1.2: An Axisymmetric Flow-Focusing Microfluidic Device .	6
Figure 1.3: Dielectrophoresis focusing .....	7
Figure 1.4: The dielectrophoretic force affecting the cell at different locations .	7
Figure 1.5: A vertical focusing device utilizing dielectrophoretic force .	8
Figure 1.6: Optical gradient flow focusing through microchannel .....	9
Figure 1.7: An optical trap-based focusing technique .	9
Figure 1.8: Magnetic focusing .....	10
Figure 1.9: Focusing of microparticles using standing surface acoustic waves .	11
Figure 1.10: An electrode-based focusing microfluidic device .....	12
Figure 1.11: The basic cell cytometer using hydrodynamic focusing .....	14
Figure 1.12; A “chimneylike” structure for single step coaxial sheathing .....	16
Figure 1.13: Three novel 3D hydrodynamic focusing designs .....	16
Figure 1.14: Three-dimensional polymer hydro-focusing .....	17
Figure 1.15: A three-dimensional hydro-focusing device using PDMS.....	18
Figure 1.16: An optimal 3D focusing technique using micro-weir structure .	19
Figure 1.17: The 3D focusing technique using micromilling .....	19
Figure 1.18: 3D focusing technique using pressure driven flow .	20
Figure 1.19: A 3D focusing technique using microfluidic drifting .	21
Figure 1.20: Forces acting on the microfluidic drifting 3D focusing technique .....	21
Figure 1.21: Absorbance based micro flow cytometer .....	22

Figure 2.1: Flow establishment region and fully developed region in a fluid flow .....	33
Figure 2.2: A symmetric rectangular channel with flow rates for velocity ratio .....	34
Figure 2.3: Single Phase Poiseuille Flow in Microfluidics.....	38
Figure 2.4: Geometry with a triangular mesh .....	44
Figure 2.5: Model validation comparison design and numerical image.....	45
Figure 2.6: Design generated for model validation .....	47
Figure 3.1: Flow establishment region and fully developed region in a fluid flow .....	56
Figure 3.2: Symmetric rectangular channel with flow rates for velocity ratio .....	57
Figure 3.3: Three dimensional focusing design I with dimensions. ....	61
Figure 3.4: Simulation result of 3D hydrodynamic focusing in Design I.....	62
Figure 3.5: Graph showing horizontal and vertical focusing in Design I.....	64
Figure 3.6: Three dimensional focusing design II with dimensions.....	65
Figure 3.7: Simulation result of 3D hydrodynamic focusing in Design II .....	66
Figure 3.8: Graph showing horizontal and vertical focusing in Design II.....	67
Figure 3.9: Three dimensional focusing design III with dimensions.....	68
Figure 3.10: Simulation result of 3D hydrodynamic focusing in Design III .....	70
Figure 3.11: Graph showing horizontal and vertical focusing in Design III. ....	71
Figure 3.12: Sliced view of three dimensional hydrodynamic focusing in Design III .....	72
Figure 4.1: Two dimensional view of 3D hydrodynamic focusing design.....	76
Figure 4.2: Two dimensional view of 3D hydrodynamic focusing design.....	77
Figure 4.3: Slice view of hydrodynamic focusing happening in this design .....	82

Figure 4.4: Graph showing horizontal and vertical focusing at velocity $V_A=150$ , $V_B=350$ , $V_C=550$ m/sec through channel A, B, C respectively when diluted glycerol is used as the sample fluid and DI water is used as the sheath fluid. ....	82
Figure 4.5: Three dimensional view of the Hydrodynamic focusing effect at the tip and channel. ....	83
Figure 4.6: Graph showing horizontal and vertical focusing at velocity $V_a=150$ , $V_b=350$ , $V_c=550$ m/sec through channel A,B,C respectively when red blood cells are used as the sample fluid and diluted glycerol is used as the sheath fluid. ....	86
Figure 4.7: Graph showing horizontal and vertical focusing at velocity $V_a=150$ , $V_b=350$ , $V_c=550$ m/sec through channel A,B,C respectively when red blood cells are used as the sample fluid and DI water is used as the sheath fluid. ....	87
Figure 5.1: AutoCAD drawings of Layers I and II with dimensions of the suggested design .....	90
Figure 5.2: Design layout of Layer I and Layer II masks .....	90
Figure 5.3: Design layout of modified Layer I and Layer II masks .....	91
Figure 5.4: Overview of the Photolithography Process (119). ....	92
Figure 5.5: The contact printing mask alignment in the photolithography process (117). ....	94
Figure 5.6: The process overview of soft lithography .....	95
Figure 5.7: PDMS fabricated structure of Layers I and II. ....	96
Figure 5.8: PDMS fabricated structure of Layer I after peeling. ....	97
Figure 5.9: The final bonded PDMS structure after oxygen plasma bonding. ....	97

## List of Tables

Table 1.1: Flow cytometry .....	4
Table 2.1: Constants used in numerical simulation using COMSOL multi physics. ....	43
Table 2.2: Meshing parameters .....	44
Table 2.3: Different mesh elements on different meshing.....	45
Table 2.4: Comparison between (69) and the current work.....	46
Table 2.5: Different velocity iterations used by making $\alpha_v$ as 1.0.....	48
Table 3.1: Parameters and values used in COMSOL Multiphysics simulation.....	60
Table 3.2: COMSOL Multiphysics simulation of design I with different iterations. ....	62
Table 3.3: COMSOL Multiphysics simulation of design II with different iterations.....	65
Table 3.4: COMSOL Multiphysics simulation of design III with different iterations. ....	69
Table 4.1: Parameters and values used in COMSOL Multiphysics simulation.....	79
Table 4.2: COMSOL Multiphysics simulation with different velocity iterations. ....	81
Table 4.3: Properties of different sample and sheath fluids used in COMSOL Multiphysics simulation.....	84
Table 4.4: COMSOL Multiphysics simulation with different velocity and viscosity iterations.....	85

## List of Symbols

$V_A$	Velocity through channel A
$V_B$	Velocity through channel B
$V_C$	Velocity through channel A
$V_D$	Velocity through channel B
$F$	Force
$M$	Mass
$A$	Acceleration
$p$	Static pressure
$\vec{U}$	Velocity vector
$\mu$	Dynamic viscosity
$\rho$	Density of the fluid
$\tau$	Shear stress
$u(y)$	Velocity of fluid at a distance ‘y’
$Re$	Reynolds number
$D$	Hydraulic diameter of the channel
$\gamma$	Kinematic viscosity of the fluid
$Re_p$	Particle Reynolds number
$D_p$	Diameter of the particle
$Pe$	<i>Péclet number</i>

$w$	Width of the channel
$D$	Diffusion coefficient of the particle
$J$	Diffusion flux of the particles
$C$	Concentration
$d$	Distance a particle moves in time $t$
$r$	Curved channel radius
$c_i$	Concentration of species $i$
$D_i$	Diffusion coefficient
$R_i$	Reaction term
$\rho_1$	Density of sample fluid
$\rho_2$	Density of sheath fluid
$\eta_1$	Viscosity of sample fluid
$\eta_2$	Viscosity of sheath fluid
$c_0$	Input concentration
$D_i$	Isotropic diffusion coefficient



## **List of Abbreviations**

2D	Two dimensional
3D	Three dimensional
DG	Diluted glycerol
DI	Deionized
DIW	Deionized water
HCL	Hydrochloric acid
IPA	Isopropyl Alcohol
LOC	Lab on a chip
MEMS	Micro electro mechanical systems
PDMS	Polydimethylsiloxane
PMMA	Poly(methyl methacrylate)
RBC	Red blood cells
UV	Ultra violet

## 1 INTRODUCTION:

In the past decades micro fabricated devices have made a huge impact and created opportunities for researchers in various fields. Microfabricated devices basically consist of miniaturized structures with moving parts for pressure sensing, channels for fluid flow, micro optics for scanning, mirror arrays for displays, piezoelectrics for temperature controls etc. Microfabricated devices are also referred to as micro electromechanical systems (MEMS), micro machines, lab on a chip (LOC), microsystems or micro total analysis systems ( $\mu$ -TAS) in different parts of the world. One of the major applications of microfabricated device is of the flow of fluids through the micro channels for biological applications. The integration of micro systems with fluid dynamics can be called as microfluidic devices, since the properties of fluids vary drastically in the micro domain. Highly precise control of fluids is possible in microfluidics systems, which is advantageous in many biological applications like molecular biology, cell cytometry, chemical reaction, enzyme synthesis, protein detection etc. Microfluidic devices can be a better replacement for the conventional cell sorting systems due to their properties. Microfluidic devices provide several benefits like portability, simplicity of operation, improved transport control, greater accessibility, reduced cost and can be integrated with other analytical techniques for various practices (1-4). In chemical and biochemical engineering, sample preparation, purification, mixing, reactions, separations and fraction collection can all be performed on integrated monolithic microfabricated devices (5-9).

MEMS fabricated Lab on a Chip (LOC) devices play an important role in biomedical applications such as tissue culture, drug discovery and point-of-care diagnostic systems,

more over a tool for chemistry, biochemistry, and for fundamental research (10). LOC devices with various techniques integrate all the equipment involved in a process such as fluid flows, optics, chemical reactions, heat exchangers, separators and mixers, in your thumb.

The ability to control parameters of microenvironment at relevant length and time scales is one of the key benefits of microfluidics technology in cellular biology (1). Existing precision fluid delivery systems are bulky, expensive, and typically employ high-power syringe pumps. Microfluidic devices for manipulating fluids are widespread and finding uses in many scientific and industrial contexts. One of the successful applications of microfluidic devices has been in flow cytometers that have become quite popular for cell sorting and cell counting analyses in fields such as medical diagnosis, bioengineering as well as MEMS in general.

In the past few years MEMS technologies has shown enormous potential for portable low-cost devices in the field of analytical chemistry and biotechnology (11,12). By using MEMS technology, it is possible to integrate several microfluidic components such as micro pneumatic pumps/valves onto a polymer-based chip device (13). Edmond W. K. Young and David J. Beebe (12) studied about the fundamentals of microscale cell culture, cellular microenvironment, translation of methods from macro- to microscale, microfluidics and microscale technology, and their effects have been discussed. Microflow, fluidmechanics of micro flow devices, theoretical and experimental studies is an ongoing process that has been discussed in various papers (14-17). Microfluidic tools, device materials and fabrication techniques have been reported in many books and publications (1-8,11,14,15,18-22).

## 1.1 Flow Cytometry

Flow cytometry is an extremely powerful technology in molecular biology and biotechnology to measure physical and chemical characteristics of individual particles as they pass under a detection source one by one. One of the important applications of flow cytometry is in the field of biotechnology and medical diagnosis for cell sorting and counting. In the past decade, dye synthesis and high-speed data analysis technology have exerted synergistic effects on flow cytometry technology and have brought this powerful analytical tool into routine clinical and laboratory use in the field of gene diagnosis, transfusion medicine, bacteria analysis, clinical hematology diagnosis, DNA molecular sizing, environmental microbial sensing, and various applications of identifying cell samples (13). Flow cytometry is a technique for counting and examining microscopic particles, such as cells and chromosomes, by suspending them in a stream of fluid and passing them through an optical detector. It is capable of measuring the properties of individual particles depending on the integrating devices. Randomly distributed injected particles should be ordered or focused into a stream of single particles that can be detected by an optical system.

Flow cytometry is based on three main steps: focusing, detection and sorting. The micro particles need first to be focused at the center of the channel, to pass through an optical source for single molecular detection. Depending on the properties and the need, the micro particles can be sorted from a diverse population. The term cell cytometry is widely used when the micro particles to be sorted are cells. The basic steps of flow cytometry and the relative techniques currently used can be depicted with the aid of Table 1.1.

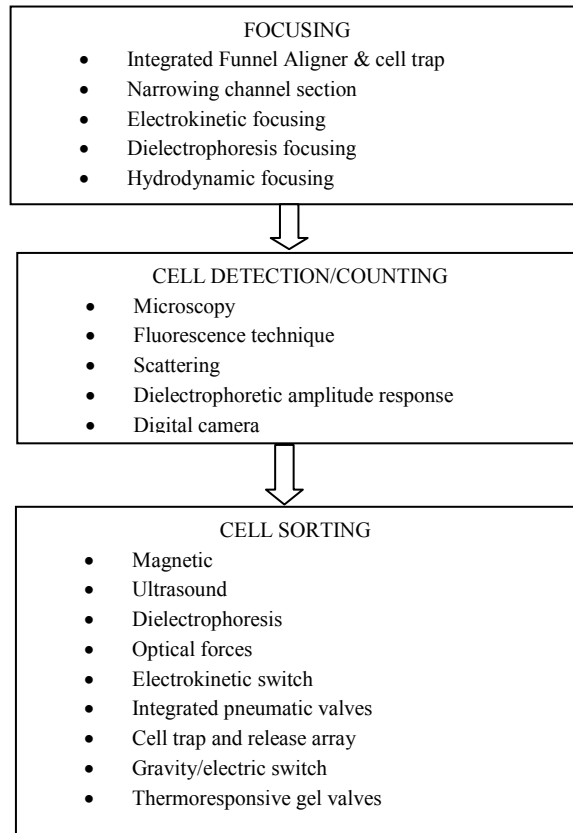


Table 1.1: Flow cytometry

Figure 1.1 shows a basic cell sorter consisting of a focusing unit, an optical source for detection of cells and a sorter that sorts the cells and the waste into different channels (23). The present research examines the fluid focusing and the design of a three dimensional hydrodynamic focusing MEMS flow cytometer. The present thesis involves the focusing of the fluid sample in a cytometer and the review of relevant literature is presented in the following section.

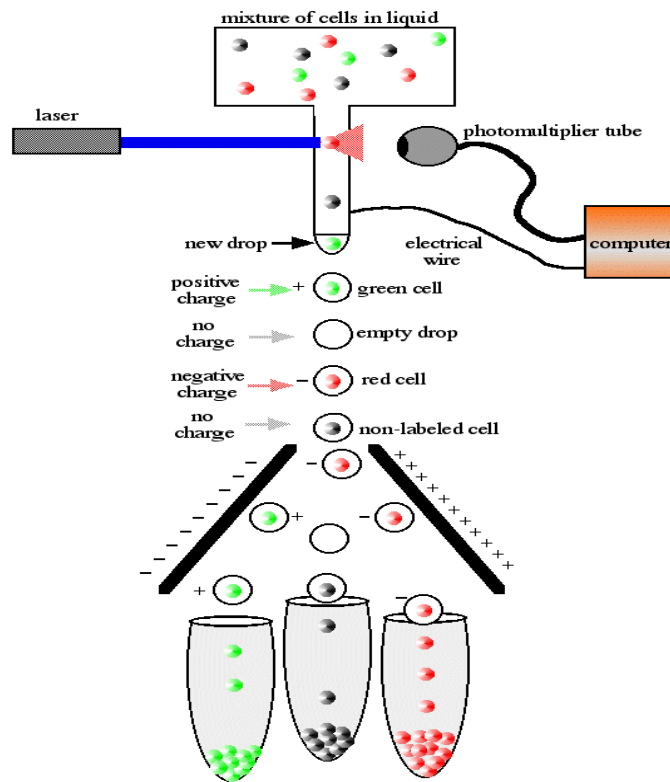


Figure 1.1: Fluorescence active Cell Sorter (12)

## 1.2 Fluid focusing in microfluidic chips

The main criteria in focusing the particles to be analyzed in the microfluidic channel are the following: the miniaturization of the fluid-handling components, the miniaturization of the optics, and integration and applications development. Optical integration and particle sorting are as challenging as the fluid handling component. The sample solution containing cells or small sized particles of research interest should be passed through a micro channel and should be aligned to the center, through which the optical detection is passing. The focusing or aligning of these particles is made possible by using different methods such as an integrated funnel aligner and cell trap, a narrowing channel section, electrokinetic focusing, dielectrophoresis focusing and Hydrodynamic focusing.

### 1.2.1 *Narrowing channel section*

An Axisymmetric Flow-Focusing Microfluidic Device has been developed by S. Takeuchi *et al* (24) as shown in Figure 1.2. The channel comprises a narrow cross section in a cylindrical tube half way down its length. The fluid is focused and breaks into aqueous droplets using the orifice in the narrow cross section as shown in Figure 1.2. To fabricate a cylindrical structure by using MEMS devices is complicated. Other methods of focusing microparticles by using a narrowing cross section are explained in various literatures (25-27).

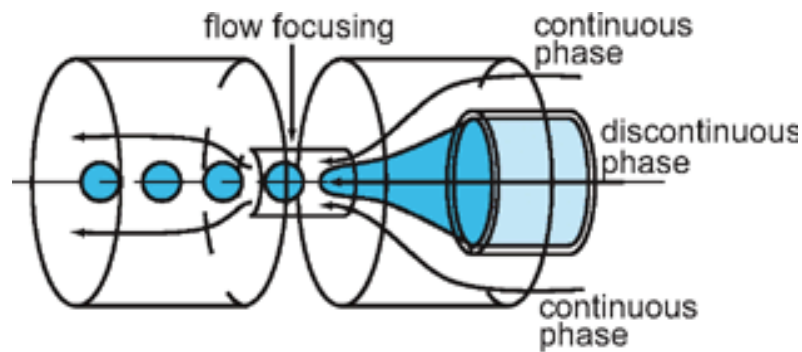


Figure 1.2: An Axisymmetric Flow-Focusing Microfluidic Device (24).

### 1.2.2 *Electrokinetic focusing*

Different research groups have studied the electrokinetic focusing of the microparticles in a microfluidic channel (28-32). C. Church *et al* (28) presented an electrokinetic focusing of yeast cells in a planar serpentine microchannel using dc-biased ac electric fields.

### 1.2.3 Dielectrophoresis focusing

In electrophoresis focusing, basic electrodes are embedded in the channel to divert the micro particles, depending on their affinity to the electric potential. Figure 1.3 shows the design of a microfluidic device fabricated on a glass substrate by Toru T *et al* (33). A valveless switch for microparticle sorting with laminar flow streams and with electrophoresis perpendicular to the direction of the fluid stream has been discussed and developed in their work. The dielectrophoretic force affecting the cell at different locations in one serpentine period and the velocity components in a streamline similar to the electric field lines is shown in Figure 1.4

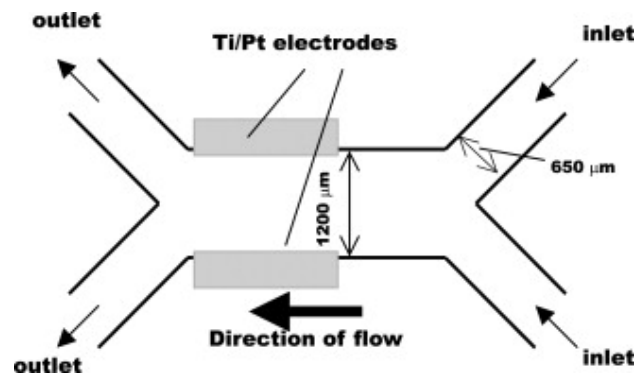


Figure 1.3: Dielectrophoresis focusing (33).

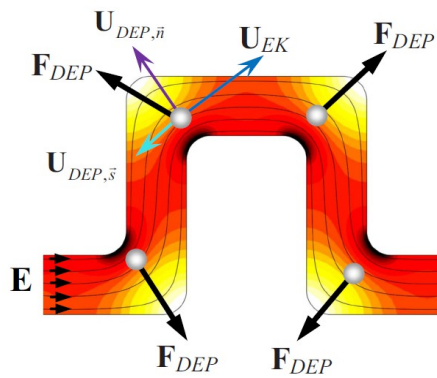


Figure 1.4: The dielectrophoretic force affecting the cell at different locations (28).



C. Lin *et al* (34) studied a vertical focusing device utilizing a dielectrophoretic force and its application on a microflow cytometer. In a microfluidic channel a pair of parallel microelectrodes as shown in Figure 1.5 is deposited on the upper and bottom surface. The pair of parallel microelectrodes provides the force for driving the micro particles to the center of the sample flow. The performance of the device has been tested using micro polystyrene beads and diluted human red blood cells (RBC). Various research groups (35,36,36,37) have discussed dielectrophoresis focusing in microfluidics.

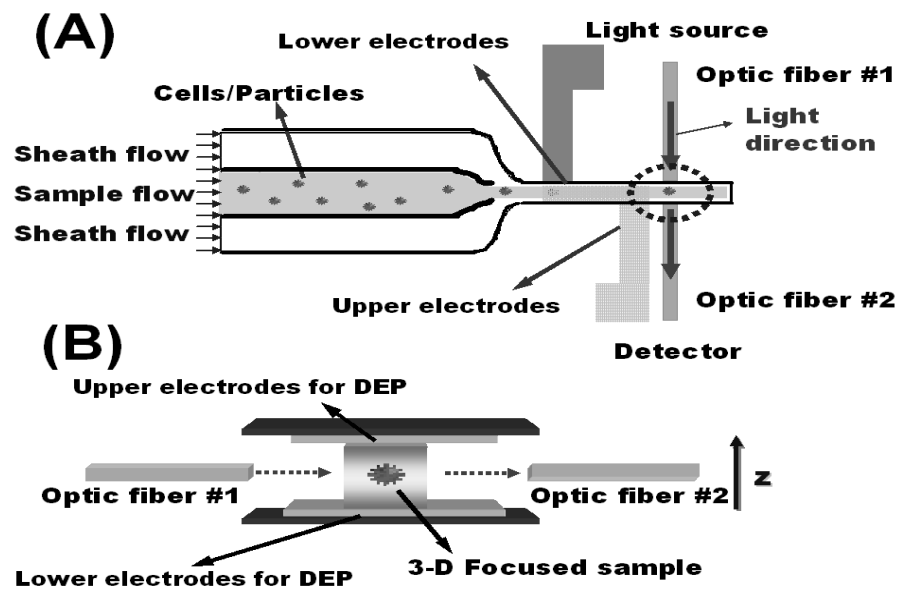


Figure 1.5: A vertical focusing device utilizing dielectrophoretic force (34).

#### 1.2.4 Optical forces

Yiqiong Zhao *et al* (38) have discussed and simulated a non-contact technique that employs an optical force field to achieve flow focusing in microfluidic systems. This technique uses an optical gradient force generated by using an elliptically shaped laser

beam in a microchannel to attract the flowing particles to the center. Figure 1.6 shows optical gradient flow focusing through the length of the microchannel.

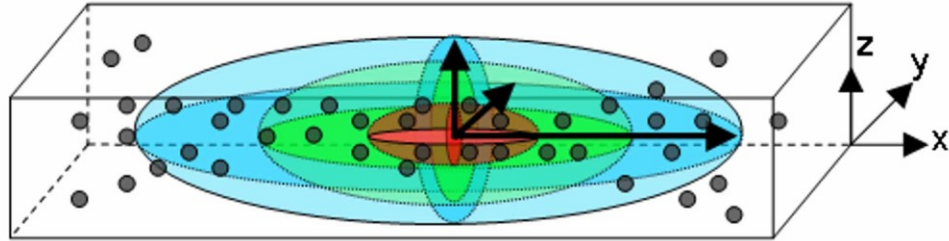


Figure 1.6: Optical gradient flow focusing through microchannel (38).

An optical trap, which can hold a particle in a tightly focused light beam, is shown in Figure 1.7. The response of a microscopic dielectric object to an applied light field can be used to arrange, guide or deflect particles inside the geometry (39). Schematic of an optical trap is shown in Figure 1.7. Chamber A consist of a blank flow stream, whereas particles to be sorted flows from chamber B to D. 3D optical lattice such as body-centred tetragonal (b.c.t.) lattice, has been introduced into the fractionation chamber (FC) which will allow one species of particle to be selectively pushed into the upper flow field as shown.

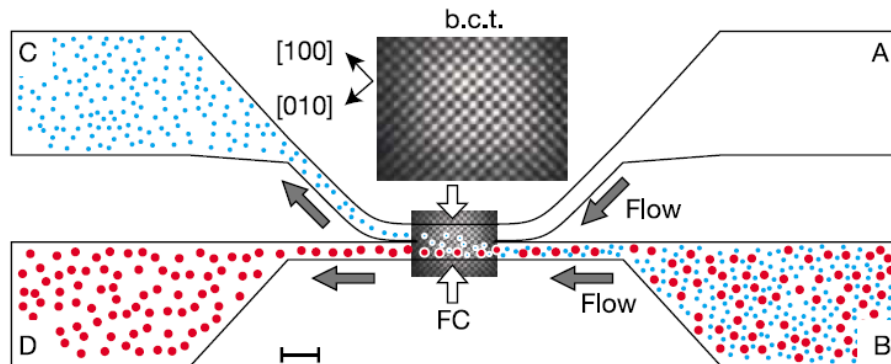


Figure 1.7: An optical trap-based focusing technique (39).

### 1.2.5 Magnetic Focusing

A magnetic-based microfluidic platform for biomolecular separation has been discussed by Qasem R *et al* (40). High magnetic field gradients generated by multi-functional magnetic microdevices have been used to demonstrate magnetic bead trapping, particle concentration, transportation and sensing in a liquid sample under static conditions and with continuous flow at different flow rates. Figure 1.8 shows the developed design and structure.

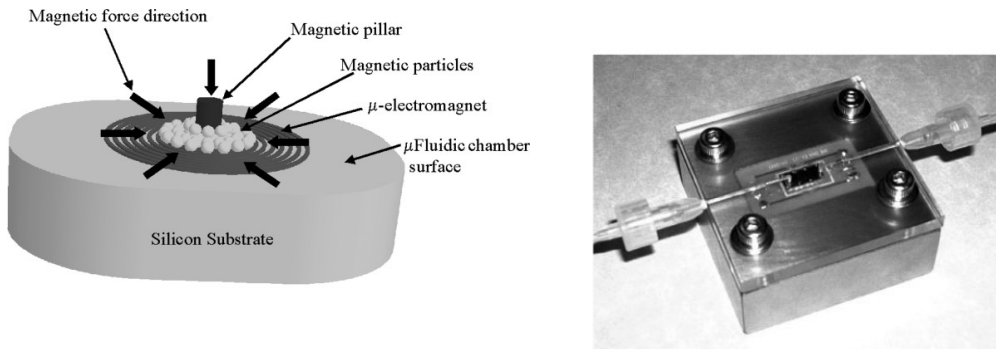


Figure 1.8: Magnetic focusing (40)

Another study shows the focusing of microparticles in a microfluidic channel with standing surface acoustic waves (41) as shown in Figure 1.9. The underlying principle is that acoustic waves generate pressure gradients in a liquid that can be used to manipulate suspended particles or a liquid medium.

Many two-dimensional focusing devices based on hydrodynamic and electroosmotic flow have been reported in microfluidic books (3-5,18) and journals (42,43). In 2D focusing it is not necessary for the micro particles in the sample fluid to pass through the focused stream one by one, even if the width of the focused stream is the same as the particle size.

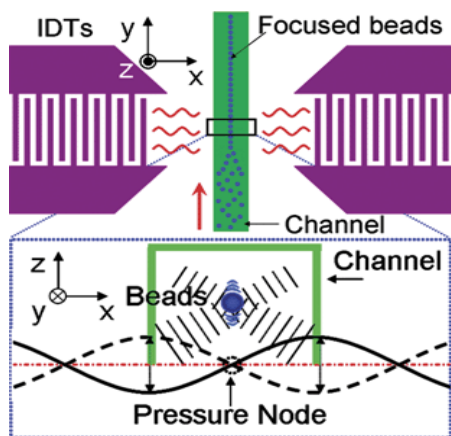


Figure 1.9: Focusing of microparticles using standing surface acoustic waves (41).

This is mainly due to the fact that the particles can still be spread vertically along the channel depth. The vertical spread of the sample is affected in several ways. For single molecule detection, the sample should pass through a minute optical detection region much smaller than the size of the channel. The use of single molecular detection with the point source of an optical device results in a large number of undetected molecules due to an unbalanced vertical spread. The other important criterion is that even if it is horizontally focused, the micro particles present in the sample may still interact with the bottom and top walls due to an unfocused stream in the vertical direction. By considering smaller cell size to be sorted, it is important to consider the third dimension, to position the particle at the center. Hence in single molecule detection and sorting, the sample flow is centered by using an additional pair of sheath flow in the vertical direction, a technique that is advantageous in cell sorting as well as in managing proteins against adsorbing and sticking to channel walls. As of now, three dimensional focusing can be achieved using dielectrophoresis and sheath-based hydrodynamic focusing techniques. Some of the reported 3D dielectrophoresis works are reviewed and subsequently attention has been shifted to 3D hydrodynamic focusing in the following sections.

### 1.3 Three Dimensional Focusing

A review of the literature shows that 3D focusing is much more advantageous than 2D, particularly in single particle detection. While various 3D focusing techniques have been developed in the past decades, both dielectrophoresis and hydrodynamic 3D focusing with their uniqueness, have found lot of research interest.

#### 1.3.1 Electrophoresis Focusing

In this technique, a non-uniform electric field with negative dielectrophoretic force is used to focus a stream of cells towards the center of a microfluidic channel from all directions. An isotropic etched elliptic-like microfluidic channel has been designed and fabricated for cytometry applications (44). It focuses biological cells by using dielectrophoresis. Using dielectrophoresis to detect and count fluorescent particles flowing through a microchannel is shown in Figure 1.10 (45).

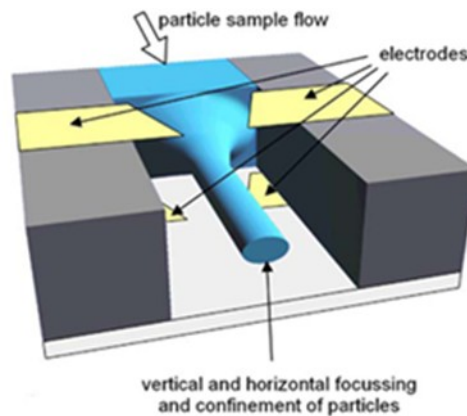


Figure 1.10: An electrode-based focusing microfluidic device (45)

A microfabricated electrode-based device focuses particles into the center of the device, which is  $40\ \mu\text{m}$  high and  $250\ \mu\text{m}$  wide within the flowing fluid stream. The method ensures that all the particles pass through a confined region that is about  $5\ \mu\text{m}$  in

diameter and formed by focusing a beam of light. The device was capable of detecting and counting up to 250 particles/s in fluorescent latex, based on the fluorescence emission intensity of the focused particles. High throughput particle analysis, in this case is achieved by combining dielectrophoretic particle focusing with confocal optical detection.

Dafeng Chen and Hejun Du presented a dielectrophoretic barrier-based microsystem that allows the separation of microparticles by aligning two layers of a microelectrode structure placed face-to-face on the top and bottom sides of the microchannel (46). Another research shows a simple method for the 3D focusing of red blood cells (RBCs) by using classical fluid mechanics with negative electrophoresis and a superimposed pressure-driven flow. In this method, particle lagging is created behind the Poiseuille upward-flow in a vertical tube and, when the density of the particle is greater than the density of the fluid, the technique creates a lift force that leads the particle to migrate toward the axis of the tube (12).

The main disadvantage of dielectrophoresis focusing and sorting is that the electrostatic field has been proved to damage the intensity of the cell membrane (47). Moreover, the particles are separated according to their sizes. The technique is also capable of separating particles of the same size if and only if the electrical properties of the particles are different. This makes 3D hydrodynamic focusing advantageous in cell cytometry.

### ***1.3.2 Hydrodynamic focusing***

Hydrodynamic focusing is a technique in which the focusing of a sample fluid is achieved by allowing two sheath fluids to conflow at different velocities inside a micro-

flow channel. By contrast, flow cytometry is a process whereby cells are analyzed on the basis of hydrodynamic focusing and sorted based the cellular properties. The principle behind the flow cytometer is expressed as the focusing effect of a center flow surrounded by two sheath flows using hydrodynamic effects. The width of the center cell flow is reduced such that only one cell is permitted to be positioned at the center, thereby facilitating detection and sorting. Since the time when cell cytometry and microfluidics were integrated, this focusing has been done on a two dimensional scale only (48).

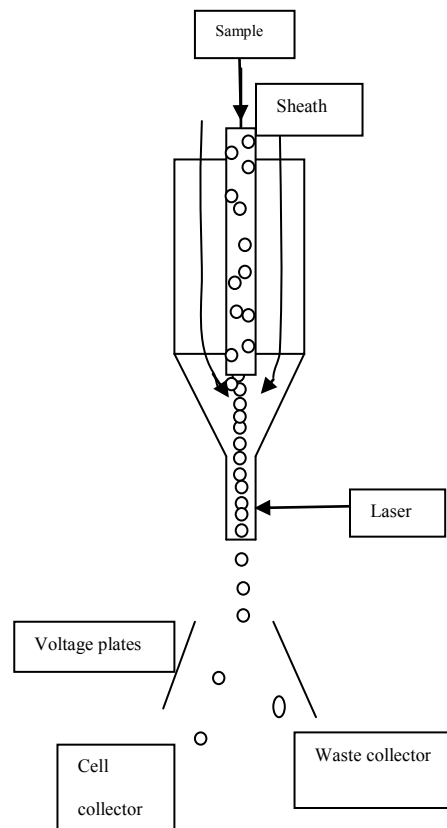


Figure 1.11: The basic cell cytometer using hydrodynamic focusing

A fluidics system consists of a central channel/core enclosed with an outer sheath through which the sample and fast flowing fluids are injected. A massive drag effect on the narrowing central chamber due to the movement of the faster sheath fluid alters the

velocity of the central fluid, giving a parabolic profile with the greatest velocity at the center and zero velocity at the sides. The particle moves to the center. The effect is called hydrodynamic focusing. Under optimal conditions in a microchannel the flow is always laminar, so that the fluid in the central chamber does not mix with the sheath fluid due to a low Reynolds number ( $Re$ ). The flow profile characteristics of the sample fluid stream can be estimated using  $Re$ .

Hydrodynamic focusing is effective in a wide variety of applications such as: on-chip flow cytometry for cell/particle counting and sorting (49-52), single-molecule detection and measurement (53), diffusion based mixtures and laminar mixers (54,55), microfluidic optical waveguides (56), cell patterning (57), fluorescent light sources (58), surface chemical patterning (59,60), flow switches for continuous sample injection (61), microchemical synthesis (62,63), and in the production of microparticles (64) and microdroplets and bubbles (65). In this work, recently evolved 3d hydrodynamic focusing techniques have been reviewed critically and a novel design is proposed.

#### **1.4 Three Dimensional Hydrodynamic focusing**

In 2D hydrodynamic focusing, a pair of sheath flows from the sides is used to focus a sample stream horizontally to the center, thereby leaving undetected particles due to unfocussed vertical spread. This leads to advancement towards 3D focusing techniques. In 2001, the 3D hydrodynamic focusing method was first proposed and fabricated for cells in a pressure driven micro cell sorter by Goranovic *et al* (66), as shown in Figure 1.12. A “chimneylike” structure for single step coaxial sheathing was modeled and



optimized through simulation. Micro machined silicon fabrication, a complex technique, was used. Moreover, the structural design was also found to be inefficient.

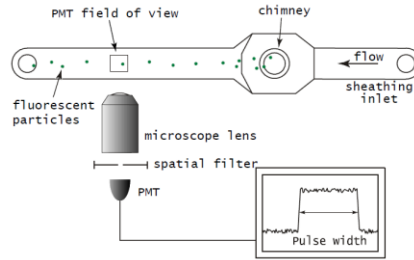


Figure 1.12: A “chimneylike” structure for single step coaxial sheathing (66)

Subsequently in 2004, N. Sundararajan *et al* (67) studied three novel 3D hydrodynamic focusing designs. The three designs are shown in Figure 1.13. In Design 1, two sheath flows, one from the top and the other from the bottom, flowing perpendicular to the sample flow, were simulated with a  $10 \mu\text{l}/\text{min}$  flow rate. Due to the asymmetrical effect of the top and the bottom sheath flows, another design, Design 2, was considered. In this design, two top sheath flows and two bottom sheath flows enter perpendicular to the sample flow.

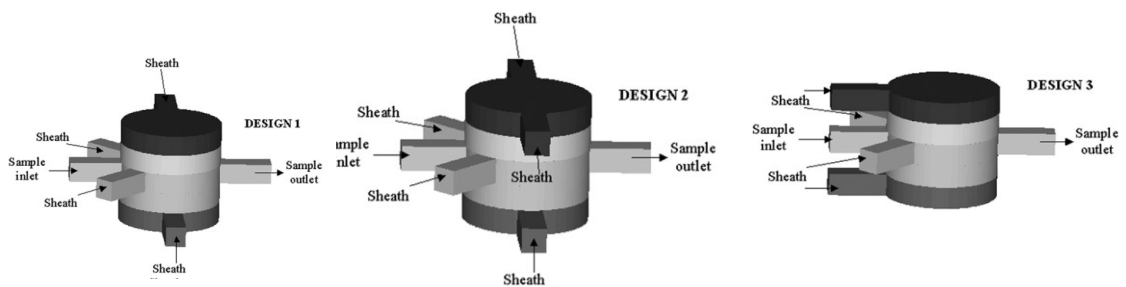


Figure 1.13: Three novel 3D hydrodynamic focusing designs (67).

To reduce the diffusion of the sample when it enters the alignment reservoir, in Design 3, the top and bottom sheath flows are aligned parallel to the sample flow. Design 2 was

selected and fabricated using the membrane sandwich method with a channel width of  $100\ \mu\text{m}$  and a channel depth of  $50\ \mu\text{m}$ . The central alignment reservoir was  $250\ \mu\text{m}$  in diameter, and the thickness of the interconnect layers was  $100\ \mu\text{m}$ . However, the main disadvantage was that the complex design required a complicated silicon-based fabrication process.

R Yanga *et al* (68), developed three-dimensional polymer hydro-focusing. A sloped microstructure for coaxial sheathing, shown in Figure 1.14, was designed, microfabricated by means of SU-8 3D lithography, and tested. A slight slanting is given to the bottom part during fabrication for vertical focusing. The horizontal focusing had been done with two coaxial sheath flows from the sides. This allowed the cells to flow in the core stream at an almost uniform velocity. This method also required complex geometric structures during fabrication.

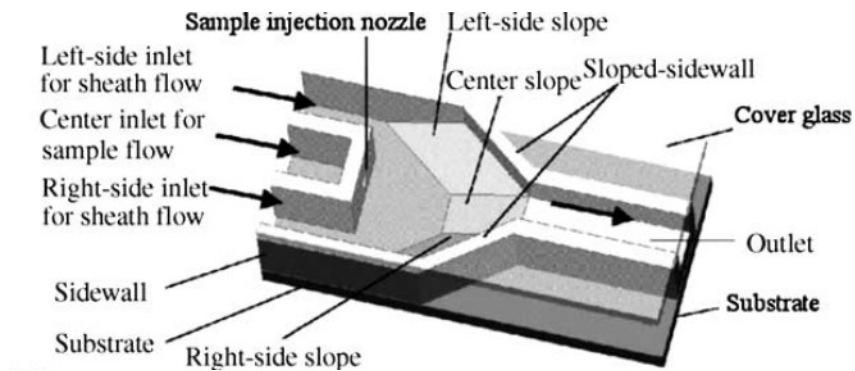


Figure 1.14: Three-dimensional polymer hydro-focusing (68).

C. C. Chang *et al* (69) first developed a 3D hydrodynamic focusing device using two-layer polydimethylsiloxane (PDMS) microchannels. There were four inlet ports and one outlet port for the fluid flow driven by a syringe pump. A sample flow stream was driven

through Channel B and was focused vertically to a narrow stream by using two sheath flows from A and C. Then it was horizontally focused to a small core region by using a cross flow through Channel D as shown in Figure 1.15. The device is fabricated using PDMS micromolding techniques. Channels A, D and E are  $100\mu\text{m}$  in width and  $95\mu\text{m}$  in depth whereas Channels B and C are  $50\mu\text{m}$  and  $45\mu\text{m}$  in width and height respectively. A flow rate of  $Q_A = Q_B = Q_C = 10\mu\text{l min}^{-1}$  and  $Q_D = 2\mu\text{l min}^{-1}$  was given respectively and a comparison was made with 2D devices in terms of focusing and structure.

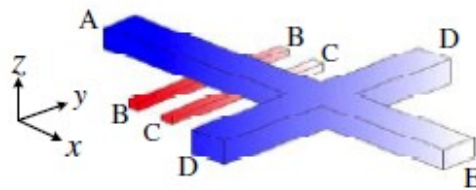


Figure 1.15: A three-dimensional hydro-focusing device using PDMS(69).

An optimal 3D focusing technique for micro-flow cytometers was suggested by C. H. Tsai (70), using hydrodynamic focusing on a microstructure. A micro-weir structure, as shown in Figure 1.16 and positioned directly beneath an optical detection system, was fabricated. The sample stream was focused in the vertical direction by a second pair of sheath flows, which were capable of achieving a focused sample stream width of between  $6$  and  $15\mu\text{m}$ . In this approach, the sample stream is focused initially in the horizontal plane using two sheath flows and is then focused in the vertical direction using a second set of sheath flows and a micro-weir structure. Most of the studies reviewed above show

that the sample flow was actually focused on the region near the bottom wall rather than at the center.

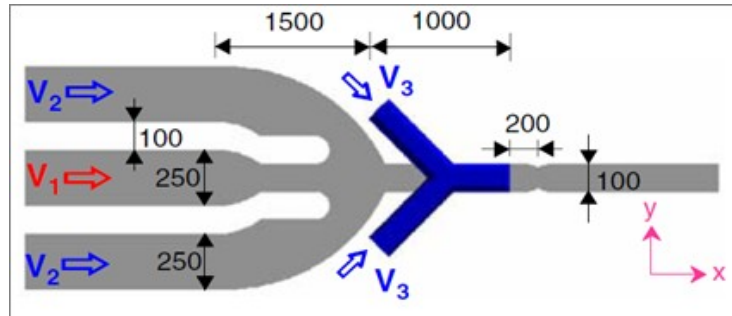


Figure 1.16: An optimal 3D focusing technique using micro-weir structure (70).

A novel two-layer microchannel structure to enable 3D hydrodynamic focusing over a wide range of Reynolds numbers ( $Re$ ) has been suggested by G. S. Zhuang *et al* (71) by keeping the flow rate constant in all the inlet channels  $Q_A = Q_B = Q_C = Q_D = 576 \mu\text{l/hr}$  in the microfabricated structure. Figure 1.17 shows the design of the 3D focusing system, in which a sample stream is passed through Channel B. Channels A, C and D denote the sheathing flows. Two smaller channels are fabricated in the lower layer (B and C,  $200 \times 200 \mu\text{m}$ ) and two larger channels (A and D,  $400 \times 400 \mu\text{m}$ ) were fabricated in the upper layer using micro milling technologies and were thermally bonded together.

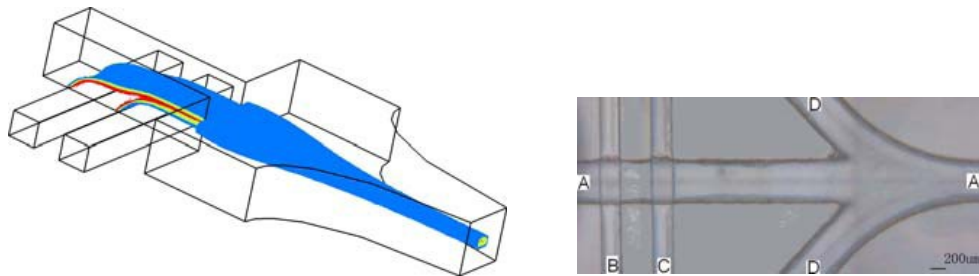


Figure 1.17: The 3D focusing technique using micromilling (71).

The focusing of the sample at the end tip seems to be in rectangular shape which is not much efficient. Also micromilling technology is an expensive and the smallest dimension of the diamond tool available is of  $200\mu\text{m}$  (72).

D. S. Kim *et al* (48) developed an efficient 3D hydrodynamic focusing microfluidic device shown in Figure 1.18. The vertical focusing of the core sample flow was achieved in the pressure-driven flow owing to a locally increased aspect ratio of thickness to width even below the global aspect ratio of 0.5 without any horizontal separation wall after a simple horizontal focusing.

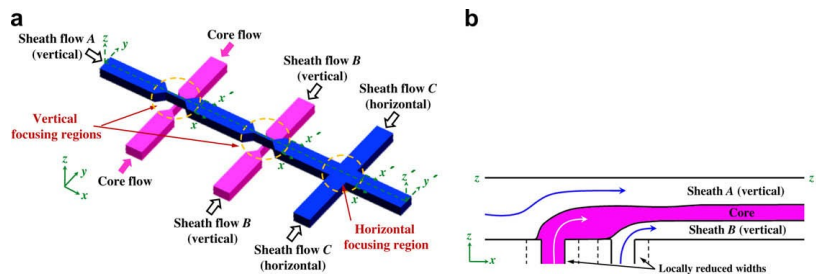


Figure 1.18: 3D focusing technique using pressure driven flow (48).

For most 3D hydrodynamic focusing devices developed so far, 3D focusing is achieved by compressing the center cell flow with sheath flows from both the horizontal and vertical directions. In order to do so, 3D multi-layer structures are needed to introduce the vertical sheath flows from the out-of-the-plane directions. The complex multilayer fabrication of these devices compromises the advantages of microfluidics and makes it virtually impossible to mass produce these devices.

Xiaole Mao *et al* (53,73,74) suggested a novel 3D hydrodynamic focusing with a single-layer planar microfluidic device using microfluidic drifting. By utilizing the viscous drag of Dean Flow induced in a curved microfluidic channel, they showed that it is possible to

achieve 3D hydrodynamic focusing in a single layer planar microfluidic device. Various forces and their effects on microfluidic drifting was further studied by (53,73) Xiaole Mao and Tony Jun Huang, showing that their device can be effectively adapted to focus microparticles with a size and density close to those of lymphocytes.

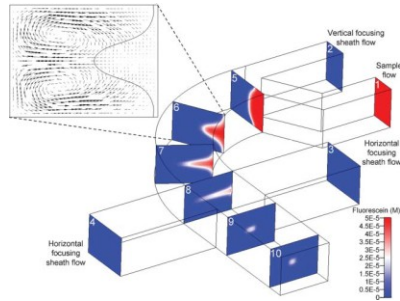


Figure 1.19: A 3D focusing technique using microfluidic drifting (53).

Figure 1.20 shows the effect of forces acting on suspended particles in the cross-sectional plane of curved channels. The forces can be classified as (i) Dean viscous (Stoke) drag force caused by secondary rotational Dean flow ( $FD$ ), (ii) centrifugal force ( $F_{cfg}$ ), and (iii) gravitational force ( $FG$ ).  $FD$  accelerates particles transversely to ensure that the particles stay on the course of the streamlines whereas  $F_{cfg}$  and  $FG$ , on the other hand, cause particles to deviate from the streamlines.

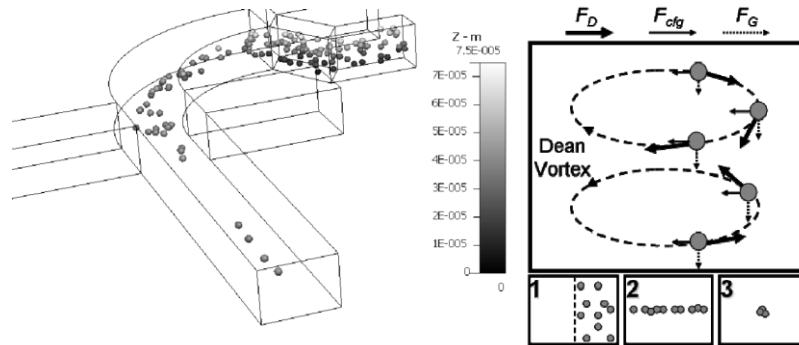


Figure 1.20: Forces acting on the particles during microfluidic drifting 3D focusing technique (73).

The theory behind microfluidic drifting and 3D hydrodynamic focusing is explained in (61). The key advantage of microfluidic drifting is that it enables 3D hydrodynamic focusing in a single-layer planar (2D) microfluidic structure that can be readily fabricated via standard soft-lithography, involving only one device layer and one photolithography mask, a technique which is ideal for mass producible flow cytometry devices.

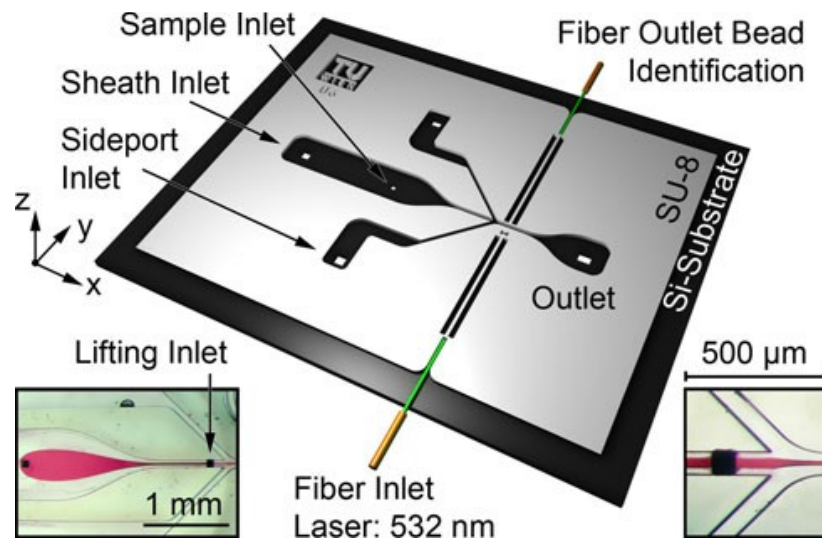


Figure 1.21: Absorbance based micro flow cytometer (75)

In 2011 Miniaturized flow cytometer with 3D hydrodynamic particle focusing has been developed by Michael *et al* (75) consisting of a silicon substrate, a single-layer SU-8 channel structure, and a PDMS cover lid. The sample flow is injected through the middle of the main sheath fluid as shown in Figure 1.21, for vertical alignment, and another pair of sheath fluid is used for horizontal alignment of the sample stream.

## **1.5 Material for Microfluidic Manufacture**

Materials such as silicon, silica, polymers, SU-8, PMMA , PDMS, etc., have been widely used to fabricate micro structures thanks to advances in MEMS fabrication technology. The details of these have been provided in Chapter 5. Biocompatible materials for microfluidic systems lead to the application of polydimethylsiloxane (PDMS) for biological studies. The biological procedures that have been miniaturized into PDMS-based microdevices include the following: immunoassays, the separation of proteins and DNA, the sorting and manipulation of cells, the studies of cells in microchannels exposed to laminar flows of fluids, and large-scale, combinatorial screening, etc (76). High-density microfluidic chips analogous to electronic integrated circuits containing plumbing networks have been fabricated by using MEMS technologies (77). Simplicity in fabrication and the control of fluid flow in PDMS microchannels make it an attractive and effective platform in the MEMS industry.

## **1.6 Thesis Motivation**

Cell cytometry is one of the important fields in cellular biology. Conventional cytometers are expensive, bulky, space consuming, involve more reagents and a considerable amount of sample consuming, etc., making microfluidics and bio MEMS suitable in this field. Cell cytometers consist of three main parts for focusing, detection and sorting. It is necessary to focus samples containing microparticles so that they are aligned at the center for single molecule detection, counting, and sorting.

Existing microfluidic cytometers use different focusing techniques such as electrokinetic, dielectrophoretic, magnetic, optical, hydrodynamic, etc. Research shows that the usage of



an electric potential ruptures the cell membrane, making it disadvantageous. Moreover, existing technologies focus mainly on two dimensional scales. However, when the micro particles, such as cells, are aligned to the center only in the horizontal direction, there is friction between the channel walls and the particles in the unfocused vertical direction. This makes it important to conduct studies in three-dimensional domains in focusing. Three dimensional focusing is achieved currently by dielectrophoresis and hydrodynamics; and the potential damage to cells due to use of electricity in dielectrophoresis makes hydrodynamic focusing as an effective alternative.

Hydrodynamic focusing is one of the important fields in micro fluidics due to microfluidic focusing, micro mixing, biological cell detection, cell counting and sorting, etc. A pair or more of sheath flows are used to align the micro particles such as cells containing a sample fluid, flowing through a main channel. The properties of the fluid and hydrodynamics play the major role in focusing. From the literature it is clear that current models focus mainly on two dimensional scales. Even though the horizontal focusing is efficient, still it gives a chance for the cells or micro particles to interact with the top and bottom of the channel walls. It is also necessary to avoid any potential voltage usage to avoid cell rupture during cellular analysis. Moreover, all the existing designs are complex structures, which require a complex fabrication process.

## **1.7 Thesis Objective and Scope**

By considering the facts reviewed above, it is necessary to develop a type of focusing without any electric potential for cell cytometry applications. The objective in this thesis is to develop a novel three dimensional design that allows the hydrodynamic focusing of

micro particles in microfluidics. The new design should be able to focus micro particles in both the horizontal and vertical directions in order to align the particles towards the center for molecular detection, counting, and sorting. It is also required to eliminate complex designs and structures. The specified objectives of the proposed research are the following:

1. Design and development of a model for three dimensional hydrodynamic focusing
2. Study of the effect of different velocity and viscosity parameters on the proposed model.

A novel three dimensional type of focusing with three pairs of sheath flows has been suggested, with the first two pairs for vertical focusing, and the third pair for horizontal focusing. The focusing ability of Design I was excellent, but based on fabrication complexity, Design II and then Design III have been proposed and simulated as discussed in detail in further chapters. The designed microchip was fabricated using photolithography, soft lithography, oxygen plasma bonding.

## **1.8 Organization of the Thesis in Manuscript-Based Format**

This manuscript-based thesis is organized in six chapters. In the present chapter, a brief introduction about micro electro mechanical systems, bio MEMS, cell cytometry, hydrodynamic focusing in microfluidics, 2D and 3D focusing are reviewed critically. The thesis motivation, the scope and objective of this work are presented. Chapter 2 presents the theory behind the hydrodynamic focusing in microfluidics. Governing equations used in numerical simulation, modeling and model introduction, constants used in simulation, mesh and validation are explained in this chapter.

Chapter 3 and Chapter 4 are duplicated from two journal articles. The chapters are organized in a cohesive manner to address the objectives of the thesis defined in Section 1.11 and formatted according to the “Thesis Preparation and Thesis Examination Regulations (version-2011)” of the School of Graduate Studies at Concordia University. The sections, figures, equations, and tables taken from the duplicated articles are numbered according to the thesis preparation regulations.

Chapter 3 is based on the following article submitted in Journal of Micromechanics and Microengineering (Article ID: RANL-8P2JSR).

Anthony Tony and Sivakumar Narayanswamy, **“A novel three dimensional hydrodynamic focusing design in micro fluidics”**

In this study, three novel designs of microfluidic devices for three dimensional hydrodynamic focusing are presented. Three pairs of laminar sheath flow are used to focus a sample fluidic flow in a micro channel. A pair of sheath flows, each from the bottom and top layers, has been provided to obtain adequate vertical focusing, whereas another pair of sheath flows has been given to achieve final horizontal focusing. Simulation has been performed with COMSOL multiphysics. The three-dimensional hydrodynamic focusing effect has been discussed in the present work. The results show that the efficient, narrow focusing of a stream of sample fluid can be obtained by using these designs. Depending on the ease of fabrication, a final three-dimensional design has been suggested. The present research can be fabricated using a two-layer PDMS microfabrication with oxygen plasma bonding.

Chapter 4 presents the following article submitted in IEEE/ASME Journal of Microelectromechanical Systems (Article ID SCH-JMEMS-2011-0358)

Anthony Tony and Sivakumar Narayanswamy, **“Study of Velocity and Viscosity Parameters Affecting Hydrodynamic Focusing In a Novel 3D Design”**

This paper presents the effect of hydrodynamic focusing caused by the change in velocity and viscosity of the fluid in a novel three-dimensional design. Various iterations of the velocity of the sheath fluid and sample fluid have been simulated to observe the three dimensional focusing effect over the end tip. The best series of velocity conditions has been found for this particular design. The effect of viscosity has been studied by considering different fluids such as diluted glycerol, red blood cells, and deionized water as sample and sheath flow fluids. Simulation has been done using COMSOL multiphysics. The results have been discussed in this work. The fabrication of the discussed design is possible using a simple two layer PDMS fabrication technique.

Chapter 5 presents the preliminary fabrication that has been carried out for the proposed design. The major steps in the fabrication process are presented. Chapter 6 presents the conclusion and summary of the thesis, giving future recommendations. A single comprehensive reference list rather than a reference list of individual papers is presented in the Reference section.

## 2 THEORETICAL DESIGN

### 2.1 Hydrodynamics of Microfluidics

Microfluidics is concentrated on circulating fluid through a channel a few micrometers wide towards the desired objective. For MEMS and Microfluidics, the dynamics of fluids is of primary interest to engineers. Compressible fluids and incompressible fluids are the two principle types dealt with in Microsystems. An incompressible steady state flow under micro channels is considered in this work.

To work with microfluidics one should understand the physics behind microfluidics. Analyzing and handling fluids in micro sized structures and channels are termed microfluidics. Due to the scaling of the dimensions to acquire micro integration the forces and their effects on the microscale need to be examined. Even at higher velocities, the inertial forces are negligible compared to the viscous forces because of the small dimensions in microfluidics.

Z.Wu *et al* (78) studied hydrodynamic interaction in microfluidic continuous cell separation in a microfluidic channel relating to classical fluid mechanics theories. Their paper gives a summary of basic laws, principles and dimensionless numbers. Considering the fluid as a Newtonian fluid that obeys 'F=ma', where 'F' is the force, 'm' is the mass and 'a' is the acceleration, the Navier-Stokes equation is produced by

$$\rho \left( \frac{\partial \vec{U}}{\partial x} + \vec{U} \cdot (\nabla \vec{U}) \right) = -\nabla p + \mu \nabla^2 \vec{U} + F \quad (2.1)$$

Where ‘ $p$ ’ is the static pressure, ‘ $\vec{U}$ ’ is the velocity vector, ‘ $\mu$ ’ is the dynamic viscosity and ‘ $\rho$ ’ is the density of the fluid. The only nonlinear term in this equation is the inertial term ( $\vec{U} \cdot (\nabla \vec{U})$ ). The Stokes equation or the Stokes flow can be calculated by neglecting this. In typical micro fluidic flow, the Reynolds number is much lower than unity (*l & u is much smaller*). Hence the flow can be approximated as creeping flow or Stokes Flow.

$$\rho(\vec{U} \cdot (\nabla \vec{U})) = 0 \quad (2.2)$$

Neglecting the surface forces when the fluid is at a steady state, the resulting flow can be described using

$$0 = -\nabla p + \mu \nabla^2 \vec{U} \quad (2.3)$$

This represents if the flow is reversible and can be predicted precisely.

The dominant effects to be considered (79) during a microfluidic design are the shear stress, Reynolds number, fluidic resistance, diffusion, entrance length, velocity ratio. They are discussed below.

### **2.1.1 Shear stress**

Fluids are aggregations of molecules. Here in the present case the particle size is considered to be much smaller than the channel dimensions. Also a sufficient driving pressure is required to overcome the viscosity and to move the fluid through the channel.

The shear stress  $\tau$ , is given by

$$\tau = \mu \frac{du(y)}{dy} \quad (2.4)$$

where,  $\mu$  = dynamic viscosity of the fluid and  $u(y)$  = velocity of fluid at a distance ‘ $y$ ’ from the stationary state at the bottom plate.

Depending on the Reynolds number, the fluid flow can be classified as a turbulent or laminar flow. In most of the cases in microfluidics, due to the small dimensions ( $10^{-6}$  scale), the flow is laminar ( $Re < 1000$  for incompressible and  $Re < 10 \cdot 100$  for compressible fluids).

### 2.1.2 Reynolds Number

The ratio between the inertial force and the viscous force is termed as the Reynolds number ( $Re$ ). It can be used to judge whether the dominant force is the inertial force or the viscous force.

$$Re = \frac{\rho u D}{\mu} = \frac{u D}{\nu} \quad (2.5)$$

where ‘ $u$ ’ is the fluid flow velocity, ‘ $D$ ’ is the hydraulic diameter of the channel, and ‘ $\nu$ ’ is the kinematic viscosity of the fluid. When the Reynolds number is low, the viscous interaction between the fluid and the wall is much stronger, and hence there is no turbulence or vortices. When a particle (cells) is suspended in the fluid, due to the influence of the fluid’s Reynolds number, there will be a viscous force and an inertial force transfer to the particle, giving

$$Re_p = Re \frac{D_p^2}{D^2} = \frac{u D_p^2}{D \nu} \quad (2.6)$$

Where ' $Re_p$ ' is the Particle Reynolds number, ' $Re$ ' is the flow Reynolds number, and ' $D_p$ ' is the diameter of the particle.

### **2.1.3 Laminar flow**

Most flows in nature can be characterized as turbulent flows since the fluid particles move in irregular regimes. In a laminar flow, the velocity of the particle in the fluid is not a random function of time. Fluid particles move along smooth paths in layers without mixing in laminar flow. If the Reynolds number is much less than 1, the laminar flow in microfluidics can be classified as a Stokes flow due to the high viscous effects.

### **2.1.4 Péclet number**

Because of the low dimensions of the channels in the microfluidics, the flow will have a low Reynolds number and hence will be laminar. Mixing happens only with respect to diffusion. The *Péclet number* provides a relation between the average velocities of the fluid flow, the width of the channel and the diffusion coefficient of the particles.

$$Pe = \frac{U_0 w}{D} \cong \frac{z}{w} \quad (2.7)$$

where,  $U_0$  is the average velocity of the fluid flow,  $w$  is the width of the channel, and  $D$  is the diffusion coefficient of the particle.

### **2.1.5 Diffusion**

The random motion of the molecules from higher concentration to lower concentration is termed diffusion, whereas the movement of the molecules within the fluids is termed convection. Fick's first law is used to relate a diffusive flux to the concentration. In



microfluidics, diffusion is the dominant particle transport mechanism over short distances and long time scales and is calculated as

$$J = -D \frac{dC}{dx} \quad (2.8)$$

where  $J$  is the diffusion flux of the particles in  $mol/m^2s$ ,  $D$  is the diffusivity or the diffusion coefficient in  $m^2/s$ ,  $C$  is the concentration in  $mol/m^3$  and  $x$  is the distance in meters. A one dimensional model of diffusion can be stated as

$$d^2 = 2Dt \quad (2.9)$$

where  $d$  is the distance a particle moves in time  $t$ .

### **2.1.6 Dean Number**

When the fluid flows along a curved channel the inertial force becomes apparent due to the increase in the Reynolds number, as the wall force changes the flow direction of the fluid, leading to an increase in the centrifugal force. This creates a vertical secondary flow with respect to the primary flow. This secondary acceleration is termed as the Dean number.

$$De = Re \sqrt{\frac{D}{r}} \quad (2.10)$$

where 'De' is the dean number, 'Re' is the flow Reynolds number, 'D' is the hydraulic diameter of the channel, and 'r' is the curved channel radius.

### 2.1.7 Entrance Length

Several factors must be considered, when designing a microfluidic focusing device. To achieve a precise control over a focused stream is important in flow cytometers. The width of the focused stream should be of the order of the cell size to get accurate features in cell sorting and counting. While designing a microfluidic channel for hydrodynamic focusing, we should consider the establishment of flow with respect to entrance length.

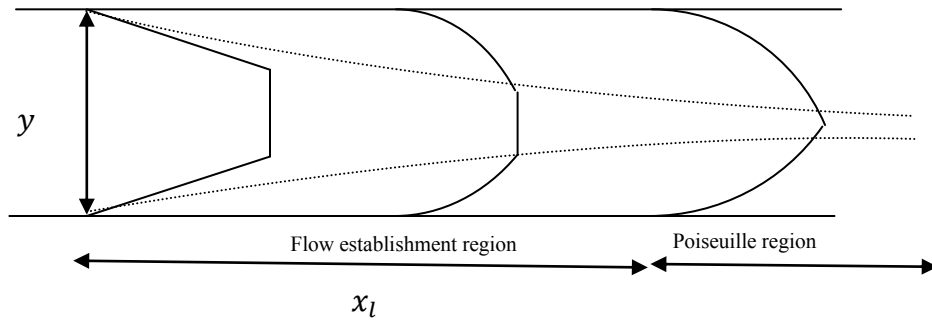


Figure 2.1: Flow establishment region and fully developed region in a fluid flow

When the fluid enters a channel, it could be classified into two regions: a flow establishment region and a fully developed region, as shown in Figure 2.1. Assume a channel with  $y$  as the width and  $x_l$  as the length of the flow establishment region. By using the Blasius layer correlation, an equation to determine hydrodynamic entrance length has been postulated by Sparrow and Schlichting (8).

$$\frac{x_l}{y} = 0.04 Re \quad (2.11)$$

Using Equation 2.11, a fluid flowing with a  $Re$  of 1 through a  $100\mu m$  channel width gives an established flow after 4 to 5  $\mu m$  in length.

### 2.1.8 Velocity Ratio

Another important factor that needs to be considered is the hydrodynamic focusing effect inside the rectangular channel (61). Consider a symmetric rectangular channel as shown in Figure 2.1, with a Newtonian fluid flow. Assuming steady and laminar flows for both the sample and sheath flows with the same density; the law of the conservation of mass states that the amount of fluid entering is the same as the amount being discharged.

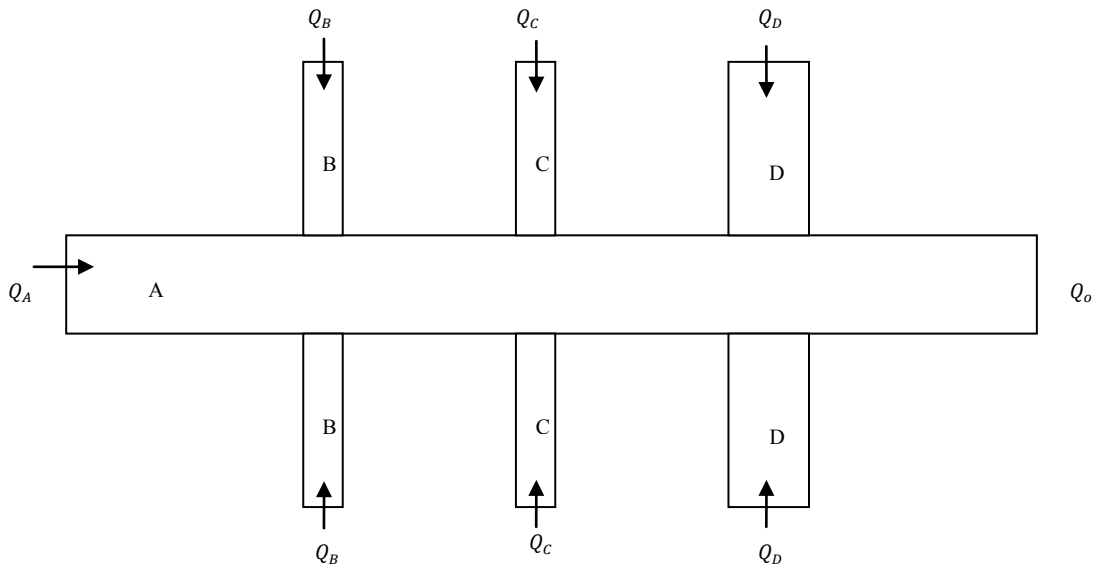


Figure 2.2: A symmetric rectangular channel with flow rates for velocity ratio

Assume that the sample is driven with a flow rate of  $Q_A$  through Channel A with a width  $w$  and a height  $h$  respectively. Three pairs of sheath flows applied sideways as shown in the figure through Channels B, C and D with a width  $w_B, w_C, w_D$  respectively. The corresponding heights are  $h_B, h_C, h_D (= h)$  respectively.

Let  $Q_o$  be the final discharge flow rate through  $w \times h$ . Applying the law of the conservation of mass gives

$$Q_A + 2Q_B + 2Q_C + 2Q_D = Q_o \quad (2.12)$$

where the flow rate can be calculated as

$$Q = w \times h \times v \quad (2.13)$$

Assume that the amount of sample entering is completely focused into a narrow stream using the sheath flows, thereby giving the corresponding width and height of the focused stream as  $w_f$  and  $h_f$  respectively.

$$Q_A = w_f \times h_f \times v_f \quad (2.14)$$

Also

$$Q_o = w \times h \times v_o \quad (2.15)$$

giving

$$\frac{w_f}{w} = \frac{v_o h Q_A}{v_f h_f Q_o} \quad (2.16)$$

The average velocity of the outlet of the rectangle channel can be found using the Poiseuille velocity profile in Equation 2.17 (61).

$$u(y) = \frac{1}{h} \int_{-h/2}^{h/2} u(y, z) dz = \frac{8h^2}{\mu \pi^4} \left( -\frac{dp}{dx} \right) \sum_{n=0}^{\infty} \frac{1}{(2n+1)^4} \times \left[ 1 - \frac{\cosh \left[ \frac{(2n+1)\pi y}{h} \right]}{\cosh \left[ \frac{(2n+1)\pi w}{2h} \right]} \right] \quad (2.17)$$

Also, the fluid velocity ratio can be determined by using the Equation 2.18. (61). By using the Equation 2.16 and 2.18 it is possible to find the velocity and width of the focused stream.

$$\frac{v_f}{v_o} = \frac{\frac{2}{w_f} \int_0^{w_f/2} u(y) dy}{\frac{2}{w} \int_0^{w/2} u(y) dy} = \frac{\left\{1 - \left(\frac{192h}{\pi^5 w_f}\right) \sum_{n=0}^{\infty} \frac{1}{(2n+1)^5} \frac{\sinh[(2n+1)\pi w_f/2h]}{\cosh[(2n+1)\pi w/2h]}\right\}}{\left\{1 - \left(\frac{192h}{\pi^5 w}\right) \sum_{n=0}^{\infty} \frac{\tanh[(2n+1)\pi w/2h]}{(2n+1)^5}\right\}} \quad (2.18)$$

### 2.1.9 Fluidic resistance

The flow rate across the microchannel can be restructured using a fluidic resistance equation.

$$Q = \frac{\Delta p}{R} \quad (2.19)$$

Where  $\Delta p$  is the pressure drop across the channel,  $R$  is the resistance offered by the channel, and  $Q$  is the flow rate across the channel. The resistance offered by a circular, rectangular channel has been studied and discussed in (80). For a rectangular channel with a height approximately equal to the width of the channel, the resistance is given in Equation 2.21.

$$R = \frac{12\mu L}{wh^3} \left\{1 - \frac{h}{w} \left(\frac{192}{\pi^5} \sum_{n=1,2,3,5}^{\infty} \frac{1}{n^5} \tanh h \left(\frac{n\pi w}{2h}\right)\right)\right\} \quad (2.21)$$

### 2.1.10 Surface tension

In environments with micro dimensions, surface tension dominates over other forces. Surface tension can be described approximately by Equation 2.23

$$\gamma = \frac{U}{\delta^2} \quad (2.23)$$

where  $\gamma$  is the surface tension,  $U$  is the average total cohesive energy of a molecule, and  $\delta$  is the characteristic dimension of a molecule and  $\delta^2$  is the surface area of a molecule. Let  $S$  be the total surface of an interface, and then the total energy stored in the interface is  $E$ ,

$$E = \gamma.S \quad (2.24)$$

Surface tension is given in units of  $J/m^2 = N/m$ , and is usually given in  $mN/m$ .

All the above properties make the microfluidic platform ideal for cell cytometry. Detailed studies of fluid flow in microfluidics, cell culture models, biomaterials, microfluidic platforms for single cell analysis, protein crystallization, etc., have been presented in the literature (80-85). In addition, very large surface to volume ratios in microdevices are advantageous in incorporating cell culture for biological studies. A highly efficient mass transport of gases through diffusion and rapid heat dissipation can be obtained when working in microscale.

## 2.2 Single Phase Flow in Microfluidics

Consider two stationary infinite parallel plates separated by a distance 'h' as shown in Figure 2.3. Since the gap between the two plates is very small, the velocity in the Y direction is negligible. The velocity  $w$  is zero, and there is no variation of properties along the Z axis. A Continuity Equation can be derived as Equation 2.25, which gives  $u$  as a function of  $y$   $\{f(y)\}$  only.

$$\frac{\partial u}{\partial y} = 0; \Rightarrow u = f(y) \quad 2.25$$

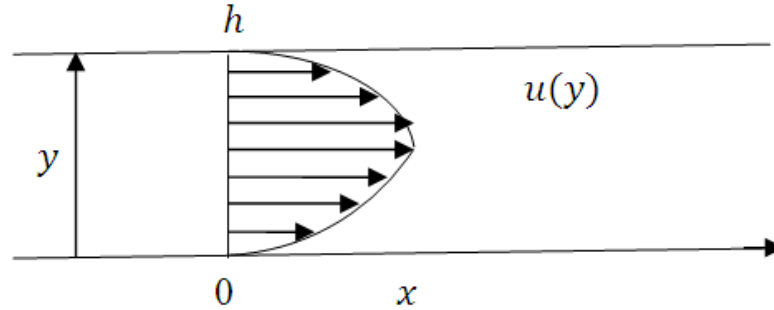


Figure 2.3: Single Phase Poiseuille Flow in Microfluidics

The above equation suggests that the velocity does not vary in the X direction. The X-Momentum and Y-Momentum can be derived as Equations 2.26 and 2.27.

$$\frac{\partial p}{\partial x} = \mu \frac{\partial^2 u}{\partial y^2} \quad (2.26)$$

$$\frac{\partial p}{\partial y} = 0; \Rightarrow p = f(x) \quad (2.27)$$

Which gives,  $p = f(x)$  only

Equations (2.25, 2.26, and 2.27) give

$$\frac{dp}{dx} = \mu \frac{d^2 u}{dy^2} = C_0 \quad (2.28)$$

From Figure 2.3, the maximum velocity condition is at the center of the plate. Applying these boundary conditions,  $u = 0$  at  $y = 0$  and  $u = 0$  at  $y = h$  gives

$$u(y) = \frac{1}{2\mu} C_0 y(y - h) \quad (2.29)$$

Also

$$\frac{dp}{dx} = -\frac{\Delta p}{L}$$

Substituting in Equations 2.28 and 2.29 gives,

$$u(y) = \frac{1}{2\mu} \frac{\Delta p}{L} y(h - y) \quad (2.30)$$

And the flow rate can be determined by using the Equation 2.31,

$$Q = \int_0^h \frac{1}{2\mu} \frac{\Delta p}{L} y(h - y) dy = \frac{1}{12\mu} \frac{\Delta p}{L} h^3 \quad (2.31)$$

## 2.3 Numerical Simulation

Numerical simulation is done using basic governing equations for the fluid flow as stated in details below.

### 2.3.1 Governing Equations

Considering conservation of mass, energy and momentum gives, continuity and Navier-Stokes Equation as explained below.

#### 2.3.1.1 Continuity Equation

Fluid flow can be modeled using continuity and momentum equations as explained below. Considering a fluid flow through a channel, conservation of mass gives the Continuity Equation 2.32.

$$\nabla \cdot \vec{U} = 0 \quad (2.32)$$

$$\vec{U} = ui + vj + wk$$

$$\nabla = i \frac{\partial}{\partial x} + j \frac{\partial}{\partial y} + k \frac{\partial}{\partial z}$$



Where  $\vec{U}$  is the velocity vector in x, y, z axis, which states that, the divergence of velocity field is zero throughout.

### 2.3.1.2 Navier-Stokes Equation

Considering,  $p$  = static pressure,  $\vec{U}$  = velocity vector,  $\mu$  = Absolute viscosity, and  $\rho$  = Density of the fluid, Navier-Stokes Equation is given can be derived as Equation 2.33

$$\rho \left( \frac{\partial \vec{U}}{\partial x} + \vec{U} \cdot (\nabla \vec{U}) \right) = -\nabla p + \mu \nabla^2 \vec{U} + F \quad (2.33)$$

### 2.3.1.3 Stokes Flow

Due to the small dimensions  $10^{-6}$  scale, in micro fluidics the inertia term dominates even though the velocity is much higher. In a typical micro fluidic flow, the Reynolds number is much lower than unity ( $l$  &  $u$  is much smaller), hence the flow can be approximated as a creeping flow or a Stokes Flow.

$$\rho \left( \vec{U} \cdot (\nabla \vec{U}) \right) = 0 \quad (2.34)$$

We can neglect the surface forces when the fluid is at a steady state. The resulting flow can be described using the following equation:

$$0 = -\nabla p + \mu \nabla^2 \vec{U} \quad (2.35)$$

This represents the flow as reversible and can be predicted precisely.

### 2.3.1.4 The Reynolds Number:

$$Re = \frac{\rho u D}{\mu} = \frac{u D}{\nu} \quad (2.36)$$

where  $u$ = fluid flow velocity,  $D$ = hydraulic diameter,  $\nu$  = kinematic viscosity of the fluid

At a low  $Re$ , the viscous interaction between the fluid and wall is much stronger; hence there is no turbulence or vortices.

### **2.3.2 Modeling**

Computational fluid dynamics (CFD) is an essential tool in fluid flow simulation between two different fluids or fluid structure interactions. Highly precise results can be achieved in fluid flow simulations such as the heat transfer, fluid structure interactions, mixing, pressure velocity viscosity variations, etc. All the complex and partial differential equations can be easily computed and solved with the help of CFD tools. COMSOL Multiphysics is a CFD tool used in designing and modeling MEMS structures. In systems like micro actuators, gyroscopes, sensors, resonators, reactors, mixers, the fluid flow can be simulated easily with the aid of COMSOL. It is possible to simulate a simple 2D model as well as complex 3D structures depending on the need. In the present research, three sets of novel three dimensional microfluidic designs for hydrodynamic focusing have been modeled and simulated.

### **2.3.3 Model Introduction**

Three-dimensional designs have been drawn using the same software. First, a 2D model was created and extruded to create a 3D design. From the theory and governing equations discussed previously, the following modules from COMSOL were chosen for simulation. Under the Model library in the MEMS module, the Stokes flow and the Convection and diffusion module were chosen for this work.

### 2.3.3.1 Stokes Flow Equations

The steady state equation for the Stokes flow in the MEMS module was chosen to observe the fluid flow and interaction in the microfluidic design. Because a low Re flow was under consideration, the Stokes flow equations were chosen. The Stokes flow equations from the COMSOL database are similar to equation (2.33) with a difference of identity matrix for iteration.

$$\rho \frac{\partial u}{\partial t} - \nabla \cdot [-pI + \eta\{\nabla u + (\nabla u)^T\}] = F \quad (2.37)$$

where  $\nabla u=0$ , and  $\rho$  is the fluid density in  $\text{kg/m}^3$ ,  $u$  represents the velocity vector in  $\text{m/s}$ ,  $p$  equals the pressure in Pa,  $\eta$  denotes the dynamic viscosity in  $\text{Pa}\cdot\text{s}$ ,  $F$  is a body force term in  $\text{N/m}^3$ , and  $I$  is the identity matrix.

### 2.3.3.2 Convection and Diffusion Equation

A steady-state equation for convection and diffusion under MEMS module was used to observe the amount of species concentration present in the particular section of the design.

The convection and diffusion equation from the COMSOL database is

$$\frac{\partial c_i}{\partial t} + \nabla \cdot (-D_i \nabla c_i + c_i u) = R_i \quad (2.38)$$

where  $c_i$  is the concentration of species  $i$  ( $\text{mol/m}^3$ ),  $D_i$  denotes its diffusion coefficient ( $\text{m}^2/\text{s}$ ),  $u$  refers to the velocity ( $\text{m/s}$ ), and  $R_i$  denotes the reaction term ( $\text{mol}/(\text{m}^3\cdot\text{s})$ ). The velocity can be expressed analytically or can be obtained by coupling a microfluidics

application mode that models the momentum balance to the Convection and Diffusion application mode.

#### 2.3.4 Constants

It is possible to create a constants library in COMSOL multiphysics for easy usage and accessibility. Certain terms and constants used in the present work are described in Table 7.1.

rho1	density of sample fluid in $\text{kg/m}^3$
eta1	viscosity of sample fluid in $\text{Pa}\cdot\text{s}$
rho2	density of sheath fluid in $\text{kg/m}^3$
eta2	viscosity of sheath fluid in $\text{Pa}\cdot\text{s}$
c0	input concentration in $\text{mol/m}^3$
D <sub>i</sub>	isotropic diffusion coefficient in $\text{m}^2/\text{s}$

Table 2.1: Constants used in numerical simulation using COMSOL multi physics.

#### 2.3.5 Mesh and Validation

The simulation was run in an Intel(R) Core(TM) 2 CPU 6300 Processor, 1.86GHz, with the help of 8GB Ram memory in Windows 7. Normal Meshing with triangular grid was chosen with the longest refinement method. Other parameters and values during meshing are given in Table 2.2.

Maximum element size scaling factor	1
Element group rate	1.6
Mesh curvature factor	0.6
Mesh curvature cut off	0.03
Resolution of narrow regions	0.5

Table 2.2: Meshing parameters

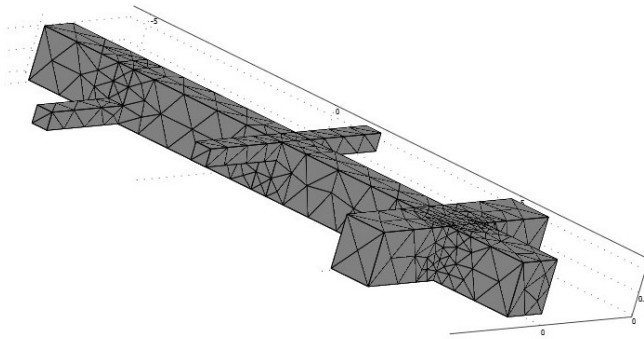


Figure 2.4: Geometry with a triangular mesh

Figure 2.4 shows the geometry with a normal triangular mesh. Mesh elements generated for this particular design is stated in Table 2.3. Mesh element is high in extra fine, which will make the simulation lengthy. In this work simulation is run as normal meshing with triangular grid.

Mesh	Extra fine	Normal	Coarse
No of mesh element	7575	1923	824

Table 2.3: Different mesh elements on different meshing

### 2.3.6 Model Validation

The model has been generated using the parameters discussed in previous section and simulations were performed and results discussed in the following chapter. Prior to performing simulations using COSMOL Multiphysics on the proposed designs, the model was validated by performing the design simulation based on the work that has been published (69). Their particular design was chosen for model verification considering the fact that the designs proposed in this study can be modified to perform the simulations. The comparison of the microfluidic hydrodynamic focusing device proposed in this thesis and the device presented in (69) are shown in Table 2.4.

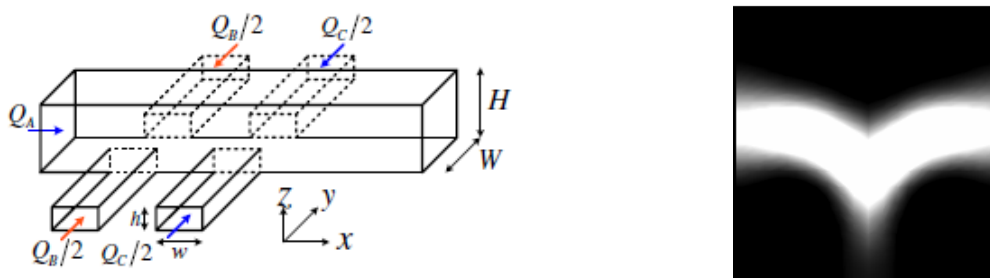


Figure 2.5: (a) Channel A, B, C of (69) showing corresponding flow rate. (b) Numerical images of the cross-sectional profiles of the vertical focused stream in the main channel from (69) with  $H/W = 1.2$ ,  $H/h = 12$ , the flow rate ratio  $\alpha v = 1.0$ ,  $Re = 1.0$ , at a distance

Parameter	In the present work	In Reference(69)
Main Channel dimensions	Channel A of 120 $\mu$ m in width(W) and 120 $\mu$ m in height(H)	No dimensions for Channel A only H/W ratio of 1.2
Side Channel dimensions	Channel B & C of 40 $\mu$ m in width (w) and 10 $\mu$ m in height (h). Where channel B is for the sample flow and channel C is for sheath fluid flow.	No dimensions for Channels B & C except H/h ratio of 12
H/h	12	12
H/W	1.0	1.2
Velocity	Since only the flow ratio is given, different velocity situations have been simulated as shown in table below	Velocity or flow rate in the simulation is not given except the flow ratio $\alpha_v$ is 1
$\alpha_v$	Ratio of flow rates of Sample ( $Q_B$ ) and sheath ( $Q_A, Q_C$ ) 1.0	1.0

Table 2.4: Comparison between (69) and the current work.

Figure 2.5a, shows the 3D schematic of the previous work, with A as main channel, B,C and D as the side channels. Sample fluid flow is given through channel B for focusing. While several design variations with respect to H/W ratio have been provided in their work, the Figure 2.5b showing one of their results has been used for the validation of the

simulation procedure performed in this work. No dimensions for Channels A, B or C is given except H/W ratio of 1.2 and H/h ratio of 12. Figure 2.5b shows the result from (69) with  $\alpha_v$  as 1.0, H/W as 1.2 and H/h as 12. The reason for selecting this particular output concentration profile is that the H/W of 1.2 is similar to the proposed design with an H/W =1 and H/h can be easily varied. While in the present work the H/h ratio is expected to be 2, for the validation, the h has been reduced to  $10\mu\text{m}$  to get the H/h ratio of 12 and the Channels B and C have been positioned along the main channel similar to the work in reference. Certain assumptions have been made while designing and the model has been generated for simulation.

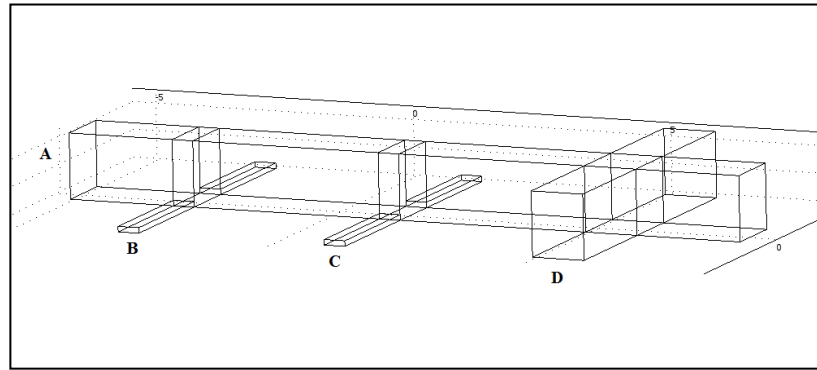


Figure 2.6: Design generated for model validation

Figure 2.6 shows the design generated for model validation. Channel A of  $120\mu\text{m}$  in width and height, channel B and C of  $40\mu\text{m}$  in width and  $10\mu\text{m}$  in height has been designed to maintain the H/W as 1.0 and H/h as 12. Moreover, in their work, the distance between channels B and C are not mentioned, so the distance of  $340\mu\text{m}$  has been assumed here for validation and the Reynolds number  $\ll$  unity. Since the result shown in figure 1b has been obtained for a flow ratio between sample and sheath fluids as 1, and



the flow rates of sample and sheaths were not given, the simulation has been performed here with various velocity conditions by keeping flow ratio  $\alpha_v$  as 1, and the results are shown in Table 2.5.

#	$V_A$	$V_B$	$V_C$	$V_D$	Slice view at 100 $\mu\text{m}$ downstream of Channel C as per ref (ref)
	$\mu\text{m}/\text{sec}$				
1	10	360	360	10	
2	17	600	600	10	
3	35	1200	1200	10	
4	50	1800	1800	10	
5	10 0	3600	3600	10	
6	20 0	7200	7200	10	

Table 2.5: Different velocity iterations used by making  $\alpha_v$  as 1.0

In the current work, since the sample and sheath fluid channels are of varying dimensions, flow rates  $Q_B$  and  $Q_A$  are made constant as 1, by varying the corresponding velocities  $V_B$  and  $V_A$ . Consider a sheath flow of  $50\mu\text{m}/\text{sec}$  in velocity through channel A, the flow rate corresponds to  $Q_A$  will be of  $720000\ \mu\text{m}^3/\text{sec}$ . Keeping  $Q_A = Q_B$  gives the velocity  $V_B$  of  $1800\mu\text{m}/\text{sec}$ . Since the channel dimensions of B and C are same, corresponding velocities  $V_B$  and  $V_C$  will be also the same so that the flow ratio remains unity.

The results from simulation shows that when the  $V_A < 17\mu\text{m}/\text{sec}$ , the results are scattered whereas when  $V_A > 100\mu\text{m}/\text{sec}$ , mixing started to occur. An efficient result similar to the published work has been obtained when  $V_A$  is taken as  $35\mu\text{m}/\text{sec}$  and  $50\mu\text{m}/\text{sec}$  as shown in rows 3 & 4 of Table 2.5. The results presented with  $V_A$  as  $35\mu\text{m}/\text{sec}$  and  $50\mu\text{m}/\text{sec}$  show good agreement with the result from the literature. While in the general sense the results are comparable, particular variation is seen in the concentration at the top portion of the channel cross section, and general smoothness of transition between sample and sheath flows. These variations are attributed to the following:

- a) Distance along Channel A between channels B and C have not been disclosed in the publication by the researchers. To perform the verification this distance was assumed to be  $340\mu\text{m}$  which is similar to the distance in the proposed design, explained in the following chapter.
- b) While the H/W ratio of 1.2 is used in the literature, the model here was performed with a H/W ratio of 1. The increase in height provides sufficient room for the sheath fluid at the top of the section as shown in figure 1b, whereas that is not possible in the proposed model. The sheath fluid layer starts forming at the top of the channel

A, when the velocity is increased beyond  $50\mu\text{m}/\text{sec}$  but beyond this value the velocity is too high for the channel dimensions that the fluids starts to mix.

- c) In the work done by CC Chang *et. al.*, the simulation has performed in CFD whereas; in this work the simulation has been performed with COMSOL.

## **2.4 Summary**

Taking into account the theory behind hydrodynamics and microfluidics, the properties of the fluid for the sample and sheath flows were chosen. Based on the governing equations, certain modules were selected from COMSOL for simulation. Validation of COMSOL model has been done in comparison with the previous published work. A design should be generated and boundary conditions should be set for the simulation, which is discussed in the next chapter.

### **3 A NOVEL THREE DIMENSIONAL HYDRODYNAMIC FOCUSING DESIGN IN MICRO FLUIDICS**

This chapter is based on the article submitted in Journal of Micromechanics and Microengineering (Article ID: RANL-8P2JSR).

#### **3.1 Introduction:**

Hydrodynamic focusing is effective in a wide variety of applications such as on-chip flow cytometry for cell/particle counting and sorting (49-52), single-molecule detection and measurement(53), diffusion based mixtures and laminar mixers(54,55), microfluidic optical waveguides(56), cell patterning(57), fluorescent light sources(58), surface chemical patterning(59,60), flow switches for continuous sample injection(61), microchemical synthesis(62,63) , and production of microparticles(64), micro-droplets and bubbles(65). In general, hydrodynamic focusing provides an effective means of controlling fluid flow along microchannels, based on the applied pressure and the channel width. In particular, using hydrodynamics small quantities of particles can be precisely positioned in micro/nano channels.

Though the objective of focusing is to align the micro particle to the center, it will also help to reduce the interaction between the sample and the channel walls. While working with microfluidic systems, manipulating fluid flow in microchannels is a highly important issue in the design. In 2D focusing it is not necessary for the micro particles in the sample fluid to pass through the focused stream one by one, even if the width of the focused stream is same as that of the particle size. It is mainly due to the channel depth where in 2D focusing it is not balanced. For single molecule detection, the sample

should pass through a minute optical detection region much smaller than the size of the channel. The vertical spread of the sample results in a large number of undetected molecules. The other important criterion is that, even if the particles are horizontally focused, they may still interact with the bottom and top walls. Hence in single molecule detection and sorting, such as flow cytometry, the sample flow is centered using an additional pair of sheath flow in the vertical direction, thereby providing 3D hydrodynamic focusing. This is especially advantageous in managing proteins against adsorbing and sticking to the walls.

### **3.2 Literature Review**

The main criteria in focusing the particles to be analyzed in the microfluidic channel are the miniaturization of fluid-handling components and the miniaturization of the analyzing methods such as optics, and integration. The sample solution containing micro particles of research interest should be passed through a micro channel and should be aligned to the center for analysis. Focusing or aligning of these particles is achieved by using different methods such as, Integrated Funnel Aligner & cell trap, Narrowing channel section, Electrokinetic focusing, Dielectrophoresis focusing and Hydrodynamic focusing(86,87). An optical trap using an applied light field can be used to arrange, guide or deflect particles inside a geometry(39). Another study shows the focusing of microparticles in a microfluidic channel with standing surface acoustic waves(41). While various focusing techniques mentioned above have been developed over the past few years, only Dielectrophoresis, Electrokinetic and hydrodynamic focusing provide the ability for 3D focusing. The main disadvantages of electrophoresis and electrokinetic focusing and sorting is that electrostatic field has been proved to damage the cell

membrane(47), which make Hydrodynamic focusing advantageous in cell cytometry, where 3D focusing is essential.

*Three dimensional hydrodynamic focusing* – Flow cytometry is a technique in which cells are analyzed and sorted depending on their cellular properties. The main principle behind the flow cytometer is the focusing effect of a center flow, surrounded by two sheath flows using hydrodynamic effect. The width of the center cell flow will be reduced such that only one cell is permitted to be positioned at the center which makes detection and sorting easy. Since the integration of cell cytometry and microfluidics, the focusing has been done on the two dimensional scale only (48). Many Two dimensional focusing devices based on hydrodynamic and electrososmotic flow have been reported in the literature (3-5,18,42,43). In this work we will concentrate on three dimensional hydrodynamic focusing techniques evolved recently and we will also suggest a novel design of PDMS microfluidic device using MEMS technology.

The first 3D focusing method was proposed and fabricated for cells in a pressure-driven micro cell sorter by Goranovic *et al* (66). A chimney like structure for single-step coaxial sheathing was modeled and optimized through simulation. Micromachined silicon fabrication is used. Sundararajan *et al* (67) studied three novel 3D hydrodynamic focusing designs and simulated with different variations. R Yanga *et al* (68), developed a three-dimensional polymer hydro-focusing. A sloped microstructure for coaxial sheathing was designed, microfabricated by means of SU-83D lithography and tested. A slight slanting is given in the bottom part during the fabrication, producing the vertical focusing. The horizontal focusing had been done by two coaxial sheath flows from the sides. This allows the cells to flow in the core stream with an almost uniform velocity. This method

also requires complex geometric calculation. For all the stated methods the structural design was also found to be inefficient. But the main disadvantage was the complex design, which required a quite complicated silicon based fabrication process.

C. C.Chang *et al*(69) first developed a three-dimensional hydrodynamic focusing device using two-layer polydimethylsiloxane (PDMS) microchannels. There are four inlet ports and one outlet port for the fluid flow driven by a syringe pump. The 3D focusing device using PDMS micromolding techniques is fabricated, and a comparison is made with a 2D device in terms of focusing and structure. An optimal three-dimensional focusing technique for micro-flow cytometers was suggested by C.H. Tsai(70), using hydrodynamic focusing on a microstructure. A micro-weir structure, which was positioned directly beneath an optical detection system, was fabricated.

The sample stream is focused in the vertical direction by using a second pair of sheath flows capable of achieving a focused sample stream width of between 6 and 15 $\mu$ m. In this approach, the sample stream is focused initially in the horizontal plane using two sheath flows and is then focused in the vertical direction using a second set of sheath flows and a micro-weir structure.

Most of the work shows that sample flow actually was focused on the region near the bottom wall rather the center. A novel two-layer microchannel structure to enable three-dimensional (3D) hydrodynamic focusing over a wide range of Reynolds numbers ( $Re$ ) has been suggested by G. S. Zhuang *et al* (71) by keeping the flow rate constant in all the inlet channels  $QA = QB = QC = QD = 576\mu\text{l/hr}$  in the microfabricated structure.

D. S. Kim *et al* (48) developed an efficient 3-dimensional hydrodynamic focusing microfluidic device (3D-HFMD). In their work, vertical focusing of the core sample flow is achieved in the pressure-driven flow owing to a locally increased aspect ratio even below the global aspect ratio of 0.5 without any horizontal separation wall after a simple horizontal focusing.

For most 3D hydrodynamic focusing devices developed so far, 3D focusing is achieved via compressing the center cell flow with sheath flows from both the horizontal and vertical directions. In order to do so, 3D multi-layer structures are needed to introduce the vertical sheath flows from the out-of-the-plane directions. The complex multilayer fabrication of these devices compromises the advantages of microfluidics and makes it virtually impossible to produce these devices massively. Xiaole Mao *et al* (53,73,74) have suggested a novel three-dimensional hydrodynamic focusing with a single-layer planar microfluidic device using Microfluidic drifting. By utilizing the viscous drag of Dean flow induced in a curved microfluidic channel, they showed that it is possible to achieve 3D hydrodynamic focusing in a single layer planar microfluidic device.

In the present work, a novel three-dimensional design for hydrodynamic focusing has been studied, simulated, and proposed. Bio-compatible materials for microfluidic systems lead to the application of polydimethylsiloxane (PDMS) for biological studies. Properties of PDMS are best suited for miniaturized biological studies<sup>40</sup>. Easy fabrication and methods for controlling fluid flow in microchannels make it attractive and an effective platform in MEMS.



### 3.3 Theoretical Design Considerations

There are several factors to be considered, when designing a microfluidic focusing device. To achieve precise control over the focused stream is important in flow cytometers. The width of the focused stream should be on the order of the cell size to get accurate features in cell sorting and counting. While designing a microfluidic channel for hydrodynamic focusing we should consider the establishment of flow with respect to the entrance length.

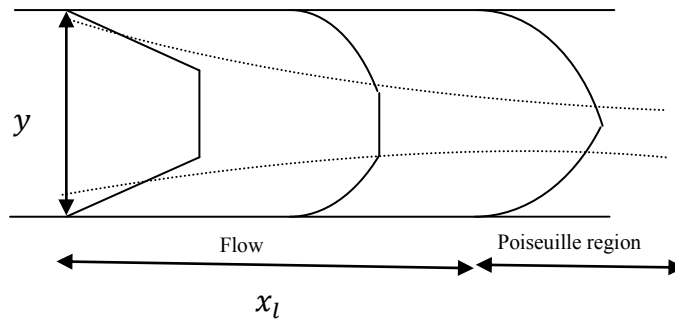


Figure 3.1: Flow establishment region and fully developed region in a fluid flow

When the fluid enters a channel, we classify it into two regions: The flow establishment region and the fully developed region as shown in Figure 3.1. Consider a channel that is  $y$  space in width, and let  $x_l$  be the length of its flow establishment region. By using Blasius layer correlation an equation to determine hydrodynamic entrance length has been postulated by Sparrow and Schlichting (8).

$$\frac{x_l}{y} = 0.04 Re \quad (3.1)$$

Fluid flowing with a Reynolds number of 1 through a  $100\mu m$  channel width gives an established flow beginning after 4 to 5  $\mu m$  of length by using this equation. Another important factor to consider is the hydrodynamic focusing effect inside the rectangular channel(61). Consider a symmetric rectangular channel as shown in Figure 3.2 below, with Newtonian fluid flow. Assuming that both the sample and the sheath flows have the same density and that the flow is steady and laminar, the law of the conservation of mass states that the amount of fluid entering is the same as the amount egressing.

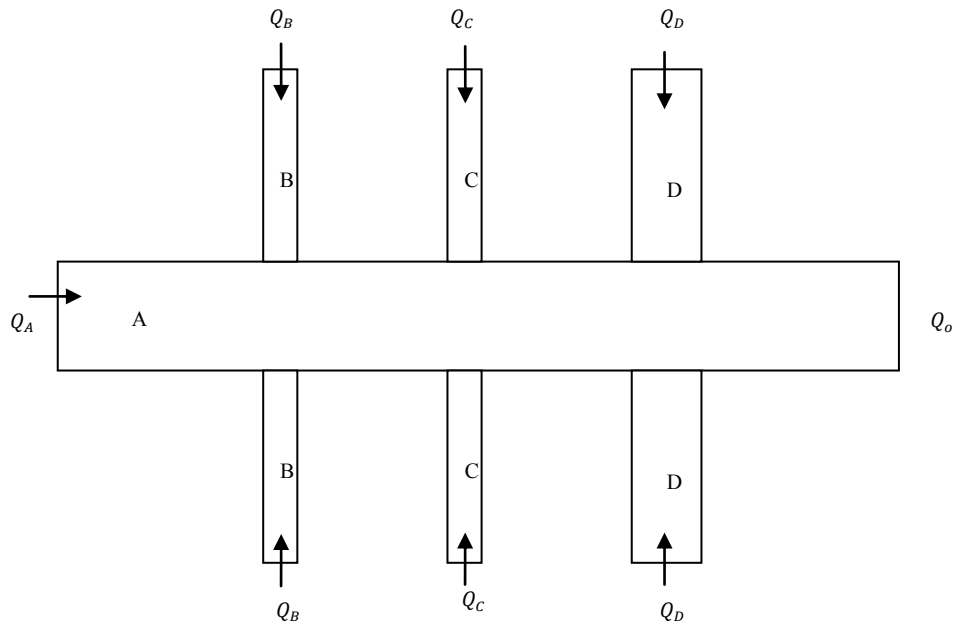


Figure 3.2: Symmetric rectangular channel with flow rates for velocity ratio

Let the sample be driven with a flow rate of  $Q_A$  through Channel A with width  $w$  and height  $h$  respectively with a velocity of  $v$ . Three pairs of sheath flow are applied

sideways, through Channels B, C and D with width  $x$ , and height equaling  $w_B \times h_B$ ,  $w_C \times h_C$ ,  $w_D \times h_D$ , respectively.

Let  $Q_o$  be the final discharge flow rate at the exit. Applying the conservation of mass gives

$$Q_A + 2Q_B + 2Q_C + 2Q_D = Q_o \quad (3.2)$$

where flow rate

$$Q = w \times h \times v \quad (3.3)$$

Let us assume that the amount of the sample entering is completely focused into a narrow stream using the sheath flows. Then the corresponding width and height of the focused stream will be  $w_f$  and  $h_f$ , respectively.

$$Q_A = w_f \times h_f \times v_f \quad (3.4)$$

Also

$$Q_o = w \times h \times v_o \quad (3.5)$$

This gives

$$\frac{w_f}{w} = \frac{v_o h Q_A}{v_f h_f Q_o} \quad (3.6)$$

The average velocity of the outlet of the rectangle channel can be found out using Poiseuille velocity profile which is (61).

$$u(y) = \frac{1}{h} \int_{-h/2}^{h/2} u(y, z) dz = \frac{8h^2}{\mu\pi^4} \left( -\frac{dp}{dx} \right) \sum_{n=0}^{\infty} \frac{1}{(2n+1)^4} \times \left[ 1 - \frac{\cosh \left[ \frac{(2n+1)\pi y}{h} \right]}{\cosh \left[ \frac{(2n+1)\pi w}{2h} \right]} \right] \quad (3.7)$$

The velocity ratio can be found out using (61).

$$\frac{v_f}{v_o} = \frac{\frac{2}{w_f} \int_0^{w_f/2} u(y) dy}{\frac{2}{w} \int_0^{w/2} u(y) dy} = \frac{\left\{ 1 - \left( \frac{192h}{\pi^5 w_f} \right) \sum_{n=0}^{\infty} \frac{1}{(2n+1)^5} \frac{\sinh [(2n+1)\pi w_f / 2h]}{\cosh [(2n+1)\pi w / 2h]} \right\}}{\left\{ 1 - \left( \frac{192h}{\pi^5 w} \right) \sum_{n=0}^{\infty} \frac{\tanh [(2n+1)\pi w / 2h]}{(2n+1)^5} \right\}} \quad (3.8)$$

Based on the design parameters and considerations, three designs have been suggested and the effect of 3D hydrodynamic focusing has been studied in the present work.

### 3.4 Simulation

A 3D hydrodynamic sample focusing flow system was numerically simulated using COMSOL Multiphysics (Comsol Inc., Palo Alto, USA) to fully understand the flow behavior and particle centering. Taking into account a low Reynolds number in the microfluidic channel due to the small dimensions, Stokes flow equations were used for incompressible steady-state simulation with convection and diffusion. All inlet flows were considered as laminar and as a fully developed flow with no-slip conditions at the channel walls.

The diffusion coefficient was defined with  $D_i = 1e-10[m^2/s]$  as the Isotropic diffusion coefficient of the substance in water and the input concentration was set to  $c_0 = 500[mol/m^3]$ . The simulation was performed by considering isotropic diffusive conductivity with the diffusion constant  $D_i$  and by choosing the properties of sample and sheath flow as different as shown in Table 3.1. Sheath fluid is considered as DI water where as properties of Diluted glycerol is considered as high viscous sample fluid(88).

rho1	1e3[kg/m <sup>3</sup> ]	Density of sample Fluid
eta1	1.803e-3[Pa*s]	Viscosity of sample Fluid
rho2	1e3[kg/m <sup>3</sup> ]	Density of sheath Fluid
eta2	1.002e-3[Pa*s]	Viscosity of sheath Fluid
c0	500[mol/m <sup>3</sup> ]	Input concentration

Table 3.1: Parameters and values used in COMSOL Multiphysics simulation

### 3.4.1 Design I

A three dimensional hydrodynamic focusing model was designed as shown in Figure 3.3. Channel A is  $100 \times 120 \mu m$  in width and height respectively. Channels B and C are  $40 \times 50 \mu m$  in width and height whereas Channel D is  $100 \times 100 \mu m$  in width and height respectively. The outlet channel is designed to be  $120 \times 120 \mu m$  in width and height. Channels B and C are placed on the bottom of the main Channel A as shown in Figure 3.3. A sample is driven through inlet Channel A with velocity  $V_A$ . Two pairs of sheath flows with velocities  $V_B$  and  $V_C$  are used to focus the main stream in the vertical direction.

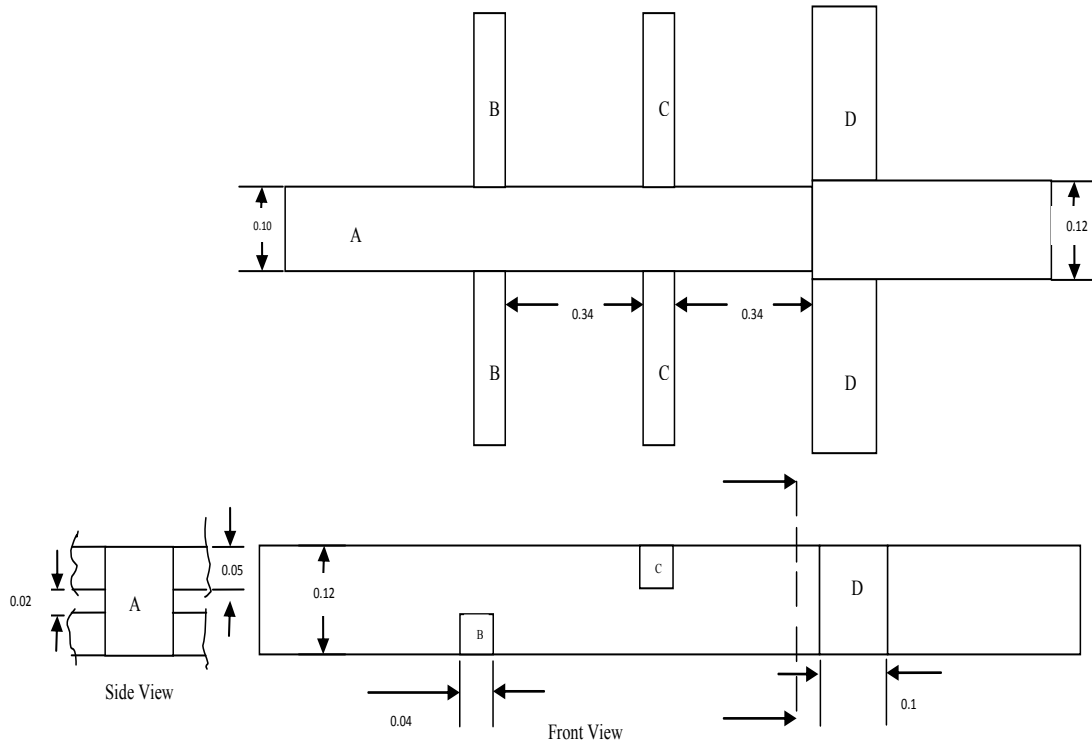


Figure 3.3: Three dimensional focusing design I with dimensions.

Since the flow is laminar and the Reynolds number is too low, there is less chance of mixing to occur. The properties of the sheath flow and sample fluid are different enough for hydrodynamic focusing to occur. Again another sheath flow through Channel D is given with velocity  $V_D$  for converging the sample stream in the horizontal direction. This results in three dimensional hydrodynamic focusing.

Keeping the inlet velocity of the sample at  $V_A = 500 \mu\text{m}/\text{sec}$  and the velocity of the sheath flow in the horizontal direction  $V_D = 15 \mu\text{m}/\text{sec}$  while changing the velocities of the sheath flows for the vertical focusing at  $V_B$ , and  $V_C$  as listed in Table 3.2, the different focusing effects on the vertical direction have been studied

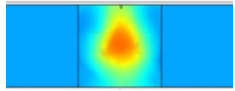
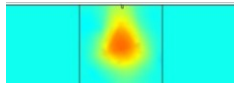
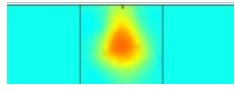
Sl no/Channel	$V_A$ $\mu\text{m/sec}$	$V_B$ $\mu\text{m/sec}$	$V_C$ $\mu\text{m/sec}$	$V_D$ $\mu\text{m/sec}$	Simulation Results
1.	500	800	800	15	
2.	500	1000	1000	15	
3.	500	1200	1200	15	

Table 3.2: COMSOL Multiphysics simulation of design I with different iterations.

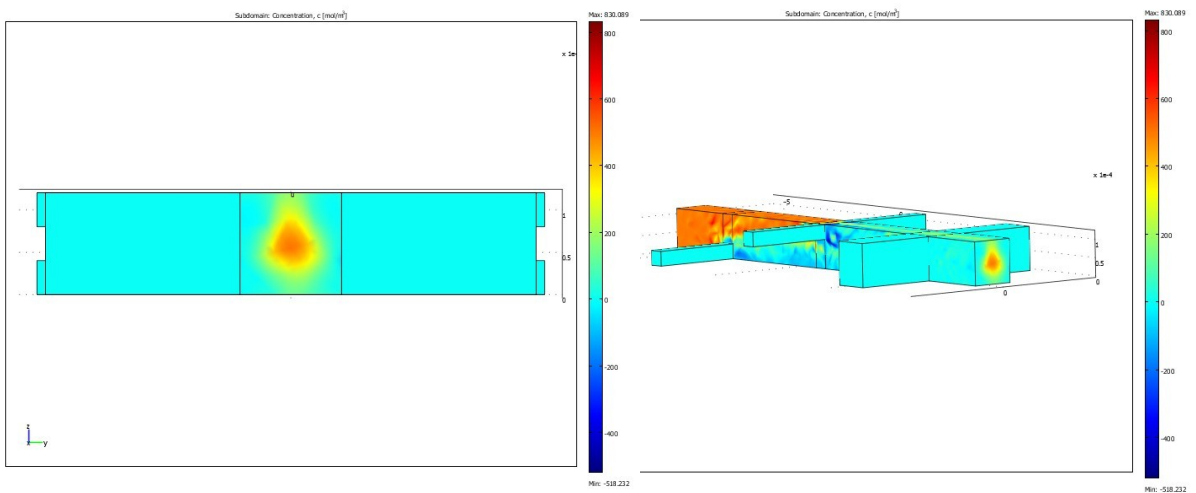


Figure 3.4: Simulation result of three dimensional hydrodynamic focusing in Design I

#### 3.4.1.1 Discussion:

On keeping the sample velocity constant at  $V_A = 500 \mu m/sec$ , it is found that any velocity of sheath flow for the vertical focusing ( $V_B$  &  $V_C$ ) should not be below  $500 \mu m/sec$ . The velocity of the sheath flow should be higher than that of the sample fluid flow to accomplish hydrodynamic focusing. And when the velocity exceeds  $1200 \mu m/sec$ , the focusing over the end tip starts to disappear due to mixing, due to the increase in Reynolds number above 1.

While very good focusing is possible at  $V_B$  and  $V_C$  at  $1200 \mu m/sec$  the main disadvantage of this design is in the difficulty of fabrication. Since the channel varies in width, it is difficult to fabricate by using existing MEMS technologies. A two layer structure should be fabricated and stitched together to achieve varying channel width. Another disadvantage is in placing the two Channels B and C at  $40 \times 50 \mu m$  with a separating distance of  $20 \mu m$ . For this kind of fabrication we need to use a three layer structure, but such a fabrication is difficult to achieve. To achieve the required design it is necessary to perform a 5-step fabrication process, thereby increasing the complexity. Taking all these considerations into account, a subsequent design has been suggested and studied.



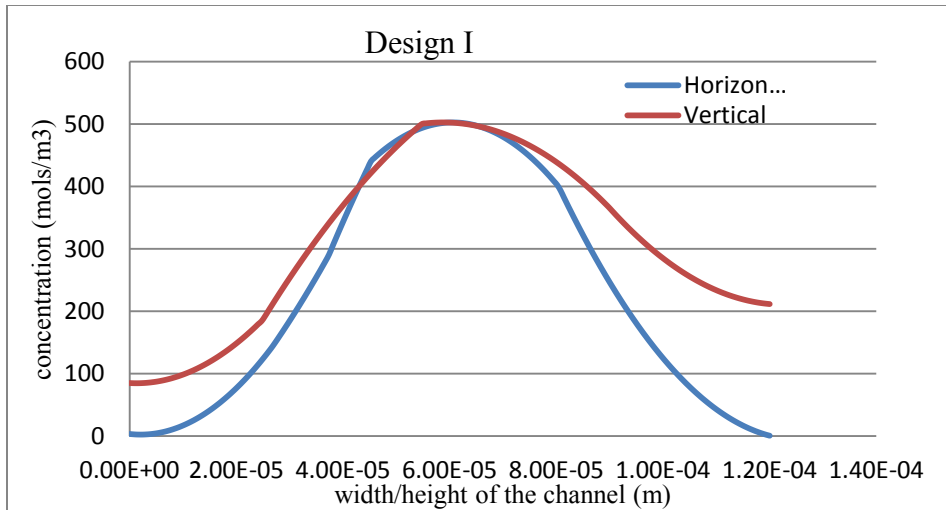


Figure 3.5: Graph showing horizontal and vertical focusing with respect to width/height at velocity condition  $V_A=500 \mu\text{m}/\text{sec}$ ,  $V_B$  and  $V_C$  at  $1200\mu\text{m}/\text{sec}$ .

### 3.4.2 Design II

By making the channel width constant throughout, the new design has been studied as shown in the figure below. Here the width and height of Channel A are made  $120\mu\text{m} \times 120\mu\text{m}$  respectively. The main advantage of this design is the ease of fabrication.

The stepped structure at the end position, as shown in Figure 3.3, is reduced to a constant width channel as shown in Figure 3.6. This reduces the bonding of the two separate pieces to achieve the stepped-block structure. Therefore, the total process has been reduced from 5 steps to 3 steps by comparison with the previous design, making the channel constant throughout. Keeping the inlet velocity of the sample at  $V_A = 500 \mu\text{m}/\text{sec}$ ,  $V_D$  equals  $15 \mu\text{m}/\text{sec}$ . While changing the velocities of the sheath flows at  $V_B$  and  $V_C$ , the different focusing effect has been studied.

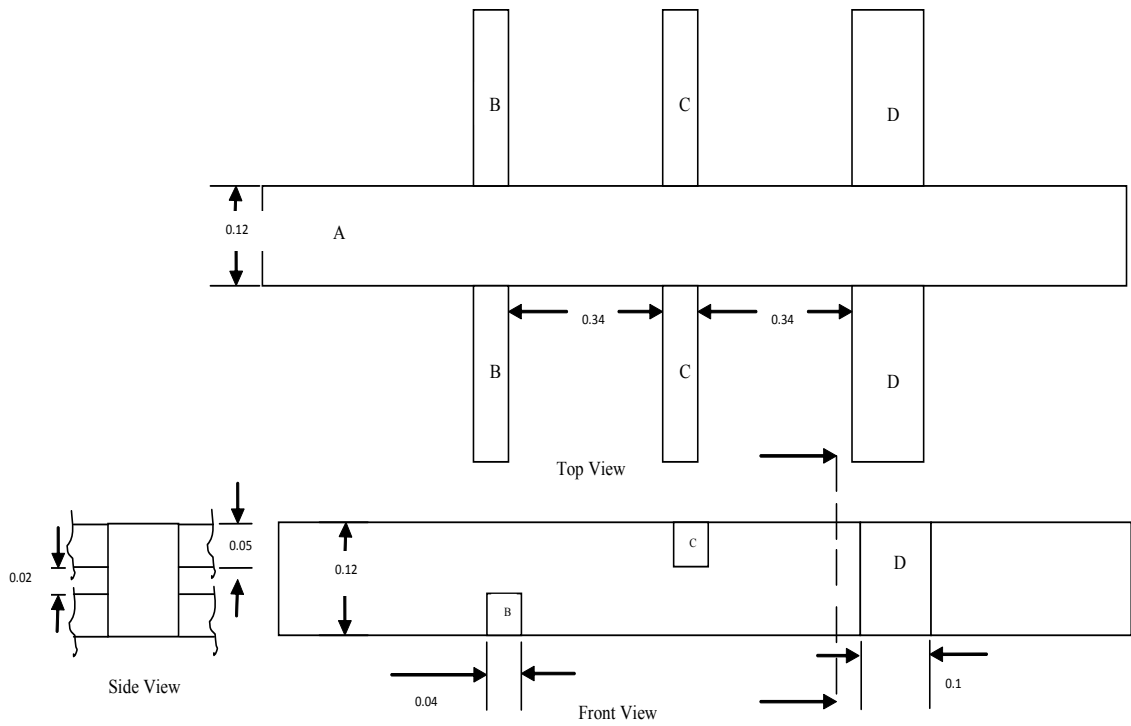


Figure 3.6: Three dimensional focusing design II with dimensions

Sl no/Channel	$V_A$ $\mu\text{m}/\text{sec}$	$V_B$ $\mu\text{m}/\text{sec}$	$V_C$ $\mu\text{m}/\text{sec}$	$V_D$ $\mu\text{m}/\text{sec}$	Simulation Results
1.	500	800	800	15	
2.	500	1000	1000	15	
3.	500	1200	1200	15	

Table 3.3: COMSOL Multiphysics simulation of design II with different iterations.

### 3.4.2.1 Discussion:

The channel width is increased to  $120\mu\text{m}$  throughout to fit the initial conditions of the fluid flow of Design 1. By reducing the channel width to  $100\mu\text{m}$ , it is necessary to reduce the inlet velocity of the fluid to accommodate the change. While keeping the sample velocity constant at  $V_A = 500\mu\text{m}/\text{s}$ , the sheath flow velocity for vertical focusing is found to be in the range between  $800\mu\text{m}/\text{s}$  to  $1200\mu\text{m}/\text{s}$ . When the sheath flows for vertical focusing  $V_B$  &  $V_C$  are  $800\mu\text{m}/\text{s}$ , the intensity of focusing at the end tip is scattered as shown in the table. While the sheath fluid velocity is increased to  $1200\mu\text{m}/\text{s}$ , the intensity becomes narrow as shown.

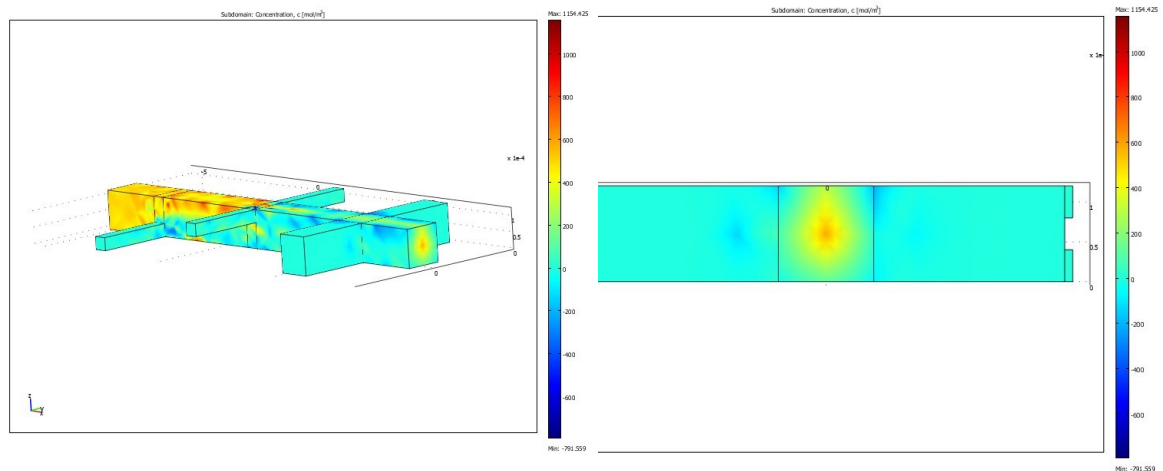


Figure 3.7: Simulation result of three dimensional hydrodynamic focusing in Design II

By comparison with the previous design (Tables 3.2 & 3.3), the focusing on the end tip has been slightly compensated for in Design II due to the alteration in design. By comparison with the previous design, the fabrication is simpler due to the constant width of the channel throughout. This reduces the difficulty in the fabrication, but again the problem with placing Channels B and C at  $40 \times 50\mu\text{m}$  with a distance of  $20\mu\text{m}$  of separation still exists. The main aim is to achieve the best focusing effect using

hydrodynamics with a minimum for the cost, time, and fabrication process. To achieve this, it is necessary to reconsider the design again by eliminating the existing problems.

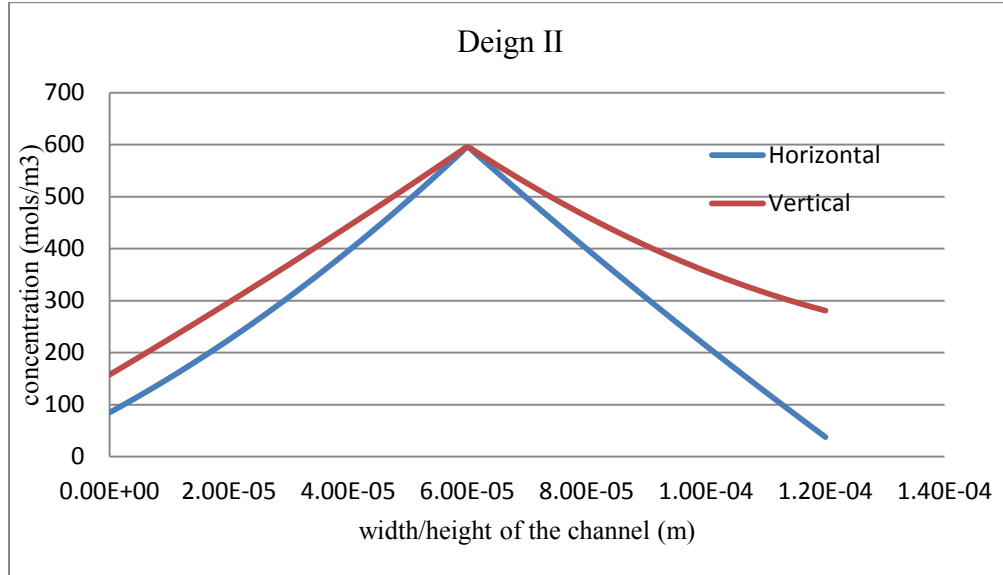


Figure 3.8: Graph showing horizontal and vertical focusing with respect to width/height at velocity condition  $V_A=500 \mu\text{m}/\text{sec}$ ,  $V_B$  and  $V_C$  at  $1200\mu\text{m}/\text{sec}$ .

### 3.4.3 Design III

By considering Designs I and II, to achieve three dimensional hydrodynamic focusing, it is necessary to place Channels B and C ( $40 \times 50\mu\text{m}$ ) according to the ease of fabrication. Design III, shown in the Figure 3.9, shows the structure that it is possible to fabricate by using a two layer MEMS fabrication process. While keeping the inlet velocity of the sample at  $V_A=500 \mu\text{m}/\text{sec}$  and  $V_D=15 \mu\text{m}/\text{sec}$  and at the same time changing the velocities of sheath flows at  $V_B$  and  $V_C$ , the different focusing effect has been studied.

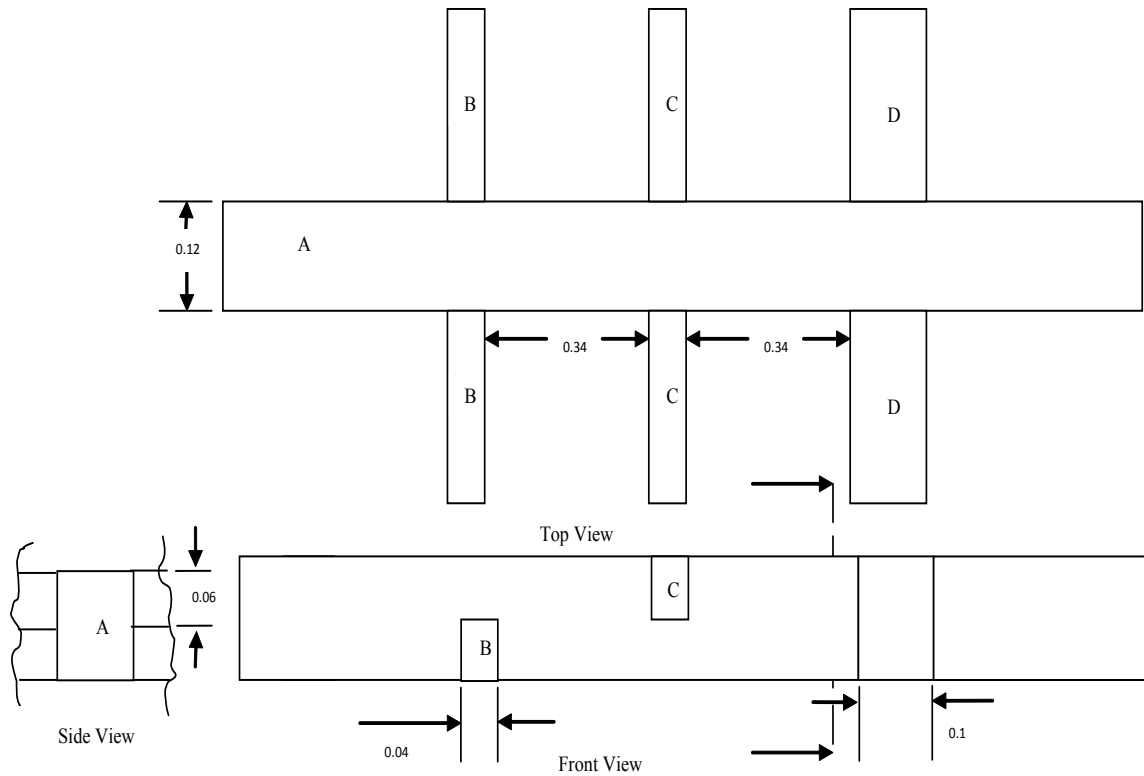


Figure 3.9: Three dimensional focusing design III with dimensions

### 3.4.3.1 Discussion:

It seems that, due to varying the dimension and design, the focusing is also being varied. The focusing started to disappear for any value above  $V_B$  as  $800\mu\text{m}/\text{sec}$  and  $V_C$  as  $1000\mu\text{m}/\text{sec}$ . At  $V_B$  and  $V_C$  as  $1200\mu\text{m}/\text{sec}$  the intensity of red shows that the device will break due to high velocity. To achieve this result, velocity  $V_C$  &  $V_B$  has been decreased by a decrement of  $200\mu\text{m}/\text{sec}$  and simulated. A better result is shown in the range between  $V_C$  &  $V_B = 500\mu\text{m}/\text{s}$  to  $800\mu\text{m}/\text{sec}$ .

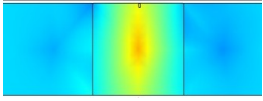
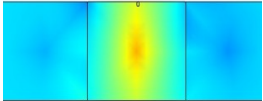
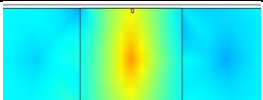
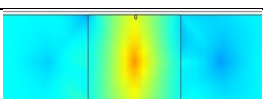
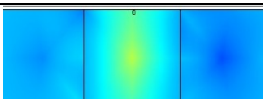

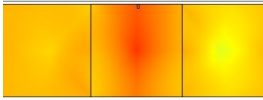
Sl no/Channel	$V_A$ $\mu\text{m}/\text{sec}$	$V_B$ $\mu\text{m}/\text{sec}$	$V_C$ $\mu\text{m}/\text{sec}$	$V_D$ $\mu\text{m}/\text{sec}$	Simulation Results
1.	500	500	500	15	
2.	500	500	600	15	
3.	500	600	700	15	
4.	500	600	800	15	
5.	500	800	1000	15	
6.	500	1000	1200	15	
7.	500	1200	1200	15	

Table 3.4: COMSOL Multiphysics simulation of design III with different iterations.

The amount of fluid entering through Channel A with  $V_A$  will be lifted by fluid entering through Channel B with  $V_B$ . Channel B is placed at the bottom of the main channel.

Removing the gap between  $V_B$  &  $V_C$  will reduce the manufacturing process to a two layer fabrication. But it will also affect the focusing due to the lack of the gap, which allows the fluid to pass through. Therefore to achieve focusing at this particular point we should look in to certain criteria's. At first the velocity of the side channels should be reduced in comparison with the previous designs. Second, to compensate for the amount of fluid lifting, velocity  $V_C$  should be greater than  $V_B$ . To achieve this result, velocity  $V_C$  has been increased by an increment of  $100 \mu\text{m}/\text{sec}$  with respect to  $V_B$ . The result shows that there is an improvement by comparison with the previous values, but the focusing is poor. Still the fluid focusing is shifted to the top of the channel. Further simulation has been performed where  $V_C$  has been increased by an increment of  $200 \mu\text{m}/\text{sec}$  with respect to  $V_B$ . Table 4 shows the simulation results of the end tip with respect to different velocity conditions. When  $V_B$  is  $600\mu\text{m}/\text{sec}$  and  $V_C$  is  $800\mu\text{m}/\text{sec}$ , the simulation shows better results in the comparison to other velocities for  $V_B$  and  $V_C$ . The above focus can be achieved either by reducing the velocity of  $V_A$  or by changing the velocity of  $V_B$  &  $V_C$  with respect to the previously stated designs.

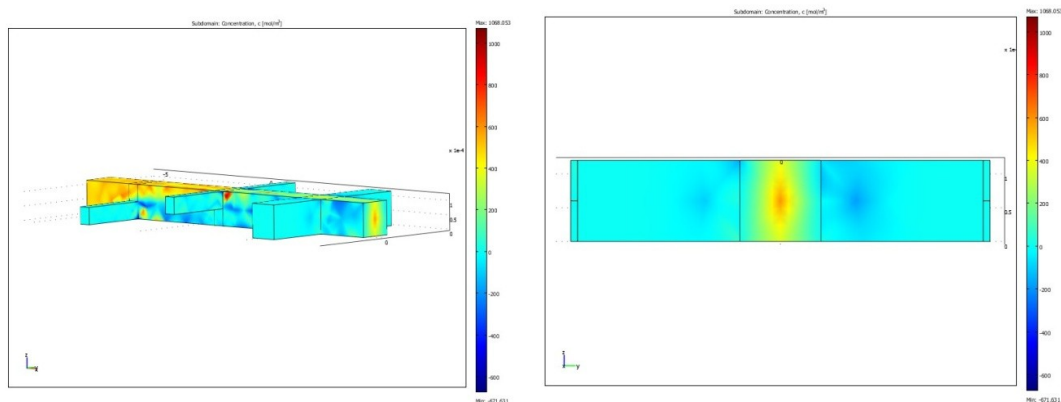


Figure 3.10: Simulation result of three dimensional hydrodynamic focusing in Design III

The ideal velocity of sheath flow when the sample velocity of  $V_A=500 \mu\text{m}/\text{sec}$  is kept constant is found to be  $V_B=600 \mu\text{m}/\text{sec}$  and  $V_C=800 \mu\text{m}/\text{sec}$ . By comparison with Designs I & II as shown in Tables 3.2 & 3.3, the fluid focusing at the end tip has been slightly reduced. However, increasing the velocity of  $V_C$  by an increment of  $200 \mu\text{m}/\text{sec}$  produces better results. Here in this design the fabrication is much simpler compared to that in the two previous designs. A two-layer PDMS fabrication technique can be used to fabricate the postulated design.

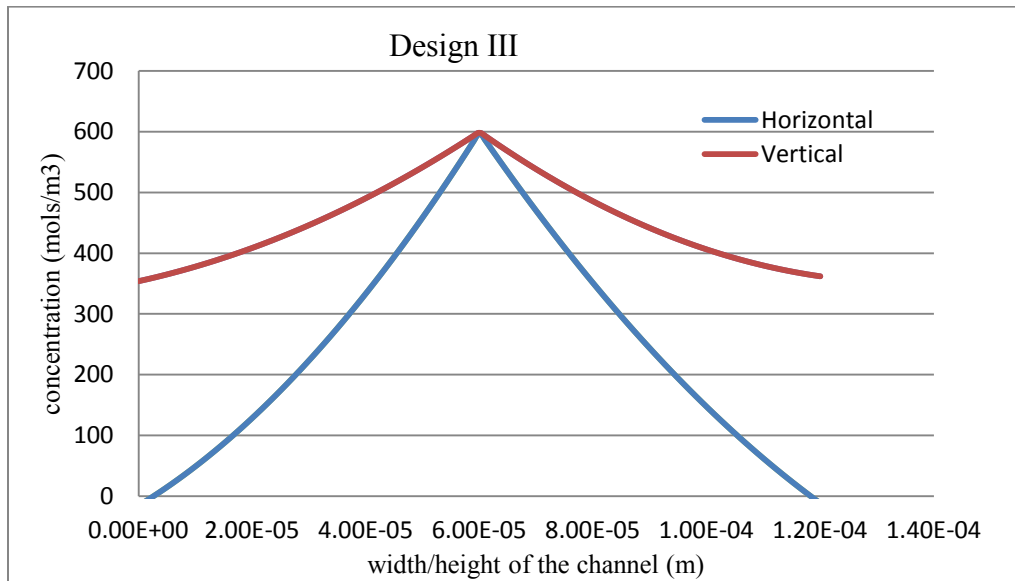


Figure 3.11: Graph showing horizontal and vertical focusing with respect to width/height at velocity condition  $V_A=500 \mu\text{m}/\text{sec}$ ,  $V_B$  at  $600\mu\text{m}/\text{sec}$  and  $V_C$  at  $800\mu\text{m}/\text{sec}$ .

### 3.5 Results and Discussion

Three dimensional hydrodynamic focusing effects over a microchannel are visualized using a COMSOL multiphysics simulation. The concentration of a sample stream



focused at the tip, after vertical and horizontal focusing by three pairs of sheath flows, is shown below.

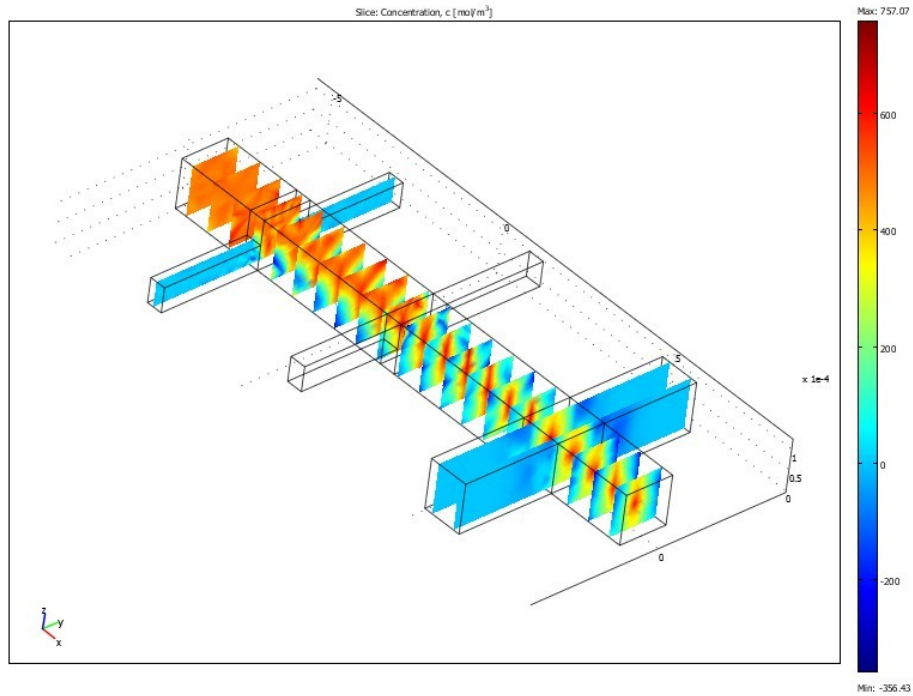


Figure 3.12: Sliced view of three dimensional hydrodynamic focusing in Design III

Figure 3.12 shows the image of the hydrodynamic focusing of the microflow cytometer after simulation. The intensity of the colored ink solution decreases due to the two sheath flows from the top, bottom, and narrows toward the tip, which is completely surrounded by the transparent sheath flow (DI-water) due to horizontal focusing. The cross-sectional close-up of the lifting inlet and of the following side port junction illustrates the good agreement of the sample centering.

Though a vertical focusing effect seems to be taking place, but it is not as good as in the case of the horizontal focusing. This could possibly be solved by locating the two initial pairs of the sheath flow at an adequate distance apart. Also the geometrical variables

should be studied more carefully. A two layer PDMS fabrication technique using an SU8 mould and Oxygen plasma bonding can be used to fabricate the postulated design.

Graphs shown in Figures 3.5, 3.8 and 3.11 have been added and discussed here in the thesis but are not in the submitted manuscript.

### **3.6 Summary**

Here in this chapter, a novel design for three dimensional hydrodynamic focusing has been proposed and simulated using COMSOL multiphysics, considering the fluid properties and fabrication easiness. It is required to find the optimum velocity for better focusing both in horizontal and vertical direction. Also it is required to study the viscosity parameter affecting the hydrodynamic focusing in this particular model. These works has been continued in the next chapter.

## **4 EFFECT OF VELOCITY AND VISCOSITY PARAMETERS ON HYDRODYNAMIC FOCUSING IN THE PROPOSED DESIGN**

This chapter is based on the article submitted IEEE/ASME Journal of Microelectromechanical Systems (Article ID SCH-JMEMS-2011-0358).

### **4.1 Introduction**

The ability to control the parameters of micro-environments at relevant length and time scales is one of the key benefits of microfluidics technology in cellular biology (1), in which one of the important aspects is fluid flow through a micro channel. Since the amount of fluid used is very small, only small quantities of reagents are required, thereby reducing the wastage. Existing precision fluid-delivery systems are bulky, expensive, and typically employ high-power syringe pumps. Microfluidic devices for manipulating fluids are widespread and find uses in many scientific and industrial contexts. Compared to conventional systems the fabrication cost is much less in microfluidic devices. To create a portable fully integrated, clinical diagnostic device for easy usage in everyday life is one of the primary goals of bioMEMS technology. The present study presents an investigation of ideal velocity parameters to achieve three dimensional hydrodynamic focusing in a novel design. Different velocities have been applied, changing the sheath flow and the sample flow conditions to observe the horizontal and vertical hydrodynamic focusing in a microfluidic channel. In the later context, different viscous fluids have been chosen so that the simulation can be performed and the effect of viscosity in hydrodynamic focusing can be observed.

## 4.2 Hydrodynamic Focusing

Hydrodynamic focusing is the technique by which a pair of sheath fluids is used to narrow the flow of a sample fluid, using their difference in fluidic properties such as velocity, viscosity or density. Over the past few decades many studies have been performed in this area, due to the application in cell cytometry for cell counting and sorting. Focusing can be mainly achieved by hydrodynamics, dielectrophoresis, electrokinetics, etc. The main advantage of hydrodynamic focusing is that it does not affect the biological cells since there is no electrical charge applied in this process. Better results have been obtained by using two pairs of sheath flow than one pair, depending on the geometry. At first the hydrodynamic effect was mainly concentrated on two dimensional (1,3-5)(6,21) focusing in which the sample fluids containing micro particles are focused only in the horizontal direction. It has been noted that while focusing only in two dimensions, there will be friction between the cells and walls in the vertical direction, necessitating focusing in three dimensional scales. Until now, only a few researchers have reported hydrodynamic focusing in three dimensional scales (67,69,71,74,89,90). Most of these designs are less efficient and also have complex structures that present difficulties during fabrication. Various researchers have studied the principle of hydrodynamic focusing with respect to the controlling parameters, fluid properties and dimensions (22,42,47,77,88,91-99). Our aim is to present a novel design that can be fabricated by using a simple two layer MEMS process that makes use of a PDMS Polymer

### 4.3 Design:

Hydrodynamic focusing is the technique by which a sample fluid is focused by using one or two pairs of sheath flow with different fluidic properties. It can be done in simple two dimensional scales and in three dimensional scales. In previous work (100)an investigation of three novel designs for three dimensional focusing was carried out. A three-dimensional model was suggested that can be fabricated by using a simple two layer PDMS fabrication technique as shown in Figure 3.1.

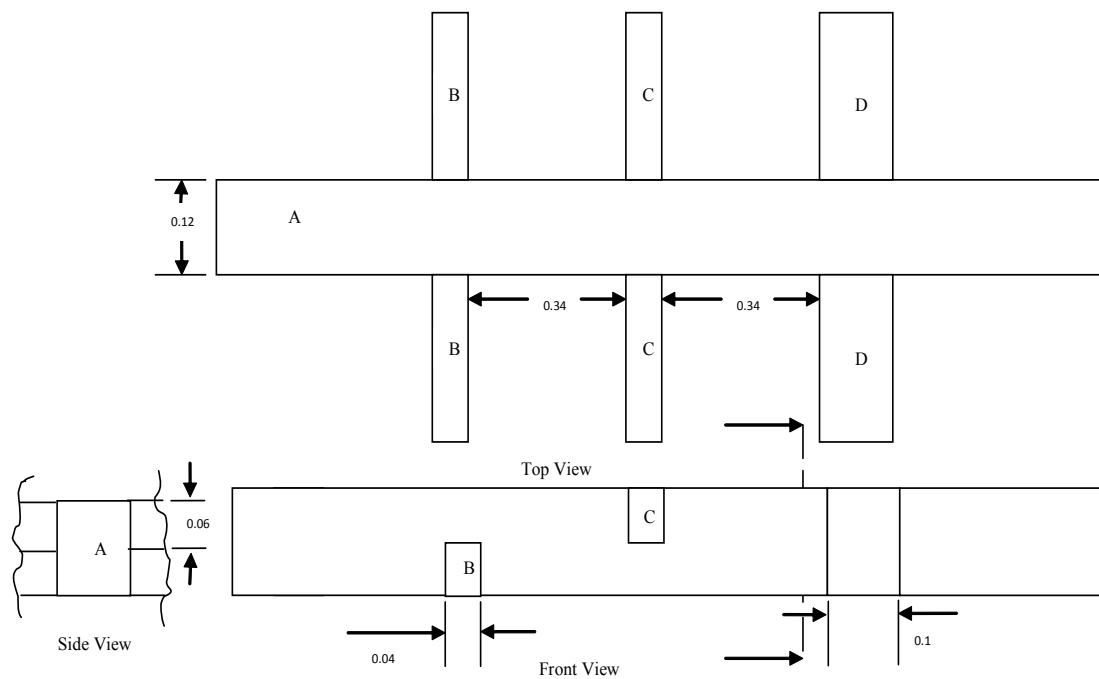


Figure 4.1: Two dimensional view of 3D hydrodynamic focusing design

Figure 3.1 shows all three views giving the dimensions of the design of three dimensional hydro dynamic focusing. In this design, the sample fluid is driven through channel A, which is  $120\mu\text{m}$  in width and  $120\mu\text{m}$  in height. The sheath fluid for vertical focusing flows through Channels B and C whose dimensions are  $40\mu\text{m}$  in width and  $60\mu\text{m}$  in height. The sheath fluid for horizontal focusing flows through Channel D, which is  $100\mu\text{m}$  in width and  $120\mu\text{m}$  in height. Channels B and D are placed at  $340\mu\text{m}$  on either side of Channel C as shown in Figure 3.1. A three dimensional view of the design is shown in Figure 3.2.

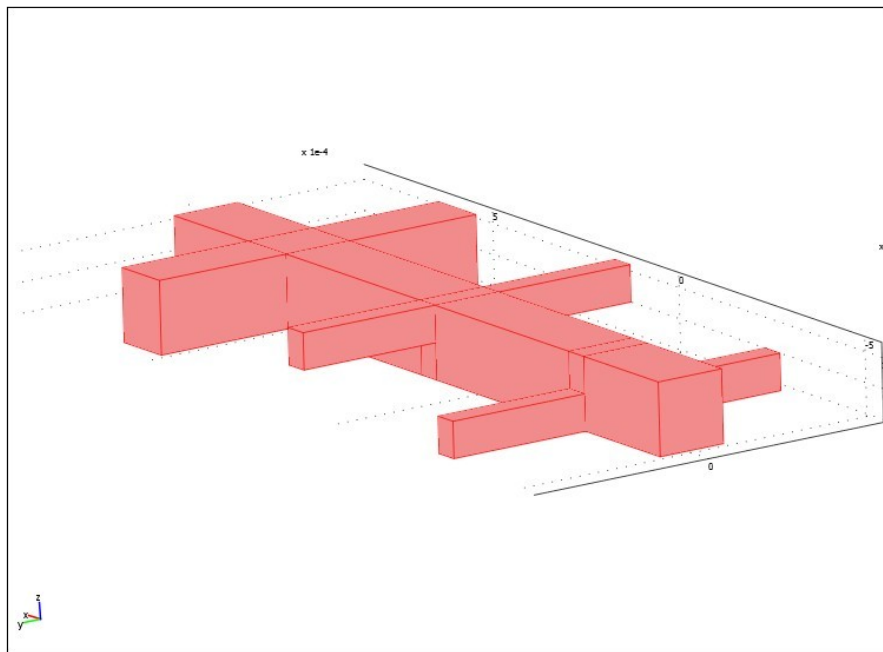


Figure 4.2: Two dimensional view of 3D hydrodynamic focusing design

The sample fluid flowing through channel A will be lifted up with the aid of the sheath fluid flowing from Channel B placed at the bottom of Channel A. To achieve centered

vertical focusing, another pair of sheath fluids driven from Channel C has been used, which is placed at the top of the main channel as shown in Figure 3.2. At the end of Channel A, another pair of sheath flow has been given using Channel D, for horizontal focusing. The dimensions and the positional features of the channels, as shown in Figure 3.2, are designed specifically, considering the feasibility of a simple two layered PDMS microfabrication.

#### 4.4 Simulation:

A 3D hydrodynamic sample focusing flow system was numerically simulated using COMSOL Multiphysics using an incompressible steady-state condition with convection and diffusion. A fully developed Laminar flow with no-slip conditions at the channel walls and Stokes flow equations were considered during the simulation. Reynolds number is used to characterize the fluid flow through the micro channel.

$$Re = \rho u D / \mu = u D / \nu \quad (4.1)$$

The fluid is considered a Newtonian fluid that obeys 'F=ma', where 'F' is the force, 'm' is the mass and 'a' is the acceleration. From this assumption we can derive the Navier-Stokes equation, which is

$$\rho \left( \frac{\partial \vec{U}}{\partial x} + \vec{U} \cdot (\nabla \vec{U}) \right) = -\nabla p + \mu \nabla^2 \vec{U} + F \quad (4.2)$$

Where  $\rho$  is the fluid density,  $\vec{U}$  is the flow velocity vector field,  $\mu$  is the dynamic viscosity, F is the volume force affecting the fluid, P is the fluid pressure. During

simulation it was considered that  $F = 0$ , since there are no volume forces affecting the fluid.

The concentration of the dissolved substance in the fluid can be described with the aid of the convection-diffusion equation stated below.

$$\frac{\partial c}{\partial t} + \nabla \cdot (-D \nabla c) = R - u \cdot \nabla c \quad (4.3)$$

where  $c$  is the concentration,  $D$  is the diffusion coefficient, and  $R$  is the reaction rate. In this model,  $D = 10^{-10} \text{ m}^2/\text{s}$ , and  $R = 0$  because the concentration is not affected by any reactions.

The initial objective is to achieve efficient three dimensional focusing by varying the inlet velocity conditions in the channel. The properties of diluted Glycerol (88) were considered as the properties of the sample fluid and DI water as the sheath fluid during simulation. The different parameters used during the simulation are stated in Table 4.1 below.

rho1	1e3[kg/m <sup>3</sup> ]	density of sample fluid
eta1	1.803e-3[Pa*s]	viscosity of sample fluid
rho2	1e3[kg/m <sup>3</sup> ]	density of sheath fluid
eta2	1.002e-3[Pa*s]	viscosity of sheath fluid
c0	500[mol/m <sup>3</sup> ]	input concentration

Table 4.1: Parameters and values used in COMSOL Multiphysics simulation



In previous work (100), taking  $V_A = 500\mu\text{m}/\text{sec}$  as constant, it was found that, for this particular design, to obtain efficient three dimensional hydrodynamic focusing it was necessary to consider a lower inlet velocity. So the simulation was carried out by changing the inlet velocity  $V_A$  of the main channel and the corresponding sheath flow velocities as stated in Table 4.1. Decrement of  $100\mu\text{m}/\text{sec}$  was considered for the inlet velocity  $V_A$  through the main channel, while varying the velocity of the sheath flow through Channels B & C. The last column of Table 4.2 shows the simulation results at the tip for the different fluid velocities.

For this particular design, it is observed that an efficient three dimensional focusing is obtained when the inlet velocity is at  $150\mu\text{m}/\text{sec}$ , the sheath flow  $V_B$  is at  $350\mu\text{m}/\text{sec}$  and the  $V_C$  is at  $550\mu\text{m}/\text{sec}$  as seen in row ten of Table 4.2. A graph corresponding to the concentration of the particle with respect to the width & height of the channel has been plotted with this velocity condition as shown in Figure 4.2. From the graph it is observed that the vertical focusing is taking place but it is not efficient compared to the horizontal focusing. When the inlet velocity is reduced to  $100\mu\text{m}/\text{sec}$ , it is observed that the intensity of focusing has disappeared. At any value of  $V_A$  above  $200\mu\text{m}/\text{sec}$  for the main channel, the amount of vertical focusing is inefficient.

	$V_A$ $\mu\text{m}/\text{sec}$	$V_B$ $\mu\text{m}/\text{sec}$	$V_C$ $\mu\text{m}/\text{sec}$	$V_D$ $\mu\text{m}/\text{sec}$	Simulation Results
1.	500	500	600	15	
2.	500	500	500	15	
4.	400	500	600	15	
5.	300	400	500	15	
6.	250	450	550	15	
7.	250	350	450	15	
8.	200	400	600	15	
9.	200	300	400	15	
10.	150	350	550	15	
11.	150	250	350	15	
12.	100	300	500	15	
13.	100	200	300	15	

Table 4.2: COMSOL Multiphysics simulation with different velocity iterations.

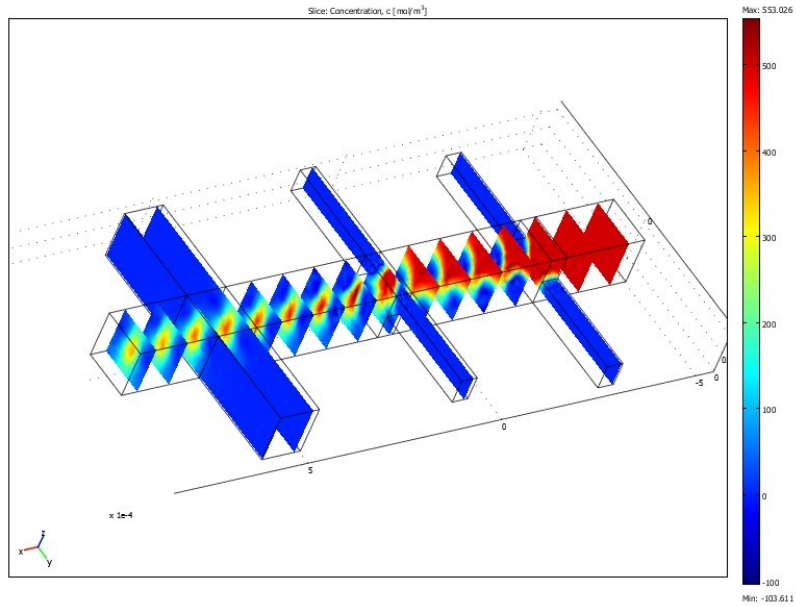


Figure 4.3: Slice view of hydrodynamic focusing happening in this design

The graph in Figure 4.4 shows the horizontal and vertical focusing with respect to the molar concentration on the Y-axis to the distance on the X-axis at the tip of the three dimensional design.

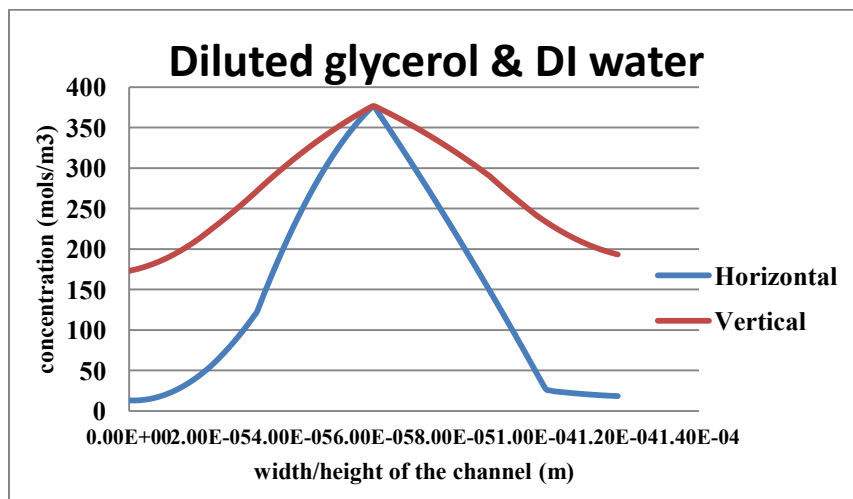


Figure 4.4: Graph showing horizontal and vertical focusing at velocity  $V_A = 150$ ,  $V_B = 350$ ,  $V_C = 550$  m/sec through channel A, B, C respectively when diluted glycerol is used as the sample fluid and DI water is used as the sheath fluid.

Even though vertical focusing is taking place, it is observed that this vertical focusing is not efficient as compared to the horizontal focusing. This is due to the insufficient gap between the layers to accommodate the fluid flow compared to the three layer design proposed in earlier work.

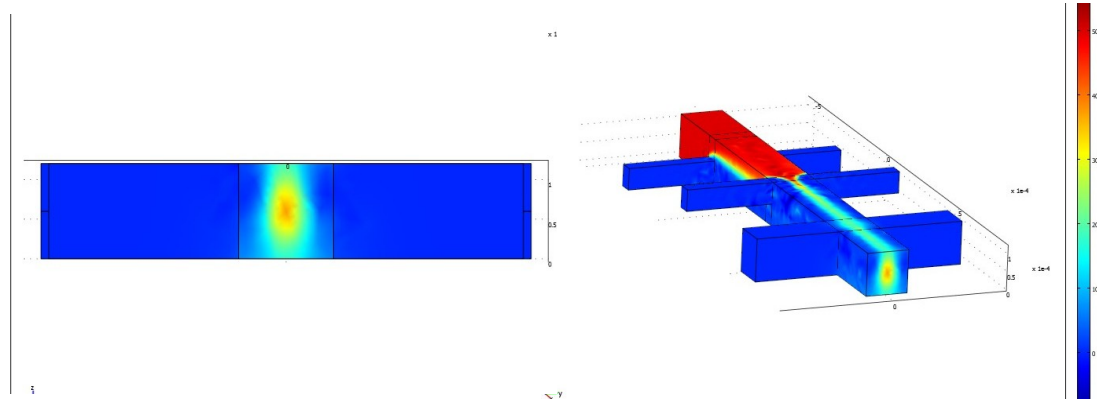


Figure 4.5: Three dimensional view of the Hydrodynamic focusing effect at the tip and channel.

#### 4.5 Viscous Effect in Focusing

Hydrodynamic focusing of the fluid is mainly dependent on the Reynolds number (Equation 5.1) of the fluid flowing through. When the Reynolds number of the fluid flowing is less than 1, the fluid flow can be considered as Stokes flow. An efficient focusing happens in microfluidics only under low Reynolds number regimes. Fluid flow through a micro channel is dependent mainly on the velocity( $v$ ) of the fluid flowing in m/sec, on the hydraulic diameter ( $D_h$ ) of the channel in m, on the density ( $\rho$ ) of the fluid in  $\text{kg/m}^3$ , and on the dynamic viscosity( $\mu$ ) of the fluid in Pa-sec.

$$\text{Re} = \rho v D_h / \mu \quad (5.1)$$

The hydraulic diameter for a rectangular channel is given in Equation 5.2

$$D_h = 2ab/(a+b) \quad (5.2)$$

where ‘a’ and ‘b’ are the channel width and height respectively. It is also possible to vary the Reynolds number by choosing fluids with different viscosities in the same design. Three different combinations of fluids such as diluted glycerol (DG) and DI water (DIW), blood (RBC) and diluted glycerol (DG), blood (RBC) and DI water (DIW) have been considered as sample and sheath fluids respectively. Simulation has been performed using their corresponding properties as mentioned in Table 5.1 [27, 28].

DG+DIW		
rho1	1e3[kg/m <sup>3</sup> ]	Density of diluted glycerol as sample fluid
eta1	1.803e-3[Pa*s]	Viscosity of diluted glycerol as sample fluid
rho2	1e3[kg/m <sup>3</sup> ]	Density of sheath fluid
eta2	1.002e-3[Pa*s]	Viscosity of sheath fluid
RBC+DG		
rho1	1.43e3[kg/m <sup>3</sup> ]	Density of RBC as sample fluid
eta1	3.5-3[Pa*s]	Viscosity of RBC as sample fluid
rho2	1e3[kg/m <sup>3</sup> ]	Density of diluted glycerol as sheath fluid
eta2	1.803e-3[Pa*s]	Viscosity diluted glycerol as Sheath Fluid
RBC+DIW		
rho1	1.43e3[kg/m <sup>3</sup> ]	Density of RBC as sample fluid
eta1	3.5-3[Pa*s]	Viscosity of RBC as sample fluid
rho2	1e3[kg/m <sup>3</sup> ]	Density of sheath fluid
eta2	1.002e-3[Pa*s]	Viscosity of sheath fluid

Table 4.3: Properties of different sample and sheath fluids used in COMSOL Multiphysics simulation

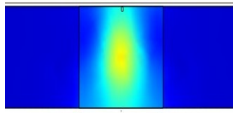
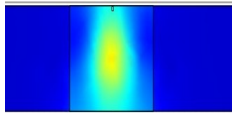
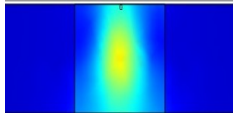
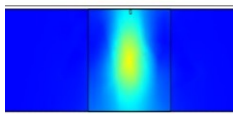
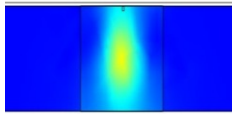
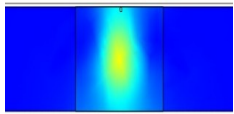
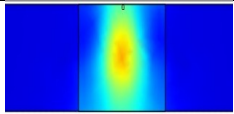
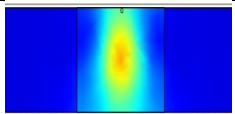
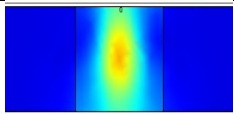
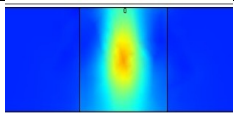
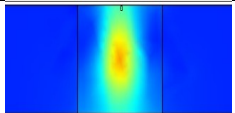
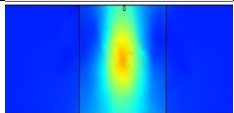
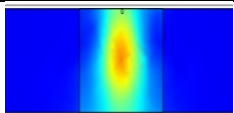
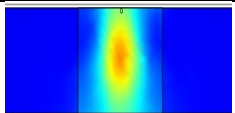
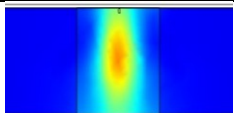
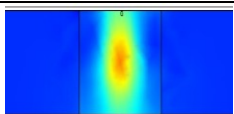
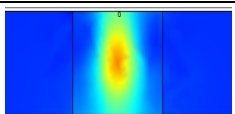
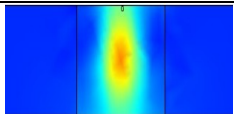
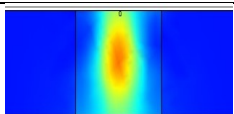
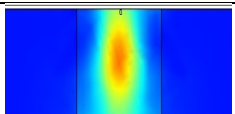
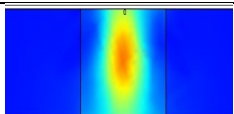
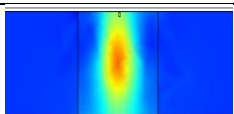
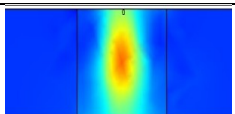
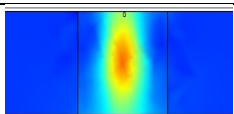
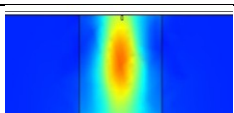
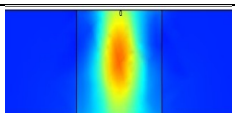
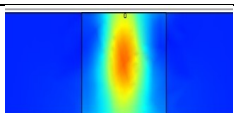
	V <sub>A</sub>	V <sub>B</sub>	V <sub>C</sub>	V <sub>D</sub>	DG+DIW	RBC+DG	RBC+DIW
	μm/sec						
1.	100	200	300	15			
2.	100	300	500	15			
3.	150	250	350	15			
4.	150	350	550	15			
5.	200	300	400	15			
6.	200	400	600	15			
7.	250	350	450	15			
8.	250	450	550	15			
9.	300	400	500	15			

Table 4.4: COMSOL Multiphysics simulation with different velocity and viscosity iterations.

Table 5.2 shows the simulation results with respect to different velocity and viscosity iterations in COMSOL multi physics.  $V_A$  at  $150 \mu\text{m}/\text{sec}$  for the sample fluid,  $V_B$  at  $350 \mu\text{m}/\text{sec}$  and  $V_C$  at  $550 \mu\text{m}/\text{sec}$  for the sheath flow, shows the best results for all the three different conditions.

Figures 4.2, 5.1, 5.2 show the plotted graphs for the three different iterations for DG, RBC and DIW. It is noted that the effect of viscosity only affects negligibly in focusing. This is because all the fluid viscosity used in the experiments falls under  $10^{-3}$  scale, which affects only minor changes. The primary criteria that alter the focusing are influenced by the velocity of the fluid flowing through the channels.

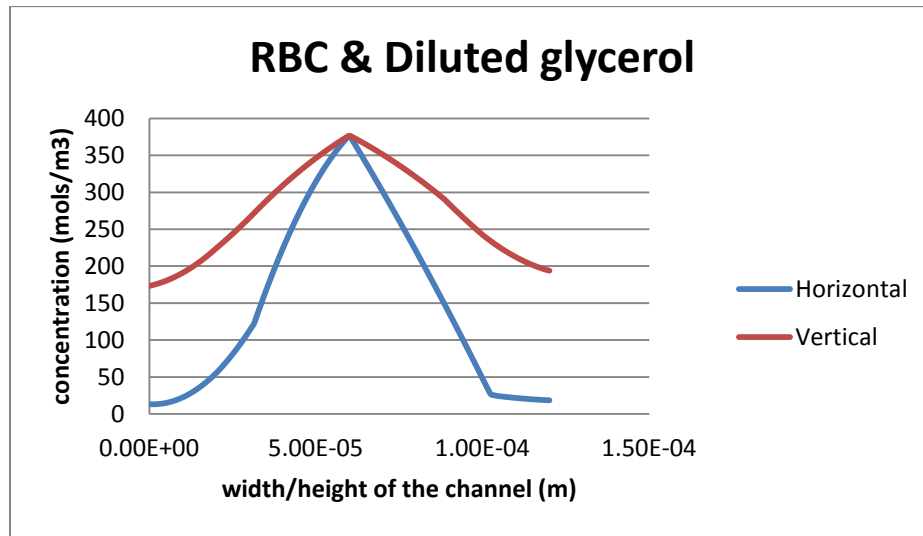


Figure 4.6: Graph showing horizontal and vertical focusing at velocity  $V_a=150$ ,  $V_b=350$ ,  $V_c=550\text{m}/\text{sec}$  through channel A,B,C respectively when red blood cells are used as the sample fluid and diluted glycerol is used as the sheath fluid.

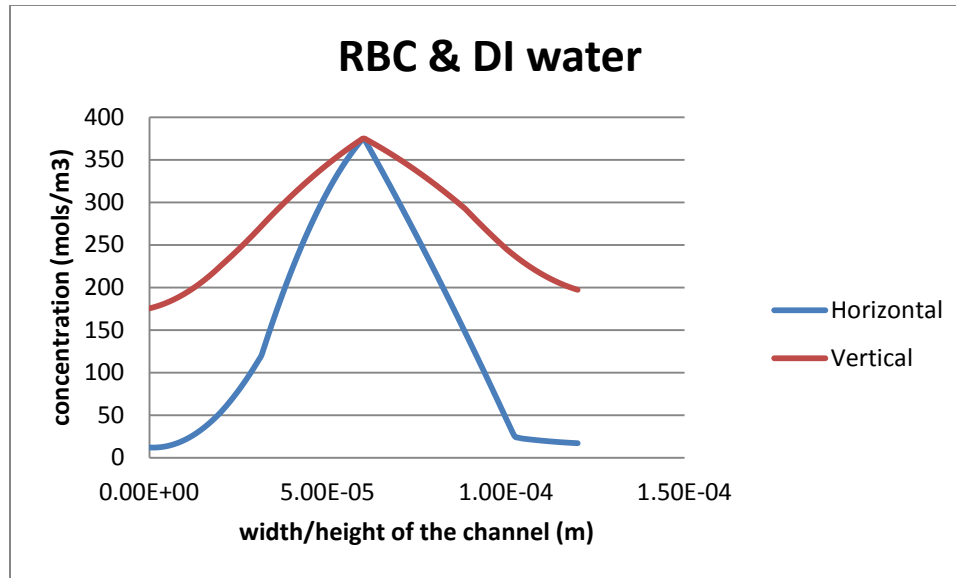


Figure 4.7: Graph showing horizontal and vertical focusing at velocity  $V_a=150$ ,  $V_b=350$ ,  $V_c=550$  m/sec through channel A,B,C respectively when red blood cells are used as the sample fluid and DI water is used as the sheath fluid.

#### 4.6 Results and Discussion:

A novel three dimensional model for hydrodynamic focusing was investigated by altering the parameters such as the velocity and the viscosity of the fluid flowing through the channels. The ideal velocity condition using COMSOL simulation was found to be  $150 \mu\text{m}/\text{sec}$  for the sample flow through the main channel, the sheath flow  $V_B$  at  $350 \mu\text{m}/\text{sec}$  and  $V_C$  at  $550 \mu\text{m}/\text{sec}$ . However, the vertical focusing is not as efficient as the horizontal focusing due to the insufficient gap between the two layers between channel B and C in the vertical direction. In future work, it will be necessary to study the effects of aspect ratio and the optimum distance to determine the best place for the channels for three-dimensional focusing to occur. The ideal distance of separation between Channel B and Channel C must be studied to obtain better results.



It was found that the effect of focusing is primarily dependent on the velocity of the fluid flowing through rather than on the viscosity of the fluid. The effect of viscosity is minimal due to the  $10^{-3}$  scale. Also when different fluids are used, both the fluid density and the viscosity vary.

#### **4.7 Summery**

Ideal, velocity conditions for better hydrodynamic focusing for the proposed deign has been found out using simulation. In the next work a preliminary fabrication of the proposed design has been done.

## 5 PRILIMINARY FABRICATION

### 5.1 Introduction

The fabrication of three dimensional microstructures is growing as microfabrication technologies advance. Several research groups have demonstrated different techniques for fabricating 3D microfluidic systems using silicon (101-103), PDMS (104-107), SU-8 photoresists (108-111), PMMA (112,113), glass (114,115), and Teflon (116-118). Up to now the majority of these devices have been fabricated with complex and time consuming silicon and related materials by using etching techniques. However, there are several limitations in wet etching when it is used to obtain specific geometrical shapes. Dry etching is much too expensive for the fabrication of complex structures. The use of PDMS in MEMS devices is advantageous in several ways such as lower cost by comparison with glass and SU-8, bio compatibility which leads to applications in biotechnology and bio engineering, optical transparency, and its permeability to gases. By comparison, the bonding property of PDMS makes it highly suitable for the fabrication of complex 3D structures. In the present work, simple microfabrication techniques such as dark field masks, negative photo resists, photo lithography and soft lithography are used to fabricate the proposed design. Two layers of PDMS are bonded together using oxygen plasma bonding at the end to construct the required three-dimensional structures.

The fabrication process is achieved by following three major steps: Layer I fabrication, Layer II fabrication, and oxygen plasma bonding before the assemblage of the layers one on top of the other. The proposed design, as stated earlier, was created in AutoCAD with

specified dimensions. Masks are then printed onto MYLAR transparency sheets at high resolution (3600 dpi), and these masks are further used for fabricating SU-8 photoresist molds on a silicon wafer. The molds of Layers I and II were then used to fabricate a PDMS microfluidic device. The entire fabrication process is explained in detail in the following sections.

Layer I consists of sample flowing Channel A with a width of  $120\mu\text{m}$ , Channel B for the first sheath flow for the vertical focusing of width  $40\mu\text{m}$ , and Channel D for the horizontal sheath flow of width  $100\mu\text{m}$ . Layer II consists of sample flowing Channel A with a width of  $120\mu\text{m}$ , Channel C for the second sheath flow for vertical focusing with a width of  $40\mu\text{m}$ , and Channel D for the horizontal sheath flow with a width of  $100\mu\text{m}$ . The schematic representation of Layer I and Layer II with dimensions is shown in Figure 5.1. The respective layer masks are shown in Figure 5.2.

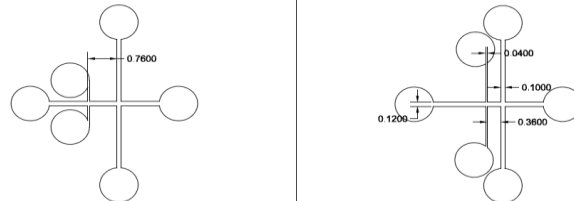


Figure 5.1: AutoCAD drawings of Layers I and II with dimensions of the suggested design



Figure 5.2: Design layout of Layer I and Layer II masks

One of the disadvantage while fabricating using this mask layout was, after bonding two layers and injecting syringe pump leads to the collapse of the channel wells which are closer to each other. A modified layer of mask has been designed as shown in Figure 5.3 in this work.

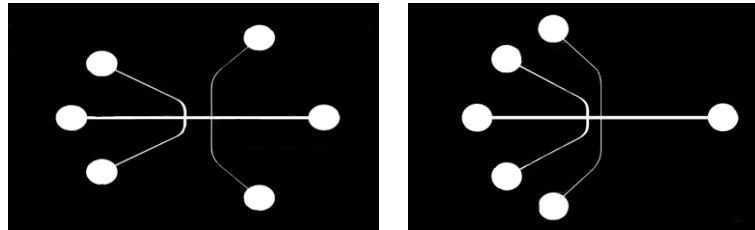


Figure 5.3: Design layout of modified Layer I and Layer II masks

## 5.2 Photolithography

Photolithography is an optical means for transferring patterns onto a substrate. It is used in microfabrication to selectively remove a thin layer or bulk of a substrate. The desired patterns can be transferred to the wafer using this technique. Masks are prepared from Auto Cad drawings as per required specifications. With this mask, patterns are then transferred to a photoresist layer. The basic steps of photolithography consist of surface preparation, coating of the photo resist, soft baking, exposure, development, and hard baking. The detailed process overview is shown in Figure 5.3.

As a preliminary step, the silicon wafers are chemically treated with a diluted HCL solution to remove particulate matter on the surface as well as any traces of organic, ionic, and metallic impurities. After cleaning the wafer, SU-8 2035 is deposited on the surface using high speed centrifugal spinning. High-speed centrifugal whirling of silicon wafers is the standard method for applying photoresist coatings in IC manufacturing

(120). "Spin Coating" produces a thin uniform layer of SU-8 photoresist on the wafer surface. To achieve a coating 60  $\mu\text{m}$  in thickness, an rpm of 2000 is used with an acceleration of 500rpm/sec for 30 seconds.

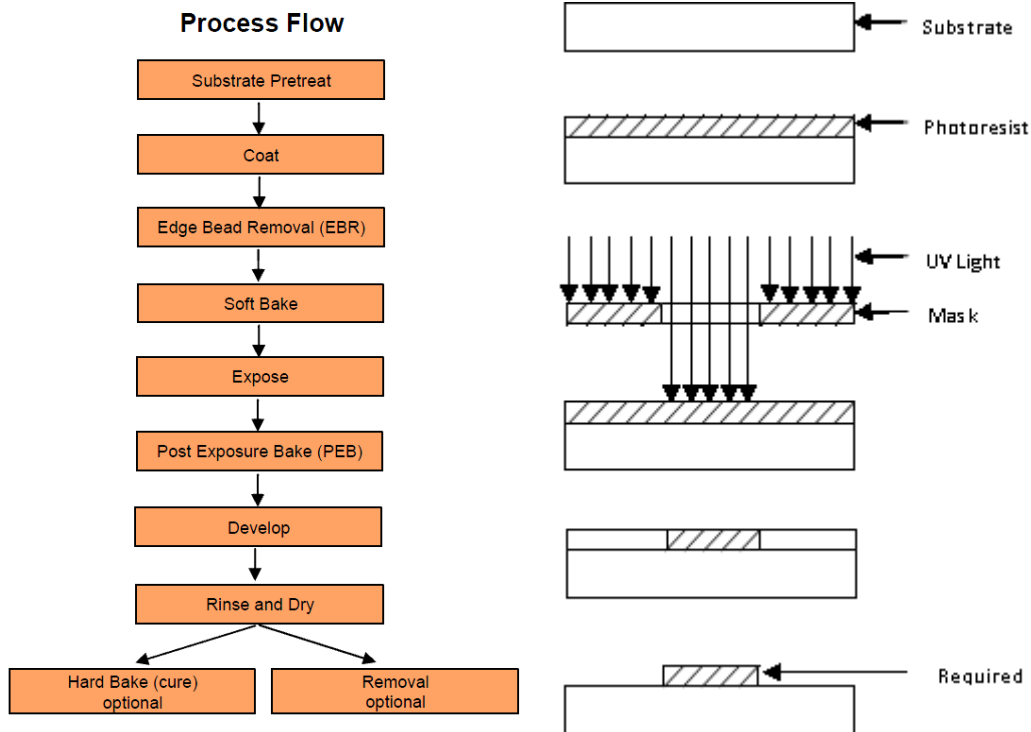


Figure 5.4: Overview of the Photolithography Process (119).

After the formation of the photoresist layer, the wafer is soft baked to remove solvents present in the photoresist coating. Moreover, this soft baking helps the coated photoresist to become photosensitive. At first the oven is set at 65°C and the wafer is baked for 3 minutes. Then the temperature is reset at 95°C, and the wafer is again baked for 7 minutes. It is important to control this baking process because over-baking reduces photo

sensitivity and under-baking resists the exposure. Under-baking results in incomplete exposure, causing less etching or less etching resistance.

The next important step in the photolithography process is mask alignment. A mask is attached to a square glass plate and aligned with the wafer. The alignment is important and should be accurate so that the pattern can be exactly transferred onto the wafer surface. Once the mask has been accurately aligned with the pattern on the wafer surface, necessary precautions should be taken before UV exposure. High intensity UV light exposes the pattern on the mask to the photoresist. The SU-8 coated silicon wafer is held on a vacuum chuck to add physical contact with the mask. The whole assembly is lifted up until the wafer and mask contact each other.

Using a vacuum, the coated photoresist in the aligned position is then exposed to high intensity UV light. Since the mask-attached glass plate and the coated wafer are in contact, it is possible to attain a high resolution by using contact printing. UV light is used for 35 seconds, and the chuck is released automatically. The process of printing with a contact mask aligner is shown in Figure 5.4. A post-exposure bake at 65°C for 2 minutes and, subsequently, at 95°C for 6 minutes is performed on the exposed wafer before developing. It is an optional step for stress reduction.

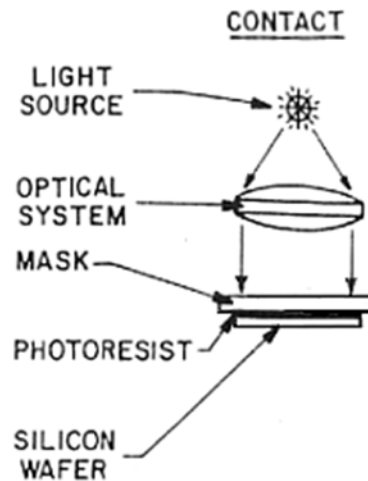


Figure 5.5: The contact printing mask alignment in the photolithography process (117).

The last important step in the photolithographic process is the development of the exposed, post-baked wafer in a developer solution. The wafer is placed for 7 minutes in a dish containing a developer solution. It is then transferred to a dish containing Isopropyl Alcohol (IPA) to rinse and wash. The required mould is produced after this step on a silicon wafer with a SU-8 photo resist. Again the wafer is transferred to the oven for a final hard baking or curing for 2 minutes at 95°C to harden the photoresist and to improve the adhesion of the photoresist to the wafer surface.

### 5.3 Silanisation

The above fabricated mould or template is used to create the original design. A layer of PDMS is poured into the mould to produce the required design or cast. There is a general problem during this step. The PDMS will stick to the surface of the mould destroying either the cast or the mould. So it is necessary to silanise the mould or template before pouring the PDMS layer. To avoid contamination due to particles, dust or moisture,

silanisation is done under a hood with a heater. A few ml of xylene is poured on the glass dish and the glass dish is kept over the heater at 50°C for 5 hours for the process to complete. The mold is then washed and cleaned using acetone and DI water. Air is blown to dry the template before storing it in the glass dish.

#### 5.4 Soft lithography

Using the prepared mould, the PDMS microfluidic device can be fabricated using soft lithography. In the present work, PDMS (Dow Corning Sylgard 184) is used to fabricate the desired microfluidic chip. Sylgard 184 has transparency and low viscosity when uncured, making it favorable for fabricating the cast. The process overview of soft lithography is depicted in Figure 5.5.

Sylgard 184 consists of a base component and a curing agent, which is curable with the help of heat. A polymer base is mixed with a curing agent in the ratio of 10:1. Good curing depends on a thorough mixing of the additives. Stirring is done on the order of 100 strokes with a stir stick to produce a high yield.

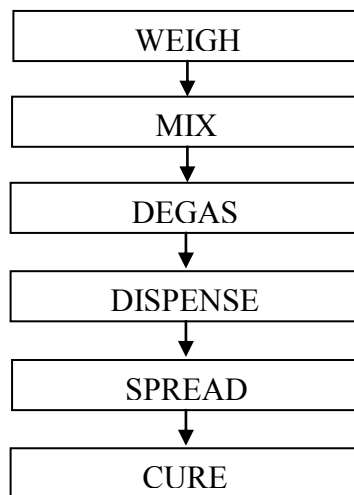


Figure 5.6: The process overview of soft lithography



The mixture will be full of trapped air bubbles from the mixing of the components. This degrades the optical properties of the PDMS after curing. So the bubbles must be removed using an exsicator using a vacuum before curing. When the silicone becomes clear and transparent, the process is finished. Now the silanised mould is firmly placed in a glass dish for proper alignment. An uncured PDMS mixture is dispensed at the center of the template from a low altitude to reduce air bubbles.

The mould assembly is left at room temperature for a few minutes to dissolve the bubbles generated during pouring. The mould is then transferred to an oven at 90°C for 5 hours. After baking the PDMS for the mentioned time span, it is taken out and cut down into the specified dimension. Figure 5.6 shows Layer I and Layer II of the cured PDMS before peeling. After curing the PDMS mixture mould Layer I and Layer II have been peeled off carefully from the dish as shown in Figure 5.7.

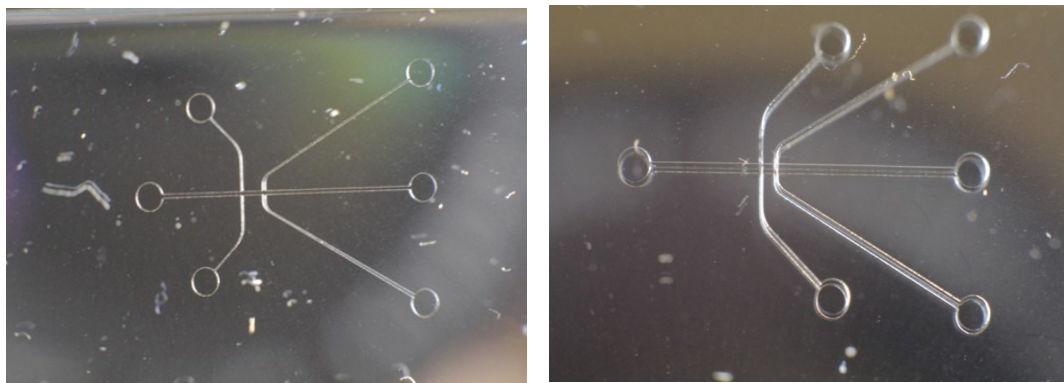


Figure 5.7: PDMS fabricated structure of Layers I and II.

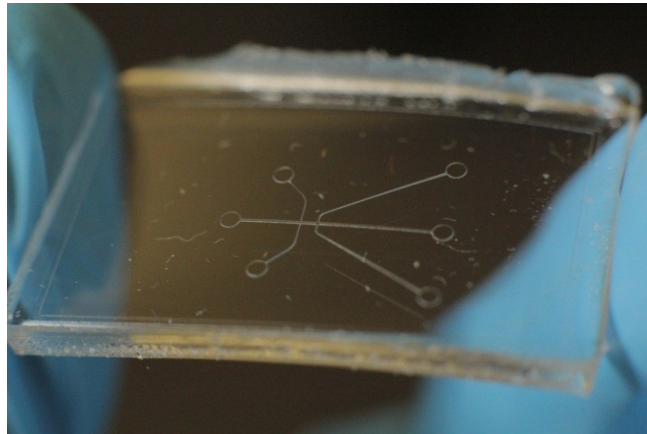


Figure 5.8:PDMS fabricated structure of Layer I after peeling.

### 5.5 Oxygen plasma bonding

The next important step is to bond the two layers of PDMS. To do that, a plasma preparation chamber that makes the PDMS hydrophilic is required. After a thorough cleaning, the two PDMS layers are placed inside the plasma chamber for 30 sec, thereby incorporating oxygen atoms into the PDMS surface. The same procedure can be used for PDMS to glass or Si bonding. Plasma is created inside the chamber, helping to bond the PDMS structure. It has been put under an optical microscope to align the two layers. Figure 5.10 shows the final bonded PDMS structure after oxygen plasma bonding.

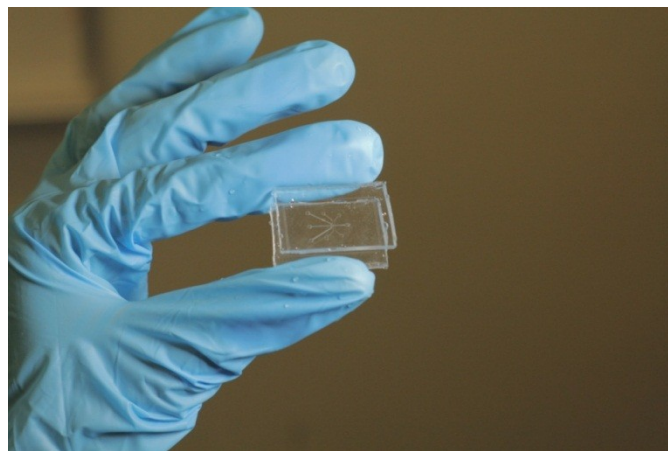


Figure 5.9: The final bonded PDMS structure after oxygen plasma bonding.

## **5.6 Summary**

As described, a preliminary fabrication of a microfluidic device for three dimensional hydrodynamic focusing was carried out. The final bonding of the device is done under an optical microscope to align the small channels. It will be necessary to conduct a detailed study of PDMS bonding in future work to obtain efficient transparent bonding. Experimentation should be conducted to validate the numerical results.

## 6 CONCLUSION AND FUTURE WORK

A brief review of flow cytometry was first carried out looking at the different uses of flow cytometry in cellular and molecular biology. Conventional flow cytometers are expensive, bulky, space consuming, reagent consuming, etc., making microfabricated flow cytometers widely acceptable. Portability, short reaction time, low cost, low power consumption, design versatility, and integration with other micro devices make microelectro mechanical systems most popular in biomedical applications. Existing microfluidics flow focusing devices use techniques such as electrophoresis, magnetic fields, optical forces, and electrokinetic and hydrodynamic methods to align the microparticles such as cells to the center for single molecular detection and sorting. Hydrodynamic focusing is advantageous due to the non use of electric potential for the focusing. Focusing is done on the basis of the differences in the properties of the fluids such velocity, viscosity, density, etc.

Hydrodynamic focusing has been investigated with respect to the current advances described in the literature. Primary attention has been paid to the focusing of micro particles only on two-dimensional scales during the past few decades. In two-dimensional focusing, the sample fluid containing the microparticles is aligned only in the horizontal direction. The disadvantages of two dimensional focusing have been discussed, leading to the study of advanced three dimensional hydrodynamic focusing of micro particles in microfluidics. A detailed study has been carried out in the present work, showing the advantages of three dimensional focusing, the existing design in 3D focusing, and their disadvantages.

Existing three-dimensional focusing designs are mainly based on electrophoresis and hydrodynamics. The main disadvantages of such designs are their complex structures and low efficiency. By considering the above points, a novel 3D hydrodynamic focusing design has been proposed and simulated using COMSOL multiphysics. Design I consists of Channel A with varying dimensions at the inlet ( $100 \times 120 \mu\text{m}$  in width and height) and at the outlet ( $120 \times 120 \mu\text{m}$  in width and height) for sample fluid focusing. Two pairs of sheath flow through side channels B and C ( $40 \times 50 \mu\text{m}$  in width and height) have been given for vertical hydrodynamic focusing, whereas at the end of the main channel A, Channel D ( $100 \times 100 \mu\text{m}$  in width and height) is placed for horizontal focusing. Channels B and C are placed on the bottom and top of main Channel A with a distance of  $20 \mu\text{m}$  in the vertical direction and a distance of  $340 \mu\text{m}$  in the horizontal direction. The sheath flow and sample fluid are different in velocity and viscosity for hydrodynamic focusing to occur.

Even though the efficiency is high, the main disadvantage of this design is the fabrication difficulty since it requires a 5 layer fabrication process. This leads to Design II with constant dimensions for main Channel A ( $120 \times 120 \mu\text{m}$  in width and height) throughout. This reduces the fabrication to a 3 layer process. Further, in Design III, the height of Channels B and C has been increased to reduce the gap between them. This proposed design can be fabricated using a simple two layer fabrication process.

Further study of the design with respect to the ideal velocity and change in viscosity parameters has been conducted. The ideal velocity for this particular design has been determined to be an inlet velocity  $V_A$  of  $150 \mu\text{m}/\text{sec}$ , a sheath flow  $V_B$  of  $350 \mu\text{m}/\text{sec}$  and a  $V_C$  of  $550 \mu\text{m}/\text{sec}$  respectively. Investigation of the changing viscosity parameters

shows a minimal effect in hydrodynamic focusing due to the  $10^{-3}$  range of viscosity values. The proposed design has been fabricated using a two layer PDMS fabrication technique using oxygen plasma bonding. Even though three dimensional hydrodynamic focusing is being used, vertical focusing is not as efficient as horizontal focusing due to the insufficient gap in the main channel to accommodate the fluid flow.

## **6.1 Future work**

It will be necessary to study the effect of the aspect ratio between the channel dimension and the fluid velocity, depending on the hydrodynamic focusing. The optimum distance for the placement of Channels B and C along the main channel A, for efficient three-dimensional focusing to occur, must also be studied in future work. In our work we determined the different velocities through the different channels. Studying the effect of velocity with respect to channels makes it possible to use a single constant velocity through all the channels by varying the width. This will help to make it possible to use a single fluid pressure pump to maintain the flow rate.

Experimentation should be conducted to validate the numerical results and to achieve better focusing through further study. Experimentation should be done with the help of fluid pumps with different fluid velocities in the current design. Four different sets of pressure-driven fluid pumps should be used and the results should be validated with the simulation results. Confocal microscopy should be used to image the focusing in the three dimensional design both in the vertical and horizontal directions. A comparison should be made with the theory and with the experimental results to evaluate the final working model and its properties.

## REFERENCES

- (1) Tabeling P. Introduction to microfluidics. Oxford [u.a.]: Oxford University Press; 2006.
- (2) Hsu T. MEMS and microsystems : design, manufacture, and nanoscale engineering. Hoboken: John Wiley & Sons, Inc.; 2008.
- (3) Hardt S, Schonfeld F. Microfluidic Technologies for Miniaturized Analysis Systems. Berlin: Springer US; 2006.
- (4) Li D,. Encyclopedia of microfluidics and nanofluidics. 2008; .
- (5) Tay FEH. Microfluidics and bioMEMS applications. Boston: Kluwer Academic Publishers; 2002.
- (6) Hesketh PJ. Bionanofluidic Mems. 2008; .
- (7) Saliterman S. Fundamentals of bioMEMS and medical microdevices. [Hoboken, NJ]; Bellingham, Wash.: Wiley-Interscience ; SPIE Press; 2006.
- (8) Berthier J, Silberzan P. Microfluidics for biotechnology. Boston: Artech House; 2010.
- (9) Ohno K, Tachikawa K, Manz A. Microfluidics: applications for analytical purposes in chemistry and biochemistry. Electrophoresis 2008;29(22):4443-4453.
- (10) El-Ali J, Sorger PK, Jensen KF. Cells on chips. Nature 2006;442(7101):403-411.
- (11) Ohno K, Tachikawa K, Manz A. Microfluidics: applications for analytical purposes in chemistry and biochemistry. Electrophoresis 2008;29(22):4443-4453.
- (12) Young EWK, Beebe DJ. Fundamentals of microfluidic cell culture in controlled microenvironments. Chem Soc Rev 2010;39(3):1036-1048.
- (13) Yang SY, Hsiung SK, Hung YC, Chang CM, Liao TL, Lee GB. A cell counting/sorting system incorporated with a microfabricated flow cytometer chip. Measurement Science and Technology 2006;17:2001.
- (14) Hetsroni G, Mosyak A, Pogrebnyak E, Yarin L. Fluid flow in micro-channels. Int J Heat Mass Transfer 2005;48(10):1982-1998.
- (15) Stone HA, Stroock AD, Ajdari A. Engineering flows in small devices. Annu Rev Fluid Mech 2004;36:381-411.

- (16) Stone H, Kim S. Microfluidics: basic issues, applications, and challenges. *AICHE J* 2001;47(6):1250-1254.
- (17) Shoji S, Esashi M. Microflow devices and systems. *J Micromech Microengineering* 1994;4:157.
- (18) Gad-el-Hak M,. MEMS : introduction and fundamentals. Boca Raton: CRC/Taylor & Francis; 2006.
- (19) Bruus H. Theoretical microfluidics. Oxford [u.a.]: Oxford Univ. Press; 2008.
- (20) Li PCH, Li PH. Microfluidic lab-on-a-chip for chemical and biological analysis and discovery. : CRC; 2006.
- (21) Liou WW, Fang Y. Microfluid mechanics. 2006; .
- (22) Tesař V. Pressure-driven microfluidics. Boston [u.a.]: Artech House; 2007.
- (23) Department of Biology, Davidson College, Davidson, NC 28036.  
Fluorescence active Cell Sorter.  
  
<http://www.bio.davidson.edu/courses/genomics/method/FACS.html>.
- (24) Takeuchi S, Garstecki P, Weibel DB, Whitesides GM. An Axisymmetric Flow-Focusing Microfluidic Device. *Adv Mater* 2005;17(8):1067-1072.
- (25) Chau LK, Osborn T, WU CC, Yager P. Microfabricated silicon flow-cell for optical monitoring of biological fluids. *Analytical sciences* 1999;15(8):721-724.
- (26) Fu AY, Spence C, Scherer A, Arnold FH, Quake SR. A microfabricated fluorescence-activated cell sorter. *Nat Biotechnol* 1999;17(11):1109-1111.
- (27) Lee GB, Lin CH, Chang GL. Micro flow cytometers with buried SU-8/SOG optical waveguides. *Sensors and Actuators A: Physical* 2003;103(1-2):165-170.
- (28) Church C, Zhu J, Wang G, Tzeng TRJ, Xuan X. Electrokinetic focusing and filtration of cells in a serpentine microchannel. *Biomicrofluidics* 2009;3:044109.
- (29) Fu LM, Yang RJ, Lee GB. Electrokinetic focusing injection methods on microfluidic devices. *Anal Chem* 2003;75(8):1905-1910.
- (30) Schrum DP, Culbertson CT, Jacobson SC, Ramsey JM. Microchip flow cytometry using electrokinetic focusing. *Anal Chem* 1999;71(19):4173-4177.



- (31) Jacobson SC, Ramsey JM. Microfabricated device and method for multiplexed electrokinetic focusing of fluid streams and a transport cytometry method using same 2000.
- (32) Fu LM, Yang RJ, Lin CH, Pan YJ, Lee GB. Electrokinetically driven micro flow cytometers with integrated fiber optics for on-line cell/particle detection. *Anal Chim Acta* 2004;507(1):163-169.
- (33) Takahashi T, Ogata S, Nishizawa M, Matsue T. A valveless switch for microparticle sorting with laminar flow streams and electrophoresis perpendicular to the direction of fluid stream. *Electrochemistry communications* 2003;5(2):175-177.
- (34) Lin CH, Lee GB, Fu LM, Hwey BH. Vertical focusing device utilizing dielectrophoretic force and its application on microflow cytometer. *Microelectromechanical Systems, Journal of* 2004;13(6):923-932.
- (35) Cheng IF, Chang HC, Hou D, Chang HC. An integrated dielectrophoretic chip for continuous bioparticle filtering, focusing, sorting, trapping, and detecting. *Biomicrofluidics* 2007;1:021503.
- (36) Zhu J, Xuan X. Dielectrophoretic focusing of particles in a microchannel constriction using DC-biased AC electric fields. *Electrophoresis* 2009;30(15):2668-2675.
- (37) Cheng IF, Chung CC, Chang HC. High-throughput electrokinetic bioparticle focusing based on a travelling-wave dielectrophoretic field. *Microfluidics and nanofluidics* 2011:1-12.
- (38) Zhao Y, Fujimoto BS, Jeffries GD, Schiro PG, Chiu DT. Optical gradient flow focusing. *Optics express* 2007;15(10):6167-6176.
- (39) MacDonald M, Spalding G, Dholakia K. Microfluidic sorting in an optical lattice. *Nature* 2003;426(6965):421-424.
- (40) Ramadan Q, Samper V, Poenar D, Yu C. Magnetic-based microfluidic platform for biomolecular separation. *Biomed Microdevices* 2006;8(2):151-158.
- (41) Shi J, Mao X, Ahmed D, Colletti A, Huang TJ. Focusing microparticles in a microfluidic channel with standing surface acoustic waves (SSAW). *Lab Chip* 2007;8(2):221-223.
- (42) Lei L, Zhou Y, Chen Y. Hydrodynamic focusing controlled microfluidic laser emission. *Microelectronic Engineering* 2009;86(4-6):1358-1360.
- (43) Yang AS, Hsieh WH. Hydrodynamic focusing investigation in a micro-flow cytometer. *Biomed Microdevices* 2007;9(2):113-122.

- (44) Yu C, Vykoukal J, Vykoukal DM, Schwartz JA, Shi L, Gascoyne PRC. A three-dimensional dielectrophoretic particle focusing channel for microcytometry applications. *Microelectromechanical Systems, Journal of* 2005;14(3):480-487.
- (45) Holmes D, Morgan H, Green NG. High throughput particle analysis: Combining dielectrophoretic particle focussing with confocal optical detection. *Biosensors and Bioelectronics* 2006;21(8):1621-1630.
- (46) Chen D, Du H. A dielectrophoretic barrier-based microsystem for separation of microparticles. *Microfluidics and Nanofluidics* 2007;3(5):603-610.
- (47) Yao B, Luo G, Feng X, Wang W, Chen L, Wang Y. A microfluidic device based on gravity and electric force driving for flow cytometry and fluorescence activated cell sorting. *Lab Chip* 2004;4(6):603-607.
- (48) Kim DS, Kim DSD, Han K, Yang W. An efficient 3-dimensional hydrodynamic focusing microfluidic device by means of locally increased aspect ratio. *Microelectronic Engineering* 2009;86(4-6):1343-1346.
- (49) Huh D, Gu W, Kamotani Y, Grotberg JB, Takayama S. Microfluidics for flow cytometric analysis of cells and particles. *Physiol Meas* 2005;26:R73.
- (50) Brown M, Wittwer C. Flow cytometry: principles and clinical applications in hematology. *Clin Chem* 2000;46(8):1221.
- (51) Wang MM, Tu E, Raymond DE, Yang JM, Zhang H, Hagen N, et al. Microfluidic sorting of mammalian cells by optical force switching. *Nat Biotechnol* 2004;23(1):83-87.
- (52) Wolff A, Perch-Nielsen IR, Larsen U, Friis P, Goranovic G, Poulsen CR, et al. Integrating advanced functionality in a microfabricated high-throughput fluorescent-activated cell sorter. *Lab Chip* 2003;3(1):22-27.
- (53) Mao X, Waldeisen JR, Huang TJ. "[rising dbl quote] Microfluidic drifting"-implementing three-dimensional hydrodynamic focusing with a single-layer planar microfluidic device. *Lab on a Chip* 2007;7(10):1260-1262.
- (54) Hansen C, Quake SR. Microfluidics in structural biology: smaller, faster... better. *Curr Opin Struct Biol* 2003;13(5):538-544.
- (55) Pabit SA, Hagen SJ. Laminar-flow fluid mixer for fast fluorescence kinetics studies. *Biophys J* 2002;83(5):2872-2878.
- (56) Wolfe DB, Conroy RS, Garstecki P, Mayers BT, Fischbach MA, Paul KE, et al. Dynamic control of liquid-core/liquid-cladding optical waveguides. *Proc Natl Acad Sci U S A* 2004;101(34):12434.

- (57) Chiu DT, Jeon NL, Huang S, Kane RS, Wargo CJ, Choi IS, et al. Patterned deposition of cells and proteins onto surfaces by using three-dimensional microfluidic systems. *Proceedings of the National Academy of Sciences* 2000;97(6):2408.
- (58) Vezenov DV, Mayers BT, Wolfe DB, Whitesides GM. Integrated fluorescent light source for optofluidic applications. *Appl Phys Lett* 2005;86:041104.
- (59) Zhao B, Moore JS, Beebe DJ. Surface-directed liquid flow inside microchannels. *Science* 2001;291(5506):1023.
- (60) Zhao B, Moore JS, Beebe DJ. Principles of surface-directed liquid flow in microfluidic channels. *Anal Chem* 2002;74(16):4259-4268.
- (61) Lee GB, Chang CC, Huang SB, Yang RJ. The hydrodynamic focusing effect inside rectangular microchannels. *J Micromech Microengineering* 2006;16:1024.
- (62) Kenis PJA, Ismagilov RF, Takayama S, Whitesides GM, Li S, White HS. Fabrication inside microchannels using fluid flow. *Acc Chem Res* 2000;33(12):841-847.
- (63) Stroock AD, Whitesides GM. Controlling flows in microchannels with patterned surface charge and topography. *Acc Chem Res* 2003;36(8):597-604.
- (64) Martín-Banderas L, Flores-Mosquera M, Riesco-Chueca P, Rodríguez-Gil A, Cebolla Á, Chávez S, et al. Flow Focusing: A Versatile Technology to Produce Size-Controlled and Specific-Morphology Microparticles. *Small* 2005;1(7):688-692.
- (65) Anna SL, Bontoux N, Stone HA. Formation of dispersions using “flow focusing” in microchannels. *Appl Phys Lett* 2003;82:364.
- (66) Three-dimensional single step flow sheathing in micro cell sorters. *Modeling and Simulation of Microsystems*; 2001.
- (67) Sundararajan N, Pio MS, Lee LP, Berlin AA. Three-dimensional hydrodynamic focusing in polydimethylsiloxane (PDMS) microchannels. *Microelectromechanical Systems, Journal of* 2004;13(4):559-567.
- (68) Yang R, Feeback DL, Wang W. Microfabrication and test of a three-dimensional polymer hydro-focusing unit for flow cytometry applications. *Sensors and Actuators A: Physical* 2005;118(2):259-267.
- (69) Chang CC, Huang ZX, Yang RJ. Three-dimensional hydrodynamic focusing in two-layer polydimethylsiloxane (PDMS) microchannels. *J Micromech Microengineering* 2007;17:1479.
- (70) Tsai CH, Hou HH, Fu LM. An optimal three-dimensional focusing technique for micro-flow cytometers. *Microfluidics and nanofluidics* 2008;5(6):827-836.

- (71) Three-dimensional hydrodynamic focusing over a wide Reynolds number range using a two-layer microfluidic design. Proceedings 12th international conference on miniaturized systems for chemistry and life sciences ( $\mu$ TAS'08), San Diego, CA; 2008.
- (72) Jackson MJ. Micro and nanomanufacturing. 2007; .
- (73) High-throughput on-chip flow cytometry system using “microfluidic drifting” based three-dimensional (3D) hydrodynamic focusing. Solid-State Sensors, Actuators and Microsystems Conference, 2009. TRANSDUCERS 2009. International: IEEE; 2009.
- (74) Mao X, Huang TJ. Microfluidic Drifting: Three Dimensional Hydrodynamic Focusing Of Microparticles.
- (75) Rosenauer M, Buchegger W, Finoulst I, Verhaert P, Vellekoop M. Miniaturized flow cytometer with 3D hydrodynamic particle focusing and integrated optical elements applying silicon photodiodes. Microfluidics and Nanofluidics 2011:1-11.
- (76) Sia SK, Whitesides GM. Microfluidic devices fabricated in poly (dimethylsiloxane) for biological studies. Electrophoresis 2003;24(21):3563-3576.
- (77) Thorsen T, Maerkl SJ, Quake SR. Microfluidic large-scale integration. Science 2002;298(5593):580.
- (78) Wu Z, Hjort K. Microfluidic Hydrodynamic Cell Separation: A Review.
- (79) Bayraktar T, Pidugu SB. Characterization of liquid flows in microfluidic systems. Int J Heat Mass Transfer 2006;49(5):815-824.
- (80) Beebe DJ, Mensing GA, Walker GM. Physics and applications of microfluidics in biology. Annu Rev Biomed Eng 2002;4(1):261-286.
- (81) Meyvantsson I, Beebe DJ. Cell culture models in microfluidic systems. Annu.Rev.Anal.Chem. 2008;1:423-449.
- (82) Ratner BD, Bryant SJ. Biomaterials: where we have been and where we are going. Annu Rev Biomed Eng 2004;6:41-75.
- (83) Li L, Ismagilov RF. Protein crystallization using microfluidic technologies based on valves, droplets, and SlipChip. Annual review of biophysics 2010;39:139-158.
- (84) Zare RN, Kim S. Microfluidic platforms for single-cell analysis. Annu Rev Biomed Eng 2010;12:187-201.
- (85) Brown M, Wittwer C. Flow cytometry: principles and clinical applications in hematology. Clin Chem 2000 Aug;46(8 Pt 2):1221-1229.

- (86) Xuan X, Zhu J, Church C. Particle focusing in microfluidic devices. *Microfluidics and nanofluidics* 2010;9(1):1-16.
- (87) Oakey J, Applegate Jr RW, Arellano E, Carlo DD, Graves SW, Toner M. Particle focusing in staged inertial microfluidic devices for flow cytometry. *Anal Chem* 2010;82(9):3862-3867.
- (88) Wu Z, Nguyen NT. Hydrodynamic focusing in microchannels under consideration of diffusive dispersion: theories and experiments. *Sensors Actuators B: Chem* 2005;107(2):965-974.
- (89) Kim YW, Yoo JY. Three-dimensional focusing of red blood cells in microchannel flows for bio-sensing applications. *Biosensors and Bioelectronics* 2009;24(12):3677-3682.
- (90) Three-Dimensional Hydrodynamic Focusing Over A Wide Reynolds Number Range Using A Two-Layer Microfluidic Design.
- (91) Sia SK, Whitesides GM. Microfluidic devices fabricated in poly (dimethylsiloxane) for biological studies. *Electrophoresis* 2003;24(21):3563-3576.
- (92) Young EWK, Beebe DJ. Fundamentals of microfluidic cell culture in controlled microenvironments. *Chem Soc Rev* 2010;39(3):1036-1048.
- (93) El-Ali J, Sorger PK, Jensen KF. Cells on chips. *Nature* 2006;442(7101):403-411.
- (94) Yeon JH, Park JK. Microfluidic cell culture systems for cellular analysis. *Biochip J* 2007;1(1):17-27.
- (95) Chen CS, Jiang X, Whitesides GM. Microengineering the environment of mammalian cells in culture. *MRS Bull* 2005;30(03):194-201.
- (96) Yamada M, Kasim V, Nakashima M, Edahiro J, Seki M. Continuous cell partitioning using an aqueous two-phase flow system in microfluidic devices. *Biotechnol Bioeng* 2004;88(4):489-494.
- (97) El-Ali J, Sorger PK, Jensen KF. Cells on chips. *Nature* 2006;442(7101):403-411.
- (98) Whitesides GM. The origins and the future of microfluidics. *Nature* 2006;442(7101):368-373.
- (99) Byun I, Kim W, Park S. A micro flow cell cytometry based on MEMS technologies using silicon and optical fibers. *J Mater Sci* 2003;38(22):4603-4605.

- (100) Anthony T and Sivakumar N. A novel three dimensional hydrodynamic focusing design in micro fluidics” submitted in Journal of Micromechanics and Microengineering (Article ID: RANL-8P2JSR) Nov 28, 2011.
- (101) Elwenspoek M, Jansen HV. Silicon micromachining. Silicon Micromachining, by Miko Elwenspoek and Henri V.Jansen, pp.419.ISBN 0521607671.Cambridge, UK: Cambridge University Press, August 2004. 2004;1.
- (102) Dry silicon etching for MEMS. Proc. Symp. Microstructures and Microfabricated Systems, ECS; 1997.
- (103) Lee S, Park S, Cho DI. The surface/bulk micromachining (SBM) process: a new method for fabricating released MEMS in single crystal silicon. Microelectromechanical Systems, Journal of 1999;8(4):409-416.
- (104) Jo BH, Van Lerberghe LM, Motsegood KM, Beebe DJ. Three-dimensional micro-channel fabrication in polydimethylsiloxane (PDMS) elastomer. Microelectromechanical Systems, Journal of 2000;9(1):76-81.
- (105) Anderson JR, Chiu DT, Jackman RJ, Cherniavskaya O, McDonald JC, Wu H, et al. Fabrication of topologically complex three-dimensional microfluidic systems in PDMS by rapid prototyping. Anal Chem 2000;72(14):3158-3164.
- (106) Judy JW. Microelectromechanical systems (MEMS): fabrication, design and applications. Smart Mater Struct 2001;10:1115.
- (107) Liu C. Recent developments in polymer MEMS. Adv Mater 2007;19(22):3783-3790.
- (108) Wang C, Jia G, Taherabadi LH, Madou MJ. A novel method for the fabrication of high-aspect ratio C-MEMS structures. Microelectromechanical Systems, Journal of 2005;14(2):348-358.
- (109) Chuang YJ, Tseng FG, Cheng JH, Lin WK. A novel fabrication method of embedded micro-channels by using SU-8 thick-film photoresists. Sensors and Actuators A: Physical 2003;103(1-2):64-69.
- (110) Song I, Ajmera PK. Use of a photoresist sacrificial layer with SU-8 electroplating mould in MEMS fabrication. J Micromech Microengineering 2003;13:816.
- (111) Lin CH, Lee GB, Chang BW, Chang GL. A new fabrication process for ultra-thick microfluidic microstructures utilizing SU-8 photoresist. J Micromech Microengineering 2002;12:590.
- (112) Becker H, Heim U. Hot embossing as a method for the fabrication of polymer high aspect ratio structures. Sensors and Actuators A: Physical 2000;83(1-3):130-135.

- (113) A PMMA-based micro pressure sensor chip using carbon nanotubes as sensing elements. Micro Electro Mechanical Systems, 2005. MEMS 2005. 18th IEEE International Conference on: IEEE; 2005.
- (114) Schroers J, Pham Q, Desai A. Thermoplastic forming of bulk metallic glass—a technology for MEMS and microstructure fabrication. Microelectromechanical Systems, Journal of 2007;16(2):240-247.
- (115) Miles MW. Method for fabricating a structure for a microelectromechanical systems (MEMS) device 2004.
- (116) Liew LA, Zhang W, Bright VM, An L, Dunn ML, Raj R. Fabrication of SiCN ceramic MEMS using injectable polymer-precursor technique. Sensors and Actuators A: Physical 2001;89(1-2):64-70.
- (117) White RM, Herko LH, Altavela RP. Teflon filled resinoid dicing blades for fabricating silicon die modules 1996.
- (118) A micromachined thin-film Teflon electret microphone. Solid State Sensors and Actuators, 1997. TRANSDUCERS'97 Chicago., 1997 International Conference on: IEEE; 1997.
- (119) [http://www.microchem.com/pdf/SU-82000DataSheet2000\\_5thru2015Ver4.pdf](http://www.microchem.com/pdf/SU-82000DataSheet2000_5thru2015Ver4.pdf).
- (120) <http://www.ece.gatech.edu/research/labs/vc/theory/photolith.html>.